Rack to the Future: Design of Payload Racks to Support Future Habitation Platform and Exploration Missions

Moon to Mars Exploration Systems
and Habitat (M2M X-Hab)
2025 Academic Innovation Challenge

Final Report
University of Maryland

Dr. David L. Akin
June 4, 2025

UNIVERSITY OF
MARYLAND

UNIVERSITY OF MARYLAND AT COLLEGE PARK

DEPARTMENT OF AEROSPACE ENGINEERING

RACK TO THE FUTURE

RACK AND STACK:

DESIGN OF PAYLOAD RACKS TO SUPPORT

FUTURE HABITATION PLATFORMS AND EXPLORATION MISSIONS

ENAE484 SENIOR CAPSTONE, CLASS OF 2025

1 Introduction

1.1 Names

Faculty Advisor: Dr. David Akin

Graduate Advisors: Nicolas Bolatto, Charles Hanner

Student Team Members:

Lukas Bieneman	Raymond Encarnacion	Allison Rahr
Christopher Blaisdell	Grace Johnson	Arul Ramachandran
Rachel Boschen	Colin Keller	Dev Shanker
Muhammad Chaudhry	Benjamin Leazer	Nicholas Varro
Sofia Correia	Avery Lowe	Yuhan Wang
Andrew Dolecki	Tadhg Martinez	Ava Ward
Mason Eberle	Alexa Patnaude	

Team Logo by Dev Shanker

1.2 Report Overview

1.2.1 Table of Contents

Table of Contents

1.2.2 Table of Figures and Tables

Figures

Tables

1.2.3 Glossary of Acronyms

Acronym	Phrase	Description
AFSS	Avionics and Flight Systems	484 Sub-team
CAD	Computer Aided Design	Design Tool
CDR	Critical Design Review	Critical Design Review with faculty and industry members
CS	Crew Systems	484 Sub-team
DC	Direct Current	Electrical Flow Direction
ECLSS	Environmental Control and Life Support Systems	Station System
ETFE	Ethylene Tetrafluoroethylene	Material (Polymer)
EXPRESS	EXpedite the PRocessing of Experiments to Space Station	Rack system currently use by NASA in conjunction with ISPR
ISPR	International Standard Payload Rack	Rack system currently in use by NASA in conjunction with EXPRESS Rack
LTL	Low Temperature Loop	ISS Water Interface
LSM	Loads, Structures, and Mechanisms	484 Sub-team
MS	Mission Statement	Established by X-Hab and 484 Team
MTBF	Mean Time Between Failure	Component Reliability Metric
MTL	Moderate Temperature Loop	ISS Water Interface
MPA	Mission Planning and Analysis	484 Sub-team
NASA	National Aeronautics and Space Administration	United States government agency responsible for aeronautics research, space exploration, and scientific discovery
NBRF	Neutral Buoyancy Research Facility	One of two operating neutral buoyancy tanks in the United States
PCS	Power Controller System	Electrical System
PDR	Preliminary Design Review	Preliminary Design Review with faculty and industry members
PPT	Power, Propulsion, and Thermal	484 Sub-team
PWB	Printed Wiring Board	Electrical Component
SASE	Systems Analysis and Engineering	484 Sub-team
SSL	Space Systems Laboratory	Aerospace Laboratory at the University of Maryland, headed by Dr. David Akin
SSPC	Solid State Power Controller	Electrical Component
SSPCM	Solid State Power Controller Module	Electrical Component
TLX	Task Load Index	Subjective workload assessment questionnaire
WCS	Water Cooling System	Cooling System
X-Hab	eXploration Habitat	NASA led academic innovation challenge

Table 1: Glossary of Acronyms

1.3 Program Introduction

1.3.1 X-Hab Program - Nicholas Varro

NASA's M2M X-Hab Academic Innovation Challenge is an annual competition that invites university students to design and develop innovative space habitat technologies and systems that align with NASA's goals in exploration. University teams propose and develop projects that are judged on technical merit, academic involvement, and outreach. Under the guidance of NASA experts, student led teams collaborate over several months to design and develop solutions that address the problems outlined in their project. The X-Hab challenge offers students a unique opportunity in hands on experience in real world engineering development.

Our team collaborated with NASA to design and develop a payload rack to support future habitation platforms and their exploration missions. This project centered around innovation towards a design to handle the primary engineering challenge of adaptability in various gravitational conditions.

1.3.2 Problem Statement - Rachel Boschen

NASA's Artemis program requires a payload rack system that supports scientific research and technology development in future lunar and Martian habitats. Current rack designs from the ISS are optimized for microgravity and do not meet the unique challenges of partial gravity environments, high-oxygen levels, and long dormancy periods.

1.3.3 Mission Statement (MS) - Benjamin Leazer & Rachel Boschen

To design, build, and test a prototype payload rack optimized for partial gravity environments, tailored for lunar with scalability to Mars surface habitats, to contribute to the development of adaptable infrastructure that supports diverse payload management for long-duration crew-based missions.

1.3.4 Project Vision - Ava Ward

To create a full-scale model of the next generation of adaptable, multifunctional payload racks that seamlessly integrate with future habitation platforms, facilitating efficient scientific experimentation and technology development, supporting NASA's Artemis and Mars exploration goals for humanity's sustained presence on the Moon and beyond.

1.3.5 Program Objectives - Mason Eberle & Rachel Boschen

The payload rack system was developed around four core objectives: adaptability, human-centered design, operational efficiency, and sustainability. Adaptability was prioritized to ensure the rack could accommodate a wide range of scientific, logistical, and storage payloads across various gravitational environments, including microgravity, lunar gravity (1/6 g), and Martian gravity (1/3 g). A focus on human-centered design led to the integration of human factors and ergonomic considerations, allowing astronauts to interact with the rack easily and perform maintenance and

repair tasks effectively in partial gravity. To promote operational efficiency, the system was designed to be easily replaceable, maintainable, and serviceable with minimal crew time, supporting overall mission productivity. Finally, the rack was engineered with sustainability and extensibility in mind, enabling it to be repurposed or modified to support multiple mission scenarios and adapt to evolving scientific and operational requirements.

1.3.6 Requirements - Christopher Blaisdell

Listed below are the major level 1 requirements (Table 2) along with requirements corresponding to sub-teams that held them (Tables 3,4,5,6).

Level 1 Requirements			
ID	**Requirement**	**Level**	**Source**
MPA-1	The rack shall be liftable by two individuals under lunar gravity and should be compatible with a lifting device to facilitate safe and efficient handling.	L1	MS
MPA-2	The rack shall be designed with interface with habitat data and power systems.	L1	MS
MPA-3	The rack shall provide accessible data and power connections.	L1	MS
MPA-4	The rack shall withstand environmental, mechanical, and operational conditions associated with a 10-year lunar habitat mission life, including up to 3 years of continuous dormancy in a high-oxygen atmosphere.	L1	MS
CS-1	The rack shall be able to support ECLSS features including potable water processor, O2 Generator, waste management system, cabin air filter, CO2 removal system, thermal control system.	L1	NASA
CS-2	The rack shall be able to monitor for and detect smoke and alert the crew in the case of a fire event.	L1	NASA
CS-3	The rack shall not have sharp edges, protruding parts, nor unsecured moving parts.	L1	NASA
PPT-1	The rack shall be able to convert Station 120V DC into Payload 28V or 120V DC power.	L1	MS
PPT-2	The rack shall be able to provide auxiliary rack components with required power.	L1	MS

Table 2: Level 1 Requirements

LSM Requirements			
ID	**Requirement**	**Level**	**Source**
LSM-1	The rack shall be able to withstand launch loads up to 6 gs.	L2	MPA-4
LSM-2	The rack shall be able to withstand vibrational loads.	L2	MPA-4
MPA-5	The rack shall have a mass not exceeding 186 lbs prior to installation	L2.	MPA-1
MPA-6	The rack shall fit within 40" x 60" hatch size	L2.	NASA
LSM-5	The rack shall be capable of withstanding a crew inadvertent contact load of 154 lb (685 N).	L2	NASA
LSM-6	The rack shall provide easy access to payloads for use and repair.	L2	MPA-3, MPA-9
LSM-7	The rack shall provide facilities to replace payloads with ease.	L2	MPA-9

Table 3: LSM Requirements

MPA Requirements			
ID	**Requirement**	**Level**	**Source**
MPA-1	The rack shall be liftable by two individuals under lunar gravity and should be compatible with a lifting device to facilitate safe and efficient handling.	L1	MS
MPA-2	The rack shall be designed with interface with habitat data and power systems.	L1	MS
MPA-3	The rack shall provide accessible data and power connections.	L1	MS
MPA-4	The rack shall withstand environmental, mechanical, and operational conditions associated with a 10-year lunar habitat mission life, including up to 3 years of continuous dormancy in a high-oxygen atmosphere.	L1	MS
MPA-5	The rack shall have a mass not exceeding 375kg prior to installation.	L2	MPA-1.
MPA-6	The rack shall fit within the dimensions of the NASA standard 40" x 60" hatch.	L2	NASA
MPA-7	The rack shall optimize internal volume for scientific equipment and storage.	L2	MS
MPA-8	The rack shall be compatible with existing ISPR payloads, adhering to relevant size and interface standards.	L2	MS
MPA-9	Payloads shall be readily accessible and interchangeable.	L2	MS
MPA-10	The rack shall be capable of fitting through a straight corridor with a minimum width of 57 inches.	L2	NASA
MPA-11	The rack shall be capable of maneuvering through a 90-degree turn within a corridor of width 57 inches.	L3	NASA, MPA-10

Table 4: MPA Requirements

Crew System Requirements			
ID	**Requirement**	**Level**	**Source**
CS-1	The rack shall be able to support ECLSS features including potable water processor, O2 Generator, waste management system, cabin air filter, CO2 removal system, thermal control system.	L1	NASA
CS-2	The rack shall be able to monitor for and detect smoke and alert the crew in the case of a fire event.	L1	NASA
CS-3	The rack shall not have sharp edges, protruding parts, nor unsecured moving parts.	L1	NASA
CS-4	The rack shall allow for storage of payloads requiring different temperatures.	L2	NASA
CS-5	The rack shall provide sufficient lighting for payload(s) and crew.	L2	NASA.
CS-6	The acoustics of the rack shall be tolerable for astronauts in 1/6 earth gravity.	L2	NASA
CS-7	The rack shall be able to withstand inadvertent contact with members of the crew.	L2	NASA

Table 5: Crew Systems Requirements

PPT Requirements			
ID	**Requirement**	**Level**	**Source**
PPT-1	The rack shall be able to convert Station 120V DC into Payload 28V or 120V DC power.	L1	MS
PPT-2	The rack shall be able to provide auxiliary rack components with required power.	L1	MS
PPT-3	The rack shall interface with the space habitat to oversee air and cool/ moderate water loops.	L2	MS
PPT-4	The rack shall provide cool air to payloads and components and circulate air through smoke detector system.	L2	MS
PPT-5	The rack shall cool auxiliary components through internal air circulation or cold-plates.	L2	CS-2.
PPT-6	The rack shall provide Nitrogen distribution to one or more payloads.	L3	S-2
PPT-7	The rack shall provide vacuum exhaust to one or more payloads.	L3	S-2

Table 6: Power and Propulsion Requirements

1.3.7 Concept of Operations - Sofia Correia

The modular payload rack is designed to house and support scientific payloads, life support systems, and general equipment within the lunar habitat. Select payloads will be installed into the rack prior to launch. To meet operational and ergonomic constraints, the combined mass of the rack and any pre-installed payloads must not exceed 375 kilograms, corresponding to a lunar apparent weight of 613 newtons (138 pounds).

Upon landing on the lunar surface, the rack is offloaded from the lander and manually transported into and through the habitat. The mass limitation ensures that two astronauts can safely carry and maneuver the rack through hallways and hatches. If transport between levels within the habitat is required, the rack is lifted using a block-and-tackle system to ensure safe handling.

Once positioned at the desired installation site, the rack is secured to the habitat structure using the established mounting points. Detailed installation instructions are provided to guide astronauts through mechanical attachments as well as the connections of power, data, and life support systems. Throughout its operational lifetime, the rack enables routine access and servicing via removable side panels and integrated sliding rails, allowing payloads to be extended from the rack for inspection and maintenance.

At the end of its service life, the rack can be repurposed for indoor or outdoor storage, depending on mission and habitat requirements, thus preserving its utility beyond its original purpose.

1.3.8 Design Reference Mission - Mason Eberle

The full life-cycle of the modular payload rack is divided into four key phases: launch and landing, transportation and integration, installation and operation, and eventual decommissioning or re-purposing. Prior to launch, the rack is loaded with selected payloads, ensuring that the combined mass does not exceed 375 kilograms (613 N). The rack is secured within the launch vehicle using vibration damping, shock absorption, and thermal protection to ensure its safety during ascent. Final system checks verify the rack's structural integrity and readiness for launch.

Upon landing on the lunar surface, the rack and payloads are inspected to ensure proper alignment and condition. The rack is then manually extracted from the launch vehicle and transported into the habitat by two astronauts. If necessary, a block-and-tackle system is used for vertical movement between habitat levels. Once inside, the rack is positioned at its designated location, and detailed installation instructions guide astronauts through securing the rack to the habitat structure and connecting power, data, and life support systems. If any additional payloads were delivered separately, they are installed at this stage.

After installation, the rack is powered on, and integrated systems are tested to ensure compatibility with the habitat. Routine servicing and maintenance are supported throughout the rack's operational life through removable side panels and sliding rails that allow astronauts to access and service payloads.

At the end of its operational life, the rack is powered down and disconnected from habitat systems. It is then either repurposed for indoor or outdoor storage or decommissioned, depending on the requirements of the habitat and ongoing mission needs.

2 Current Design

2.1 Structural Design

2.1.1 Structural Overview - Muhammad Chaudhry & Grace Johnson

General feedback from multiple meetings with the NASA team was that the rack should have flexibility in width, based on certain payloads or habitat constraints. Because of this, two different rack frame designs were created: a "double" rack with dimensions more akin to EXPRESS Rack sizing to allow for compatibility with existing payloads, and a "single" rack measuring half the width of the "double" rack for smaller payloads and easier maneuverability (Thompson et al, 2014). Both racks reserve the back 0.25 m in depth for maintenance and servicing volume. Figure 1 shows the single rack design, measuring 0.59 m in width, 1.91 m in height, and 0.90 m in depth, and featuring 0.68 m^3 of payload volume as well as 0.25 m^3 of maintenance volume. Figure 2 shows the double rack design, measuring 1.16 m in width, 1.91 m in height, and 0.90 m in depth, and featuring 1.39 m^3 of payload volume as well as 0.51 m^3 of maintenance volume. For a more in-depth discussion on the dimensions of individual beam members, see Section 3.2.1.

Figure 1: CAD Model of Single Rack Frame

Figure 2: CAD Model of Double Rack Frame

Both rack designs include horizontal members that will have rails mounted on their inside faces (see Section 3.1.2), and vertical members with holes cut out at 76.2 mm intervals along their height. Each payload will have a flooring to be mounted on (see Section **??**), which will directly connect to the rails on each horizontal member. These horizontal members can move up and down along the height of each vertical member using spring-loaded pins to accommodate payloads of various heights. Additionally, each rack will have removable side panels to easily access the maintenance area and service payloads. For a more in-depth discussion of these panels, see Section 2.1.2. A preliminary mass estimate of these rack frame designs, outfitted with horizontal members to accommodate six standard payloads (see Section **??**) yields 14.5 kg for the single rack and 15.2 kg for the double rack.

2.1.2 Side Panel Design - Yuhan Wang

Following requirement LSM-6, the team aimed to design side panels that would allow ease of service and accessibility to payloads while also considering the strength, durability, and environmental resistance factors of various materials. Since the rack is designed to bear loads without side panels attached, the panels are not designed to physically support the overall structure of the rack.

The payload section and the service section of the rack each have their own individual panels. Therefore, operations needed on only one of the two sections will not require both to be exposed while conducting maintenance. For accessibility, the side panels are hinged onto the edges of the side faces of the rack and are secured to the beam separating the payload and service sections via Dzus fasteners. From a side view, the hinges would be located on the exterior corners of the rack, and the Dzus fasteners would be located in the same position on the interior side, connecting to the beam via flanges. This creates a simple swinging door style design, in which the side panels

remain securely attached to the rack during maintenance. Dzus fasteners can be unfastened one at a time, which allows maintenance to be done by one person.

The material for the side panels was chosen to be Aluminum 7075-T6, the same type of aluminum as the structural beams, in order to match the physical properties of the rest of the rack. This ensures that the side panels will not fail due to factors such as extreme heat or corrosion sooner than the rest of the rack does.

The thickness of the panels was determined via flat plate equations from mechanics theory. The main constraint for the panel thickness is the maximum allowable deformation distance from the resting location of the panel to the payloads within the rack, which is equivalent to the width of one structural beam: 13.5 millimeters. Therefore, the maximum allowable force that the panels experience must be considered. NASA standard LDR-025 (NASA JSC-65829 Rev B), from Loads and Structural Dynamics Requirements for Spaceflight Hardware, calls for designs to consider a maximum force due to inadvertent contact of 685 Newtons. The equation for maximum displacement for an edge-clamped rectangular flat plate with a concentrated load at the center is

$$y_{max} = k\frac{Fb^2}{Et^3} \tag{1}$$

where k is a constant based on the ratio of the longer dimension to the shorter dimension of the plate, F is the applied force, b is the shorter length of the rectangle, E is the modulus of elasticity, and t is the thickness. For the payload area, the ratio of length to width gives a k value of 0.0791.

Using a safety factor of 1.25, the minimum thickness for the side panels is 3 millimeters. The total mass of the panels for one side of the rack including both sections is 13.71 kilograms.

2.1.3 Mounting to Launch Vehicle and Lunar Habitat – Andrew Dolecki

The rack will be bolted to both the floor and the wall of the launch Vehicle. The possibility of mounting the rack through the use of bolts exclusively on the floor was initially discussed, but ultimately ruled out due to the 2 g's of loading in the lateral direction. This 2g's of loading will result in more stress than the 6 g's of axial loading, so it is essential to secure the rack to the wall during launch.

However, on the Lunar Habitat the rack will no longer undergo these significant loads in the lateral direction, so it is possible for our rack to be bolted to only the floor. However, it would still be preferred to mount the rack to the wall in order to prevent tipping.

2.1.4 Earth Frame Model - Muhammad Chaudhry & Grace Johnson

For testing purposes, a mock-up rack frame was constructed using 80/20 aluminum, various gusset plates and fixtures, and assembled with similar outer dimensions as the double rack design. 80/20 aluminum allows for modular assembly, easier adjustments, and is cost-effective. This 80/20 structure enables us to test the assembly process, payload integration, and structural feasibility before committing to the final lunar material. Figure 3 shows the design of this Earth Frame Model, and Figure 4 shows the LSM team constructing the actual rack frame in the Space Systems Laboratory on the University of Maryland College Park campus. This rack frame measures

1.17 m in width, 1.80 m in height, and 0.920 m in depth. A parts list for the 80/20 frame is included in Appendix B, Evolution 6. Testing done with this frame is detailed in Sections 3.3 and 3.4.

Figure 3: CAD Model of 80/20 Earth Frame Model

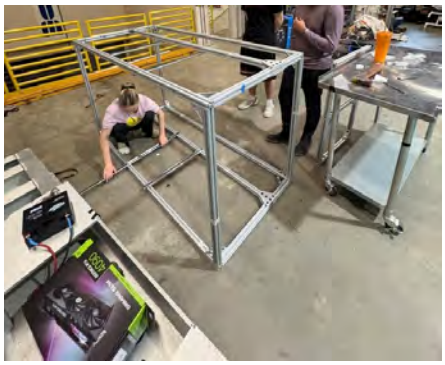

Figure 4: LSM team constructing the Earth Frame Model in the Space Systems Laboratory

2.1.5 Payload Floor - Arul Ramachandran

The low strength of the rails with drawer release and payload installation issues that occurred while manufacturing our Earth Frame Model led the team to pursue an alternative method of

integrating payloads onto the rack. The conclusion was to create a payload floor that would attach to the rack via the rail system. The payloads then attach to the flooring via DZUS bolts allowing for easy access and removal. For payloads without data requirements, the floors are to be constructed of aluminum 7075-T6 sheet metal with 2.54 mm thickness. Payloads with data will use the data hub as their payload floor. More information on the data hub can be found in Section .

Material and thickness analysis for the non-data floor was performed to minimize the additional mass added to the system from the floors. The floors were modeled as flat plates that undergo a uniformly distributed vertical load using Roark's Stress and Strain Formulas. For single rack floors, boundary conditions were long edges fixed with short edges simply supported, and for double racks boundary conditions were short edges fixed with long edges simply supported. Load was modeled as 6g's acceleration on 80 kg of payload mass distributed over the area of the floor. Analysis was performed in two parts with the first pass determining the minimum thickness to survive load conditions with a safety factor of 1.25. The second pass analysis was performed using the closest commercially available thickness of each material rounding up. The results of the first pass are shown in figure 5 while the results of the second pass are seen in figure 6. In both passes, Aluminum 7075-T6 was determined to add the least mass to the system, with Titanium being a close second. As mass was our primary concern Aluminum 7075-T6 was chosen as the non data payload floor material. It should be noted that the mass depicted in the tables is the mass for one floor.

Material	Al7075_T6	Al6061_T6	AL2024_T4	Titanium Annealed
Single Rack Thickness (mm)	2.05	3.069	2.763	1.559
Double Rack Thickness (mm)	2.083	3.119	2.809	1.585
Single Rack Floor Mass (kg)	2.056	3.011	2.771	2.613
Double Rack Floor Mass (kg)	4.268	6.252	5.775	5.428

Figure 5: First Pass Analysis of Floor Thickness and Mass

Material	Al7075_T6	Al6061_T6	AL2024_T4	Titanium Annealed
Thickness (mm)	2.54	3.175	3.175	1.588
Single Rack Floor Mass (kg)	2.547	3.115	3.184	2.661
Double Rack Floor Mass (kg)	5.204	6.364	6.505	5.437

Figure 6: Second Pass Analysis of Floor Thickness and Mass

2.2 Power and Thermal Systems

2.2.1 Power and Cooling Requirements - Luke Bieneman

The power system aims to provide standard 28 Volts at 5, 10, 15, or 20 Amps or 120 Volts in special circumstances. The minimum and maximum power and cooling requirements are based on the worst expected case of power draw and cooling needs per payload.

$$P_{max} = V_{max} A_{max} \tag{2}$$

The worst-case power draw for each payload is 560 Watts (28 Volts at 20 Amps). This estimation

is supported by two single-payload size Environmental Control and Life Support System (ECLSS) payloads (Water Processor Assembly - 343 Watts and Urine Processor Assembly - 424 Watts).

The worst-case heat dissipation for each payload will be set to 560 Watts as well, accounting for the worst theoretical case of all input power needing to be dissipated thermally.

Number of Payloads	Power Requirements (W)	Heat Dissipation Requirements (W)
1	560	560
2	1120	1120
3	1680	1680
4	2240	2240
5	2800	2800
6	3360	3360

Table 7: Power and Heat Dissipation Requirements per Payload

Additional thermal considerations must be taken into account in lunar, martian, and transient habitats. Within a station with simulated Earth atmosphere, the largest differentiating factor for cooling systems is convective efficiency.

Convective heat transfer can be generically described as:

$$Q_{\text{conv}} = hA\Delta T \tag{3}$$

where h is the convective heat transfer coefficient. This coefficient is dependent on the Nusselt Number (Nu) and for a flat plate can be written:

$$h = \text{Nu} \cdot k/L \tag{4}$$

where the Nusselt Number (Nu) can be written empirically as a function of the Rayleigh Number (Ra) as:

$$\text{Nu} = C(\text{Ra})^n \tag{5}$$

Lastly the Rayleigh Number is dependent on gravity such that:

$$\text{Ra} = g\rho\beta\Delta T L^3/\nu\alpha \tag{6}$$

This allows for heat transfer to be rewritten with a dependence on gravity:

$$Q_{\text{conv}} = (g\rho\beta\Delta T L^3/\nu\alpha)^n \cdot CkA\Delta T/L \tag{7}$$

From this derivation a connection between convective heat transfer and gravity can be drawn. Values for n vary, but are typically below 1, thus for the worst case scenario:

$$Q_{\text{conv}} \propto g \tag{8}$$

So for the various habitats:

Habitat	Gravity (m/s^2)	$Q_{\text{conv-Earth}}/Q_{\text{conv-Habitat}}$
Earth	9.81	1
Lunar	1.62	0.165
Martian	3.73	0.380
Transfer	0	0

Table 8: Effective Convective Heat Transfer for Various Habitats

While this derivation likely provides an underestimate for the efficiency of natural convection outside of Earth, it eliminates the option of using natural convection as a method of heat dissipation. This leads to the proposed methods of cooling for the rack system:

- Forced Convection with air, cooled via an air to water heat exchanger (Air Cooling System)
- Conduction through optional cold-plates and water (Water Cooling System)

The rack must also comply with the lunar station requirements:

- Water Moderate Temperature Loop (MTL) return no greater than 49 C
- Water Low Temperature Loop (LTL) return no lower than 21 C
- Electronics over 50 V should be isolated from astronauts.
- The rack must be grounded to lunar station.
- The rack must comply with acoustic limits (see Crew Systems).

2.2.2 Power System - Luke Bieneman

The power system aims to provide the maximum power required to rack subsystems while also providing redundant safety systems. The lunar station will provide 120 V DC power to the rack. The rack will then adjust this to the payload power or rack subsystem power. Typical payload voltage is 28 V DC, although some rack subsystems or payloads may require 120 V DC.

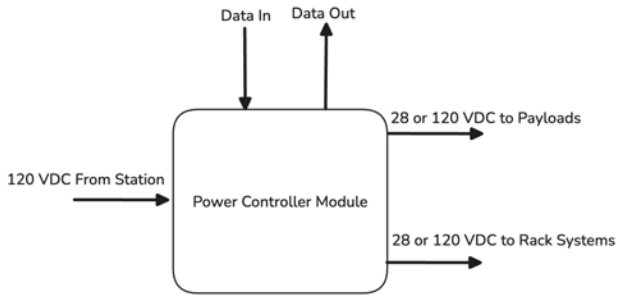

Figure 7: Power System Diagram

Within the Aerospace and Defense industry power regulation is done by either Solid State Power Controllers (SSPC's) or Electromechanical Relays. SSPC's and modules of them SSPCM's

are typically used in space application due to their wattage density (Figure 8).

	Electromechanical Switching	DDC SSPC Module
Voltage	28 V	28 V
Current	80A	480 A
Loads	8	32
Dimensions	4.25" x 7" x 10.9"	11" x 7.8" x 3.1"
Volume	324 in^3	266 in^3
Weight	11.5 lbs	15 lbs
Power-to-Volume Density	6.9 W/in^3	**50.5 W/in^3**
Power-to-Weight Density	194.8 W/lb	**896 W/lb**

Figure 8: SSPC vs Relay: Power Density (Mike Glass, 2010)

Power Controller Module

Modern SSPC's are capable of handling the maximum loads outlined in section 2.3.1. A commercial example is the SPDC150D28 from Sensitron Semiconductor which provides 28V DC at up to 150 Amps, providing 4200 W of power regulation, well above our estimated maximum power. For lunar and martian mission durations:

$$R = e^{-\frac{t}{\text{MTBF}}} \tag{9}$$

$$R_{\text{sys}} = 1 - (1 - R)^N = 2.89 \text{ (lunar) or } 16.45 \text{ (martian)} \tag{10}$$

Mission	Mission Duration (Days)	Number of SSPC's
Lunar	28-60	3
Martian	Up to 1200	17

Table 9: Number of SSPC's Required for R = 0.9999

Table 9 assumes a system reliability (R_{sys}) of 0.9999 and a Mean Time Between Failure (MTBF) of 34kHrs (from above example).

It can be concluded that 3 SSPC's can make up the lunar rack SSPCM. For longer duration missions, like the Mars mission, back-up SSPC's should be brought as replacements.

Voltage conversion will be done via a DC-DC converter. This converter will be modular to account for the racks high power needs. A commercial example is the SGRB12028S DC-DC Converter from VPT Power, which provides 120V to 28V DC conversion at 360-400 Watts. A single DC-DC Module would then need to include around 10 DC-DC Converters providing 3600 - 4000 Watts of power conversion. The electrical system must also have a way to communicate with the rack avionics and monitoring systems, so a printed wiring board (PWB) must also be included. Thus, the Power Controller System (PCS) would consist minimally of:

The Power Controller System Enclosure will be constructed using Aluminum-6061. This provides a lightweight and sturdy frame, whilst also being space rated. The enclosure is made to fit in the maintenance area behind the payloads. This area is easily accessible via the side and back panels but outside of frequently accessed areas. The PCS will be mounted to a backplate via 4 NASA Spec Fasteners located on the backside of the PCS Enclosure. A NAS6204-XX fastener is

Part	Sub parts	Purpose
SSPCM	3 SSPC's	Power Regulation
DC-DC Module	10 DC-DC Converters	Power Conversion
PWB	N/A	Rack communication and monitoring

Table 10: Power Controller System (PCS) Breakdown

recommended due to its high resistance to shear stress.

Power System Wiring Considerations

The PCS will also have 2 input power connectors (1 main, 1 redundant) (Mil-Spec-38990), 6 output power connectors (Mil-Spec-38990), a data-interfacing cable (Micro-D), and a grounding wire to the chassis.

Wire Type	Predicted Length (m)	Adjusted Length 1.2x (m)
Power In	less than 0.2	less than 0.2
Payload 1	0.16	0.19
Payload 2	0.48	0.57
Payload 3	0.80	0.96
Payload 4	1.1	1.3
Payload 5	1.4	1.7
Payload 6	1.8	2.1
Data	2.5	3
Grounding	less than 0.2	less than 0.2

Table 11: Wire Lengths for Electrical Connections

The payload lengths assume the connection is to the middle of the payload (1/6 rack height) and start from the top of the rack. There will need to be 2 of each payload wire for both power and return connection. The Power in and Grounding wires would attach to the chassis power interface (at top of chassis), and thus are assumed to be short. The data wire will span the length of the chassis (shared bus), and have splitting wires (0.1 m) to connect to each payload. The adjusted length is 1.2x the predicted length in order to account for bends and strain in the wires.

Power System Mass Estimations

Wire Type	Total Length (m)	Mass (kg)
Power In (MIL-W-22759/11-12)	0.4	0.018
Payloads (MIL-W-22759/11-14)	13.7	0.45
Data (MIL-W-22759/32-24)	3	0.054
Grounding (MIL-W-22759/11-12)	0.2	0.009
Total	N/A	.53

Table 12: Wire Mass Estimations

The above estimation uses Mil-Spec wires that fit the estimated voltage and amperage requirements with wire densities estimated based on wire gauge.

A PCS Mass Model (Figure 9) was created in CAD in order to estimate it's mass. Its dimensions are: .25 m (W) x .15 m (H) x .1 m (D) and has a thickness of 5 mm. It contains representative SSPCs, DC-DC module, and PCB. The Mass Model estimated the total mass to be 2.14 kg.

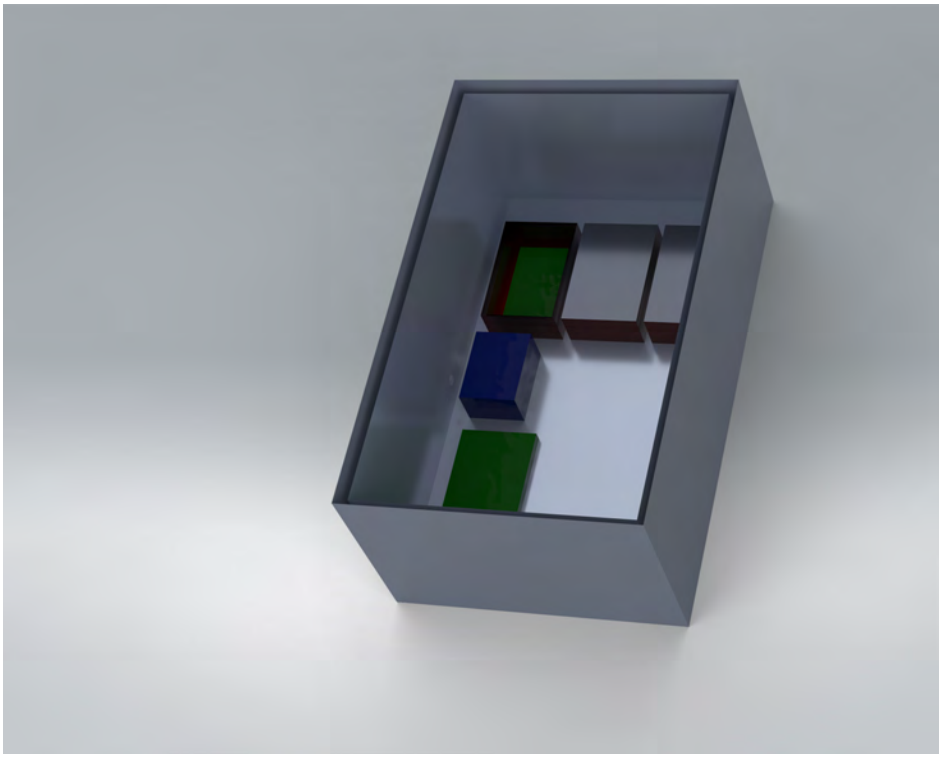

Figure 9: PCS Mass Model CAD

Safety Considerations

A safety concern found upon review of this design is the inclusion of high voltage (120V) wires and connectors. While it is anticipated these connections will be sparse, careful routing and insulation must be provided to ensure all high-voltage wires are either touch-safe or contained within the rack structure. The majority of the power in connection can be housed by the top rack cross member. For parts of the wire located in the maintenance area, the recommended power-in wires are ETFE insulated, but could be shrink-wrapped in insulating material or housed in a separate channel if needed. Furthermore, all electrical systems should be NASA-4000 compliant.

2.2.3 Air Cooling - Raymond Encarnacion

The air-cooling system is powered by the power controller module, and is cooled by the Moderate Temperature Loop (MTL). The primary purpose of this system is to sufficiently cool up to six payload positions at a time and keep them within their operating temperatures. The entire air cooling system will be housed inside a 250 x 400 x 200mm Aluminum-6061 box and will consist of 10 fans at the bottom of the box, and a water-to-air heat exchanger placed near the top of the model.

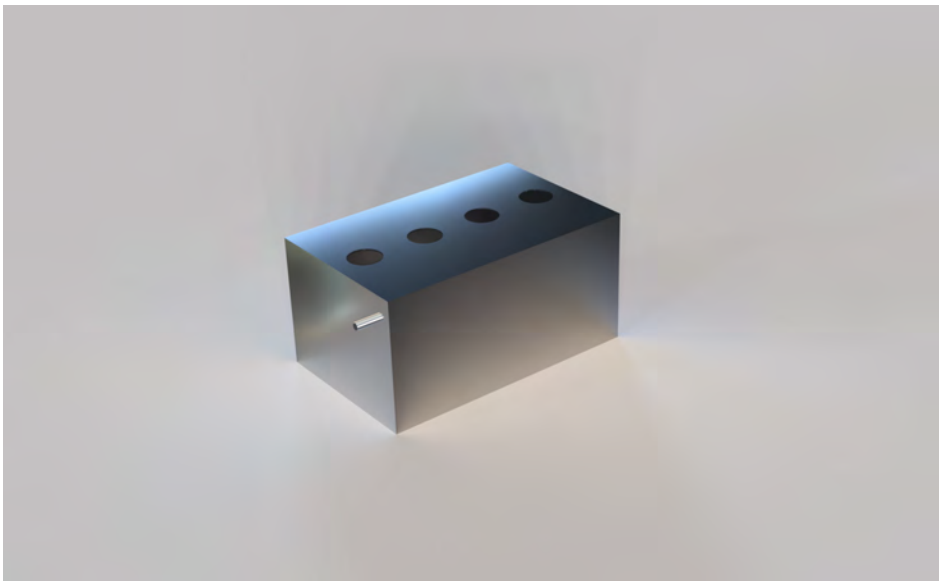

Figure 10: Air-Cooling System CAD Model

As shown above, this representative model provides payload cooling by allowing the MTL to enter the air-cooling system and pass through the heat exchanger, collecting heat from the water loop. At the same time, fans blowing at the bottom shall collect heat from the heat exchanger and blow cool air toward the payloads. While fans provide air-cooling, the MTL inside the air-cooling system shall exit both the water-to-air heat exchanger and the cooling system to pass through a separate radiator. This is done so that heat can be rejected until the water is cooled enough to return back to the MTL. The air-cooling system shall include an interface for the power controller module to power the fans and control their RPM, and an interface for the MTL to pass through. There shall also be air ducts connected to the outlets of the cooling system that lead directly to the payload positions that act as a supply air duct, along with a return duct back to the cooling system, so that the air can be recirculated and continue to provide cooling to the payloads. From Fusion, the total mass estimate of the air-cooling system was found to be 4.09 kg.

Air-Cooling System and MTL Thermal Capabilities

As described in 2.3.1, the power system provides electrical energy to different components of the avionics, including the air-cooling system. The cooling system is provided with a voltage and current of 28 Volts, 20 Amps respectively. Similar to 2.3.1, the air-cooling system's total electrical power can be calculated by:

$$P_{max} = V_{max} A_{max} \tag{11}$$

$$P_{max} = (28V)(20A) = 560W \tag{12}$$

At a maximum anticipated heat dissipation of 560 Watts, we require the MTL to be able to remove that amount of thermal load. The MTL provides water at a flow rate of 198 kg/hr, at a specific heat of c_p = 4182 J/kg-C. At an operating temperature of 17 C, and knowing that the return temperature of the MTL cannot exceed 49 C, we can calculate the amount of cooling the water

loops provide to the air-cooling system.

$$\dot{Q} = \dot{m} c_p \Delta T \tag{13}$$

$$\dot{m} = 198\,\text{kg/hr}(1\,\text{hr}/3600\,\text{sec}) = 0.055\,\text{kg/sec} \tag{14}$$

$$\dot{Q} = (0.55\,\text{kg/sec})(4182\,\text{J/kg-C})(49\,\text{C} - 17\,\text{C}) = 7360.32W \tag{15}$$

At 7360 Watts, the MTL provides more than enough cooling to the air-cooling model to keep it running at all times while accommodating for the lunar station requirements.

Air-Cooling System Design Analysis

Now that it is certain that the air-cooling system can operate constantly without causing thermal failure, the system's interior components can be designed for to ensure enough cooling reaches the payloads, assuming the rack will house 6 payloads at all times. At a normal cabin temperature of 18 C, the maximum temperature that payloads receive shall be constrained to not exceed 38 C under any circumstances, such that they all stay within their operating temperatures. Information about the fans inside the air-cooling system can be designed for and is obtained by solving for the max flow rate of the air-cooling system required to remove 560 Watts of heat, per payload. Rearranging the same heat transfer formula where the specific heat of air, $c_p = 1004$ J/kg-C, and the heat load per payload is 560 Watts, we get:

$$\dot{m} = \dot{Q}/(c_p \Delta T) \tag{16}$$

$$\dot{m} = (560\,\text{J/sec})\,/[\,(1004\,\text{J/kg-C})(38\,\text{C} - 18\,\text{C})\,] = 0.02788\,\text{kg/sec} \tag{17}$$

Fans typically describe the amount of airflow in units of volumetric flow rate, usually in ft^3/min, or cubic feet per minute (CFM). This can be quickly calculated from the mass flow rate, knowing that the density of air on Earth is 1.293 kg/m^3.

$$\dot{V} = \frac{\dot{m}}{\rho_{\text{air}}} = \frac{0.02788\,\text{kg/sec}}{1.293\,\text{kg/m}^3} = 0.021568\,\text{m}^3/\text{sec} \tag{18}$$

$$\dot{V} = \frac{0.021568\,\text{m}^3}{\text{sec}}\left(\frac{3.2808\,\text{ft}}{1\,\text{m}}\right)^3\left(\frac{60\,\text{sec}}{1\,\text{min}}\right) = 45.7\,\text{CFM per payload} \tag{19}$$

$$\dot{V}_{total} = \dot{V}(\text{num of payloads}) = 45.7\,\text{CFM}(6) = 274.2\,\text{CFM} \tag{20}$$

At the worst case scenario when all 6 payload positions are being cooled solely by the air-cooling system, the rack would require a total of 274.2 CFM to be able to sufficiently cool all payloads. This means we need a certain number of fans to provide this amount of constant cooling, given it can fit inside the air-cooling model. Since our model is 250L x 400W x 200H mm, space at the bottom is limited so the cooling system requires small fans with a high CFM rating. The team decided to use a conventional axial fan size of 80L x 25W x 80H mm, as it's a popular fan size and commonly produced. The fans inside the air-cooling system can only be placed at the bottom face and with its 80 x 80 mm side laying down, the system can conformably fit up to 15 fans if necessary. Many fans at this size produce different volumetric flow rates ranging from 30-40 CFM per fan. Using the worst case example, if we use a fan of 30 CFM, it would take 10 fans (274.2 CFM/30 CFM = 9.14) to cool all 6 payload positions with only the air-cooling system being used. This means we can fit enough fans inside the model without too much crowding. Another important consideration for

fan design, other than size constraints, is to make sure the fans all together produce a reasonable sound level during its operation. If one fan produces noise at a high decibel, and more fans get added, the total noise level could potentially be damaging to the people around the rack and cause hearing loss. At this size, the 80 x 25 x 80mm fans produce a noise level of 25 dB per fan, which is normal for a fan that size. The total noise level can then be calculated by:

$$L_{total} = 10log_{10}(10^{L_1/10} + 10^{L_2/10} + \ ... \ 10^{L_n/10}) \tag{21}$$

Where n is the number of fans and L_n is the noise level of the nth fan, in dB. Plugging in everything, the total noise level is determined to be:

$$L_{total} = 10log_{10}(10^{25/10} + 10^{25/10} + \ ... \ 10^{L_n/10}) \tag{22}$$

$$L_{total} = 10log_{10}(10[10^{25/10}]) = 35\,dB \tag{23}$$

With 10 fans, all running at 30 CFM and producing 25 dB of noise each, the total noise produced by the air-cooling system by the fans is 35 dB. This is a very reasonable sound level, as a range of 30-40 dB indicates noise level similar to leaves rustling, or the sound of a refrigerator humming. This total noise level ensures that the air-cooling system shall not produce noise that is potentially harmful to humans, even when supplying air cooling to all 6 payloads.

Air-Cooling Thermal Control System

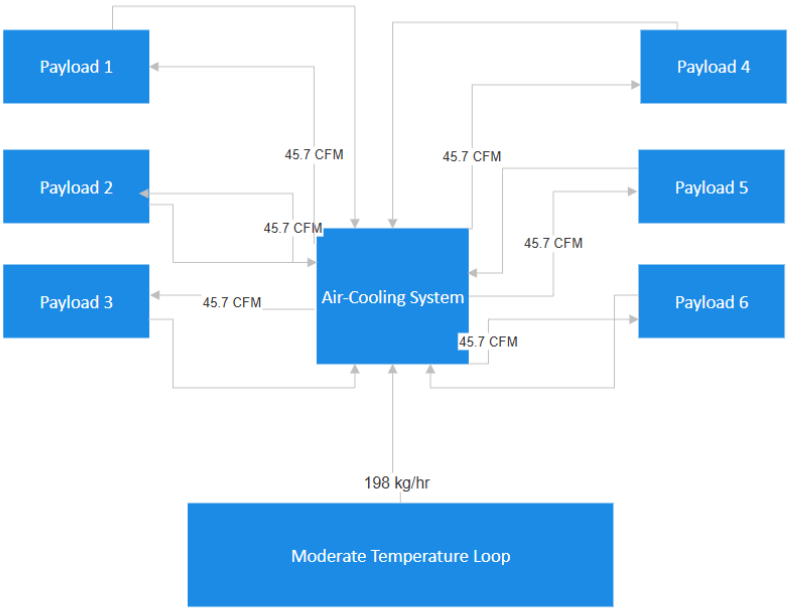

Figure 11: Air Thermal Control System Diagram

As described earlier in 2.3.3, the air-cooling system will interface with the MTL and is primarily responsible for cooling payloads, up to 6 at a time in case if cold plates aren't available for liquid

cooling. Figure 11 shows the thermal control system in the case where every payload is cooled by the air-cooling system. The cooling system is powered by the power controller and constantly receives 198 kg/hr of water from the MTL at 17 C to cool the system while the rack is powered on. The air-cooling system shall then be able to provide sufficient cooling to the payloads such that temperatures do not exceed 38 C, at a volumetric flow rate of 45.7 CFM per payload. To keep it a closed system, the exhaust air inside the payload positions shall then be redirected back into the air-cooling system via a return duct. This is done so that the air can be recirculated inside the air-cooling system and return back to the payloads for constant air-cooling.

2.2.4 Water Cooling - Luke Bieneman

The Water Cooling System (WCS) will interface with the Low Temperature Loop (LTL) of the station (4 C) and use Aluminum-6061 cold-plates to cool payloads. These cold-plates will be an additional option for payloads that have greater heat dissipation needs than the Air Cooling System can provide.

A general layout is outlined in Figure 12. Flow will be regulated by low power pumps and solenoids with corresponding flow and temperature sensors to regulate flow rate and temperature in each branch. Each payload will also be able to communicate with the main control system to demand more or less cooling.

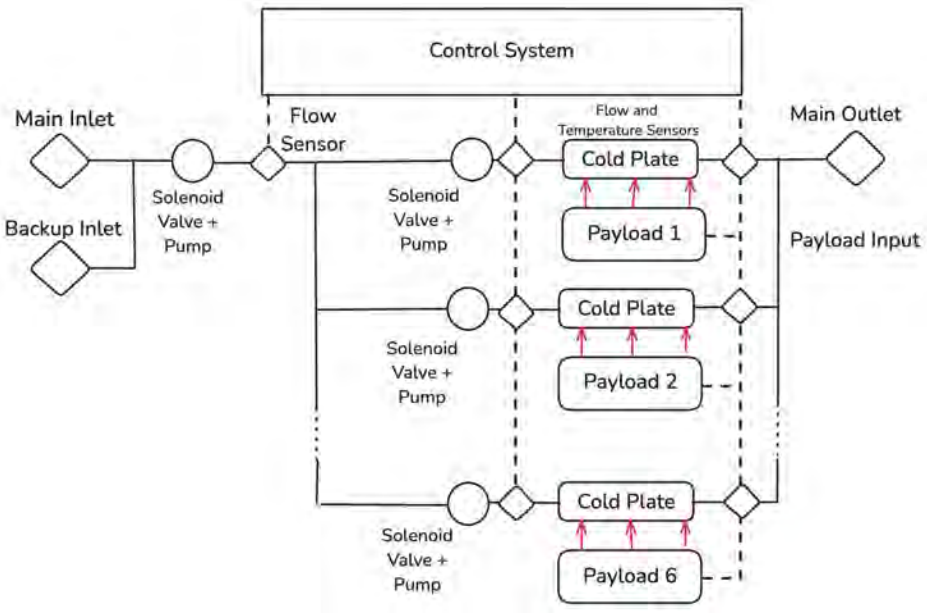

Figure 12: Water Control System (WCS) Schematic

WCS Temperature Considerations

According to the Power and Cooling Requirements, the maximum anticipated heat dissipation is 560 W. The LTL return temperature shall be below 21 C, giving a maximum ΔT of 17 C. The maximum mass flow rate of the LTL is 232 kg/hr.

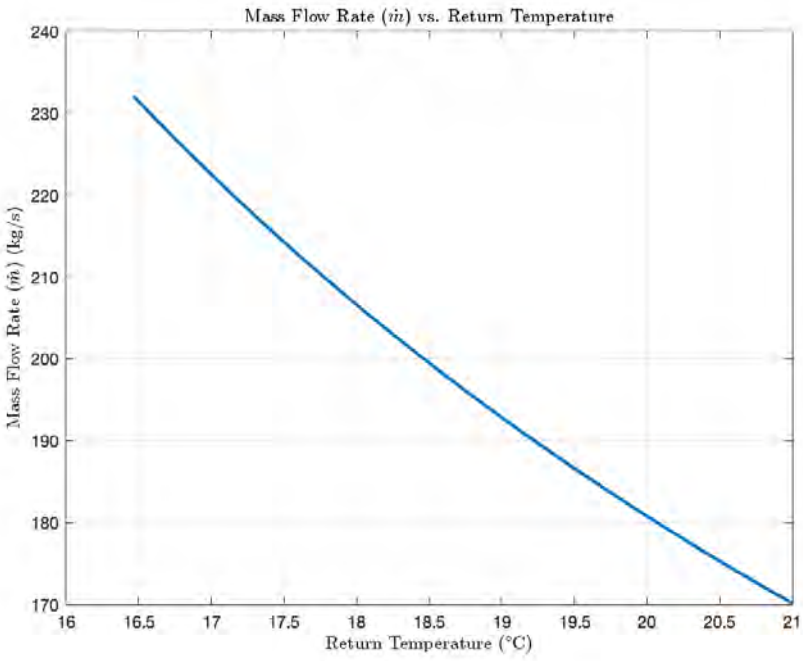

H

Figure 13: LTL Mass Flow Rate vs Return Temperature

Calculating the maximum heat the LTL can accommodate:

$$Q = \dot{m} c_p \Delta T = 4582 \text{ Watts} \tag{24}$$

where $c_p = 4182$ J/kg-C This is well above the system maximum of 3360 W and means the LTL could provide 764 W per payload position at its maximum return temperature.

An equation for mass flow rate as a function of return temp:

$$\dot{m} = 21600 \cdot Q_{\text{payload}} / (4182 \cdot (T_{\text{return}} - 4)) \tag{25}$$

For six 560 W payloads returning water at 19 C, the mass flow rate required is 193 kg/hr. This provides some leniency with regards to both mass flow rate and return temperature. A more detailed systems analysis could provide an optimal combination.

WCS Pressure Considerations

In order to determine the pump requirements an analysis of the system pressure was conducted. This analysis uses the 193 kg/hr flow rate described above. The tubing is Aluminum-6061 3/8" (9.58 mm) outer diameter tubing, with a wall thickness of .89 mm and inner diameter of 7.75 mm. The system will use Quick Disconnect connectors.

$$\dot{V} = \dot{m}/\rho = 5.36(10^{-5}) \text{ m}^3/\text{s} \tag{26}$$

$$A = \pi D^2/4 = 4.717(10^{-5}) \text{ m}^2 \tag{27}$$

$$v = \dot{V}/A = 1.136 \text{ m/s} \tag{28}$$

$$Re = \rho v D/\mu \approx 9892 \tag{29}$$

This Reynolds Number is fully turbulent. Using the Moody chart the friction factor is:

$$f \approx 0.031 \tag{30}$$

The pressure drop due to friction in a straight pipe (2.28 m, approximately the same length as payload wiring) is:

$$\Delta P_f = f \cdot (L/D) \cdot (\rho v^2/2) = 5885 \text{ Pa} \tag{31}$$

Local pressure drops can be calculated using the minor loss equation with K values listed in Table 13:

$$\Delta P_L = K \cdot \rho v^2/2 = 16131 \text{ Pa} \tag{32}$$

Local feature	K	# Per Payload
Tee (Split)	1	1
90° Turn	0.5	2
Quick Disconnect	1.5	2
Cold-plate	20	1
Total	25	N/A

Table 13: K Values For Minor Losses

This gives a total power drop per payload of:

$$\Delta P_{\text{total}} = \Delta P_f + \Delta P_L = 22016 \text{ Pa} = 3.19 \text{ psi} \tag{33}$$

6 low power pumps (about 3-4 psi) will be needed to moderate/maintain pressure throughout the WCS for each payload. A larger pump (about 5 psi) will also be needed at the inlet to drive flow from the LTL station loop.

WCS Cold-Plate Considerations

The cold-plate will have the dimensions 660.4 mm (W) x 508.6 mm (D) x 10 mm (t), the same footprint as a standard payload. These cold-plates are optional, for high power payloads, thus will take up payload area (10 mm). The cold-plate will be made of Aluminum-6061 with rectangular channels 5 mm (H) x 20 mm (W). The cold-plate will maintain a pressure drop of under 27579 Pa (4 psi) and be able to support over 560 W of heat dissipation. Appendix D contains:

- Material and Coolant Trade Studies
- Analytical and Computational Fluid Dynamics Analyses

To briefly summarize the studies:

- Material Trade Study: Aluminum-6061 provides the most heat transfer per kg of cold-plate mass outside of graphite, but without the structural limitations that come alongside it. Copper provides the most absolute heat transfer although it is the most dense material analyzed. Lastly, graphene composites or coatings promise great thermal conductivity, but the material science is relatively new and comes with similar structural issues to graphite.

- Coolant Trade Study: For conductive heat transfer within a cold plate water provides the most robust heat dissipation of the coolants analyzed.
- Analytical Cold-Plate Analysis: A cold-plate with dimensions 660.4 mm (W) x 508.6 mm (D) x 10 mm (t) and single serpentine channel would have its best pressure drop performance or thermal performance at the above channel dimensions and number of turns. A shorter path will minimize pressure drop, whereas a longer path will maximize heat transfer. Furthermore, a larger channel area will provide better performance provided the Reynolds Number is turbulent.
- Computational Fluid Dynamics (CFD) Analysis: for a 16 channel aluminum cold-plate with dimensions 660.4 mm (W) x 508.6 mm (D) x 10 mm (t) and 5 mm (H) x 20 mm (W) channels. The inlet temperature was 300K (27C) with a mass flow rate of 193 kg/hr. The resulting outlet temperature was 302K (29C) and outlet pressure 30247 Pa (4.39 psi), with a total heat transfer of 1159 W. The resulting heat distribution across the plate surface area was skewed cold near the inlet and warm near the outlet.
- The second take CFD analysis was performed with parameters more representative of the mission, a larger heat flux to determine a steady-state outlet temperature, and more revised model. The two key changes were an inlet temperature or 277 K (4 C) and a surface mass flux of 5000 W/m^2. The resulting pressure drop across the plate was 26729 Pa (3.88 psi), outlet temperature of 284.7 K (12 C), and total heat transfer of 3475 W. This second take CFD analysis demonstrates the thermal capabilities of an aluminum-water cold-plate with the geometry given are more than sufficient for 560 W payloads. This simulation demonstrates similar drawbacks to the previous: the serpentine channel layout in a cold-plate this large creates a large temperature and pressure gradient across the payload.

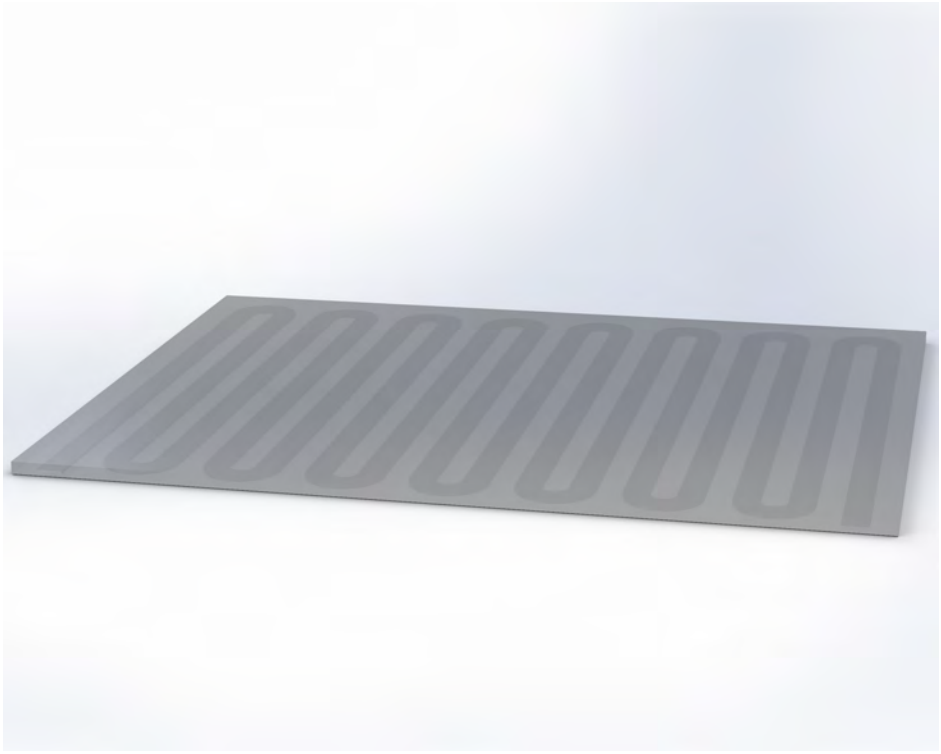

Figure 14: 16 Channel Cold-Plate Mass Model

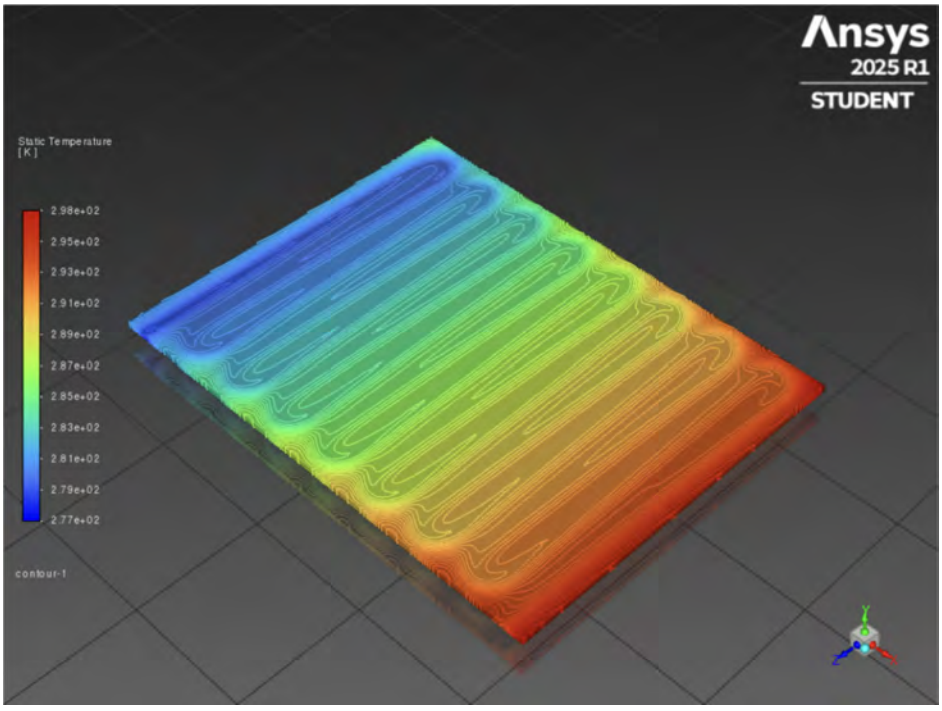

Figure 15: CFD Cold-Plate Surface Heat Map (Second Take)

Further Cold-Plate Study

The single serpentine channel provides a simple geometry that passes through the entire cold-plate. It does although have a large drawback in a plate as large as this. The channel length is very long. This creates two main issues, a large pressure gradient and a large temperature gradient. The next step in optimizing the cold-plate design is to change the channel layout. One possible variation is the addition of multiple shorter individual channels with turbulent features with the channels (ribs, fins, etc.) Although, this has the cost of needed more inlet/outlets and more external tubing.

WCS Mass Estimations

Feature	Mass (kg)	# Per Payload
Tubing (Aluminum 6061)	0.15	2.28 m, $6.6(10^5)$ m^3
Quick Disconnects	0.02	2
Cold-Plate	8.00	1
Total	8.19	N/A

Table 14: WCS Mass Estimations

The above analysis uses an Aluminum 6061-T6 cold-plate with dimensions 660.4 mm (W) x 508.6 mm (D) x 10 mm (t), and 16 5 mm (H) x 20 mm (W) channels. The tubing is also Aluminum 6061 with a 3/8" (9.525 mm) OD and .035" (0.889 mm) thickness. The density $\rho = 2700$ kg/m^3. For a fully fitted rack with cold-plates on each payload, the WCS would have a mass of $M_{\text{total}} \approx 49.1$ kg.

2.3 Payload Integration

2.3.1 Standardized Payload Sizing - Arul Ramachandran

On the express rack standard payload sizes were defined, with the payloads of larger sizes being considered double, triple, or quadruple payloads depending on how many payload sizes they took up. To maintain fluidity with EXPRESS Rack systems we have developed our own standard payload sized based on our internal dimensions and various payload numbers. The focus of our analysis was to maximize the number of payloads while still maintaining fluidity with existing payloads. Since our width and depth are set dimensions the height and number of payloads were our independent variables. To constrain our analysis, we developed target heights that would determine whether a payload number and size was a viable solution.

For payloads with data/power requirements it was determined that the payloads would already have to be redesigned to reflect technological improvements, therefore the target payload was set such that the volume would be greater than or equal than the available volume on an EXPRESS rack middeck locker.

For payloads without data/power requirements our assumption was that the lack of those systems would not necessitate a payload redesign so we set the target height to be the height of the middeck locker on the EXPRESS rack (273.2 mm) to ensure the payloads can just slot into our system. The following figures show the results of our payload number analysis (Figure 16) and the subsequent comparison to EXPRESS rack payloads (Figure 17). It should be noted that these

numbers were optimized for a single rack which better reflects the standard single payload size on the EXPRESS rack over the Double rack.

# of Payloads	No Data Payload Height (mm)	Data Payload Height (mm)
4	469.1	395.4
5	374.8	301.1
6	311.9	238.2
7	266.6	193.3
8	233.3	159.6

Figure 16: Number of Payloads and Respective Height

	Express Rack	No Data PL	Data PL
Height (mm)	253.24	311.9	238.2
Width (mm)	440.44	548.2	548.2
Depth (mm)	516.13	660.4	660.4
Volume (m^3)	0.06	0.11	0.09

Figure 17: Single Payload Sizes Compared to EXPRESS Rack

2.3.2 ECLSS System Integration - Avery Lowe & Tadhg Martinez

ECLSS- Mass Analysis - Avery Lowe

The design of our standardized payload rack was heavily influenced by the integration requirements of Environmental Control and Life Support Systems (ECLSS), which served as a primary reference for defining the rack's payload capabilities. As stipulated in Requirement **CS-1**, the rack must support ECLSS functionalities. Although our team was not directly tasked with enhancing ECLSS subsystems, conducting extensive trade studies and analyzing key parameters—such as mass, volume, power requirements, and interface connectivity—allowed us to develop a more versatile and robust rack design that effectively meets these requirements.

As outlined in the preceding section on payload integration, our rack features six shelving platforms, each following dimensional standards (seen in the previous subsection) to ensure modular compatibility. However, integrating ECLSS subsystems into our design presents a unique challenge due to their inherent lack of standardization. Unlike uniform payloads, ECLSS components often require customized configurations to fit within a rack structure, as evidenced by existing implementations such as the Collins Aerospace ECLSS pallets (Fig. 18). These systems exhibit custom layouts for their specific functions, underscoring the need for a flexible yet structured rack design.

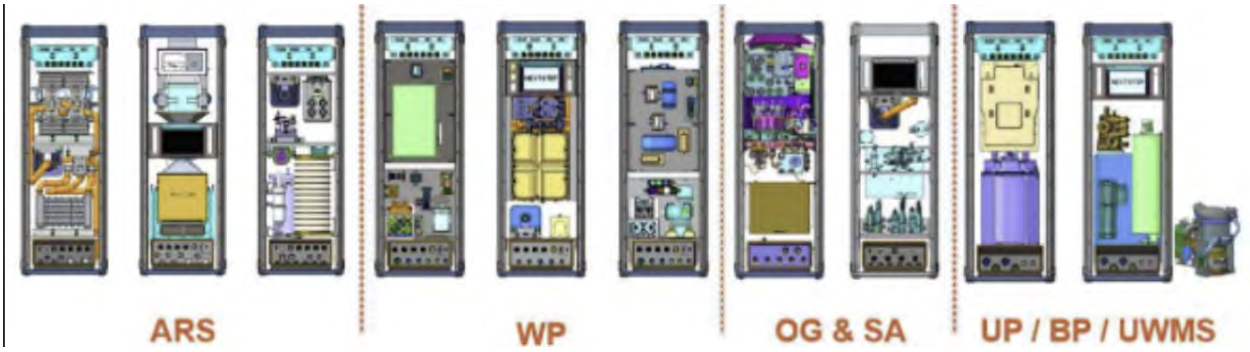

Figure 18: Different Collins ECLSS Pallets Layout (O'Neill et al., 2019) .

Despite these challenges, certain ECLSS subsystems align closely with our standardized dimensions, providing critical data for structural and load-bearing assessments. For instance, the Distillation Assembly (DA), a core component of the Water Recovery System (WRS), occupies an entire shelf platform and has a documented mass of approximately 75 kg. To account for potential discrepancies across data sources, this value was conservatively rounded to 80 kg in analyses conducted by the MPA and LSM sub-teams. Such tolerances were deemed necessary due to observed variations in reported mass values across technical literature.

Additional Integration Complexities - Avery Lowe

Beyond dimensional and mass considerations, several other factors complicate the integration of ECLSS subsystems into our rack design:

- Precise metrics for mass and volume are often unavailable, forcing reliance on International Standard Payload Rack (ISPR) benchmarks and comparable systems.
- ISPR systems are optimized for microgravity environments, whereas our lunar habitat rack must operate under partial gravity conditions. This discrepancy necessitates further research to validate the compatibility of existing ECLSS hardware with our design.
- Not all ECLSS subsystems are designed for rack integration. For example, temperature and humidity control systems (THC) in current habitats are typically embedded directly into the habitat's infrastructure rather than housed within dedicated racks.

Mass Estimation and Density-Based Analysis - Avery Lowe

Despite gaps in subsystem specifications, using the available data, combined with the defined payload volume constraints for both the single and double rack, allowed our team to develop a high-level mass estimation for a fully loaded rack. By plotting the mass against the density of known systems, we established a predictive framework to approximate the average mass of a fully loaded system.

This approach provided context on the mass of our equipped rack for the MPA mass testing further discussed in Section 3.3 and 3.4. From this study, we found that the average mass of a single rack to be 310kg and a double rack to be 630kg. This analysis can be seen in Fig. 19, and the values from the table were taken from (NASA, n.d.), and (Wieland, 1998).

Tabulated ECLSS components weight vs mass			
Payload	mass (kg)	volume (m^3)	density (kg/m^3)
DA	75.5	0.15	500.1
PCPA	44.77	0.07	612.3
FCPA	45.58	0.07	628.3
TCCS	77.2	0.25	308.8
TCCS Charcoal Bed	11.7	0.046	254.3
Activated Charcoal Bed	32.2	0.12	268.3
Blower Assembly	3	0.003375	888.9
CCAA fan assembly	12.7	0.04	317.5
Condensing heat exchanger	20.6	0.04	515.0
TCCV	6.3	0.027	233.3
Water Separator	11.95	0.054	221.3
MCA	54	0.081	666.7
		Mean Density:	451.2
	Double rack (1.39m^3)		627.2
	Single rack (0.68m^3)		306.8

Figure 19: Mass vs volume of ECLSS components .

Additional Integration Complexities - Avery Lowe

Beyond dimensional and mass considerations, several other factors complicate the integration of ECLSS subsystems into our rack design:

- Precise metrics for mass and volume are often unavailable, forcing reliance on ISPR benchmarks and comparable systems.
- ISPR systems are optimized for microgravity environments, whereas our lunar habitat rack must operate under partial gravity conditions. This discrepancy necessitates further research to validate the compatibility of existing ECLSS hardware with our design.
- Not all ECLSS subsystems are designed for rack integration. For example, temperature and humidity control systems (THC) in current habitats are typically embedded directly into the habitat's infrastructure rather than housed within dedicated racks.

CAD Integration of ECLSS Subsystems - Tadhg Martinez

In our later design stages, the Crew Systems sub-team identified an opportunity to visually and spatially simulate the integration of Environmental Control and Life Support System (ECLSS) components within the payload rack. The objective was to develop an assembly model showcasing a fully populated rack layout using realistic geometry of representative systems. This visual

integration would enable early assessments of fit, interference, crew access, and subsystem loading compatibility.

Initial CAD modeling efforts focused on three major ECLSS components:

- **A Desiccant/CO_2 Absorbent Bed**, which removes moisture to protect downstream systems and prevents CO_2 absorbent degradation while also absorbing carbon dioxide for crew safety and atmospheric control.
- **A Trace Contaminant Control System (TCCS)**, responsible for removing low-level airborne contaminants such as ammonia, formaldehyde, and ethanol vapor.
- **A Urine Processor Assembly (UPA)** component, specifically the Distillation Assembly (DA) subassembly, which performs water recovery from urine via rotary vacuum distillation.

To support this spatial visualization effort, component dimensions were derived from NASA technical documents and CAD estimates:

- TCCS: 75.55 cm (height) × 79.3 cm (depth) × 52 cm (width) (Wieland, 1998)
- CO_2/Desiccant Beds: 129.64 cm (height) × 25.4 cm (depth) × 27.94 cm (width) (Wieland, 1998)
- UPA (DA subassembly): 46.02 cm (height) × 83.82 cm (depth) × 47.75 cm (width) (NASA, n.d.)

These dimensions informed model scaling and enabled us to estimate realistic spatial volumes and mounting options within the payload rack. A completed CAD assembly integrating all three elements was developed (See Below) to assess internal clearance, stowage feasibility, and visual alignment with crew-interaction safety standards.

However, this modeling effort was constrained by the limited public availability of verified engineering drawings, images, and connector standards for these hardware systems. Consequently, while the models are geometrically and proportionally accurate, they are approximations meant to demonstrate feasibility, not final integration.

The finalized assembly highlights spatial compatibility within our rack's internal volume and serves as a conceptual framework for how future subsystems might be laid out. It supports discussions on mounting schemes and servicing access. Looking forward, we intend to expand this integration effort as additional subsystem details or hardware specifications become available. In the interim, this assembly provided a functional visual aid for ongoing design reviews and cross-team coordination.

DA Front Right

DA Front Left

Distillation Assembly (DA) - Tadhg Martinez

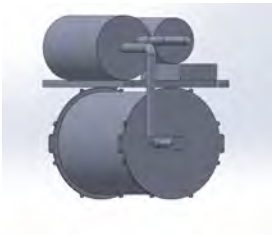

TCCS Front Left

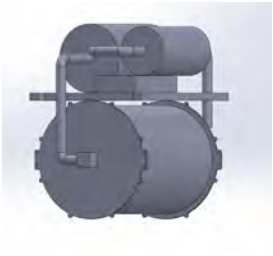

TCCS Front Right

Trace Contaminant Control System (TCCS) - Avery Lowe

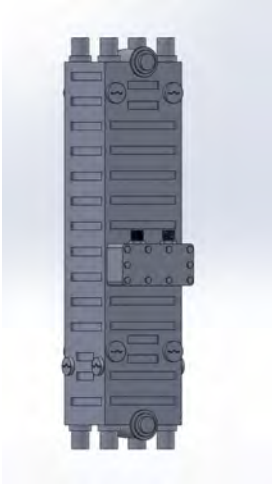

Beds Front Left

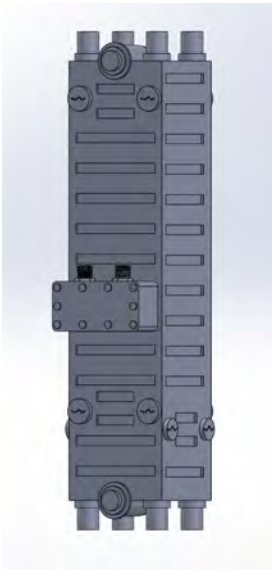

Beds Front Right

CO_2/Desiccant Beds - Tadhg Martinez

Figure 20: CAD Models of Subsystems Used in Rack Integration. Each group shows paired front views of the Distillation Assembly (DA), Trace Contaminant Control System (TCCS), and CO_2/Desiccant Beds.

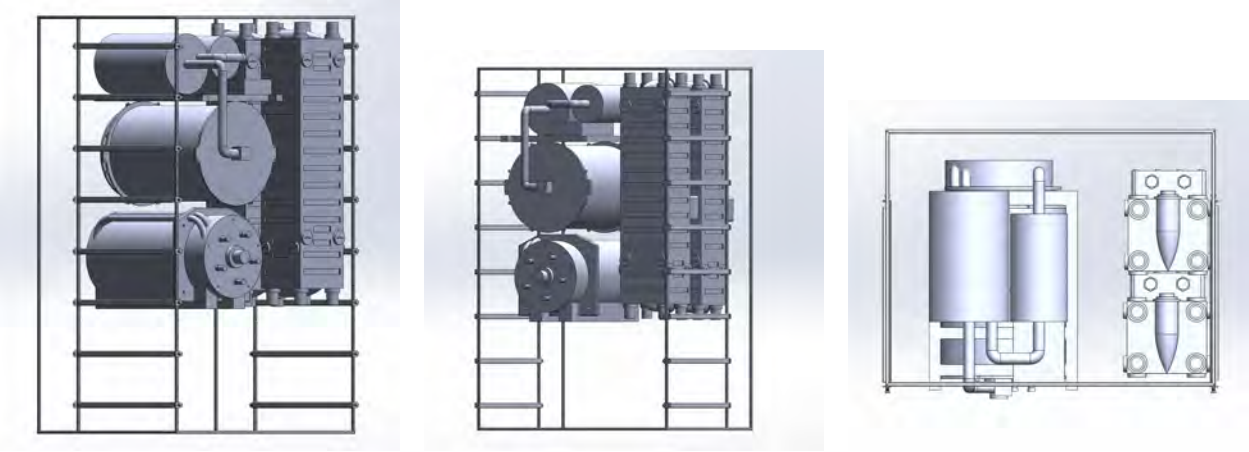

(a) Front Left View (b) Front Right View (c) Top View

Figure 21: Final CAD Assembly of ECLSS Rack Integration. Images show left, right, and top views of the rack populated with the DA, CO_2/Desiccant Beds, and TCCS.

—

2.4 Human Factors and Crew Integration

2.4.1 Crew Interaction Focus Areas - Tadhg Martinez

At the start of the project, the Crew Systems sub-team initiated its work by defining the core human-system interaction domains relevant to the design of the payload rack for the habitation of the lunar surface. Recognizing that the success of science operations and payload utilization is inherently dependent on the crew's ability to interface effectively and safely with rack systems, the team established a structured approach to assess these interactions through six overarching focus areas:

- **Life Support** – How many crew members are being supported?
- **Interface** – How is the crew expected to interact with the rack?
- **Weight** – Can the rack be handled or repositioned by crew members?
- **Safety** – Are there physical or environmental hazards posed by the rack?
- **Acoustics** – Is the operational noise generated by the rack within tolerable limits?
- **Space** – Is there sufficient clearance for crew maneuverability and task execution?

These focus areas formed the basis for a deeper investigation aimed at identifying functional design requirements and evaluation criteria for the payload rack. Each area was broken down further into specific considerations to be analyzed over the course of the semester, with the following being the earliest considerations from our team:

Life Support

The rack must be capable of supporting a to-be-determined number of astronauts within the habitat environment.

Interface

A successful interface between the crew and the rack hinges on usability and serviceability. Key topics explored include accessibility, repair-ability, modularity, and the integration of handles and labeling systems. Considerations were also made for power and data connectivity, ensuring payloads can be readily interfaced and maintained.

Weight

The feasibility of crew movement and reconfiguration of the rack is dependent on its structural design and material selection. The team wanted to focus toward a design that would allow the rack to be transported, repositioned, or serviced by astronauts in partial gravity without overburdening crew workload.

Safety

Crew safety was established as a priority. The rack must be designed to minimize injury risk with early consideration beginning with thermal management, fire protection, and the integration of secure locking and latching mechanisms compatible with gloved operations.

Acoustics

Recognizing that long-duration missions demand high standards of habitability, the team established a preliminary requirement that the rack not exceed 60 dB over a 24-hour period, referencing acoustic tolerances from ISS documentation.

Space

To ensure efficient operations, the rack must not encroach upon required crew clearance zones. Preliminary spatial constraints were outlined, including volume envelopes and aisle widths, with the rack expected to provide sufficient clearance to allow crew members to perform installation, removal, and maintenance tasks comfortably and safely.

2.4.2 Safety Requirements Assessment and Application - Tadhg Martinez

To ensure that the design of the payload rack aligns with NASA's stringent human safety and interface standards for space habitation, the Crew Systems sub-team conducted an early and thorough review of two key guiding documents: *NASA-STD-3001* ("NASA Space Flight Human-System Standard, Volume 2: Human Factors, Habitability, and Environmental Health") and the 'International Space Station (ISS) Program Pressurized Payload Interface Requirements Document' (SSP 57000). Requirements that are not directly applicable to the payload rack, such as pressure vessel design or toxic material handling, were marked as non-relevant to this hardware and excluded from detailed implementation. These documents are considered essential for evaluating the safety of crew interaction, compliance with hardware design, and general habitability during long-duration missions.

Our objective was to identify the requirements relevant to the design and integration of the rack system, with an emphasis on mechanical safety, fire protection, access to the crew and interaction. This process informed a design baseline that balances functionality with stringent safety margins.

Documentation Review Method

The sub-team systematically parsed sections of both standards, flagging applicable 'shall' statements related to:

- Structural load capacity
- Sharp edge and corner radii
- Fire and thermal safety
- Crew-induced loading conditions
- Ventilation compatibility
- Fastener retention
- Access to fire extinguishers and smoke indicators
- Protrusion clearance within crew translation paths

Where possible, thresholds and constraints were extracted directly and either embedded in CAD design decisions or tagged as verification criteria for future testing and review.

Key Requirements Incorporated into the Rack Design

Crew-Induced Load Tolerance
Per SSP 57000 Section 3.1.1.1.2, the rack must safely withstand loads up to 556.4 N (125 lbf) applied across a 4 in $\times$ 4 in area on any exposed panel and 222.6 N (50 lbf) concentrated on handles or corners in any direction.

Corner Radius Compliance
Following NASA-STD-3001 Volume 2, Section 6.3.3.1, all exposed corners and edges were filleted to a minimum of 3.2 mm (0.125 in) to reduce injury risk during accidental contact or translation in microgravity environments.

Fastener Retention
Threaded fasteners in safety-critical connections will be required to incorporate locking mechanisms such as safety wire, safety cable, or thread-locking adhesives, per SSP 57000 Section 3.1.1.5, to prevent loosening during dynamic loading or vibration.

Fire Protection Access
Design must ensure unobstructed access to Portable Fire Extinguisher (PFE) ports and visibility of fire indicators, per SSP 57000 Appendix N.3.10.2.1 and N.3.10.2.2. Protrusions and cables are to be minimized in high-traffic areas to avoid interfering with emergency egress or extinguisher discharge paths.

Translation and Egress Path Clearance
Clearance zones around the rack must meet the 32 in $\times$ 45 in egress path and 50 in $\times$ 72 in crew translation path specifications defined in SSP 57000 Section 3.1.1.1, ensuring safe access even during emergency operations.

Thermal Surface Limits
The rack surface and all components must maintain surface temperatures that do not exceed safe touch thresholds (45°C) in occupied zones, per NASA-STD-3001 Volume 2, Section 6.5.3.

Wire and Connector Covering

All exposed wires, fluid fittings, and airflow ducts shall be covered, strain-relieved, and routed to avoid direct contact with astronauts or sensitive hardware. Per SSP 57000 Sections 4.3.2.2.5.3 and 4.3.2.2.5.4, wiring must be terminated with shielded backshells, shield exposure limited to 2 inches, and all bundles securely enclosed.

Cable Routing and Bend Radius Compliance

All data, power, and fluid lines shall be routed in accordance with minimum bend radius requirements defined in SSP 57000 Table 3.1.4.2-1. For example, Ethernet lines maintain a 2.4-inch radius, while power cables are limited to 0.75 inches. These constraints minimize connector strain and preserve long-term cable integrity during repeated handling and maintenance cycles.

Dual Power Isolation

If multiple independent power inputs are used, a minimum of 1 MΩ of isolation with $<$0.03 μF mutual capacitance must be maintained to prevent a single failure from electrically bridging the two, per SSP 57000 Section 3.2.1.1.

Electrical Grounding and Bonding

All rack-integrated electrical systems shall comply with SSP 57000 Section 3.2.2.8. Specifically, Class H bonding will be implemented to ensure personal safety from shock hazards. Exposed conductive surfaces or enclosures must be bonded to a structure with DC resistance of 0.1 ohms or less. Bonding jumpers or straps are acceptable if they meet the resistance criteria. Ground continuity will be verified via inspection and resistance measurements during integration.

Acoustic Emissions and Noise Limits

To maintain habitability and prevent crew fatigue or communication interference, the rack must comply with acoustic thresholds defined in SSP 57000 Section F.3.12.1 and Appendix G, Table G.3.12.1-1. All powered components (e.g., fans, pumps, electronics) shall be evaluated to ensure that their combined acoustic output does not exceed 60 dBA Leq over a 24-hour period, with an absolute peak limit of 85 dBA. Acoustic measurements shall be taken at crew ear level, and mitigation strategies, such as vibration isolation mounts, baffling, or acoustic insulation, will be considered if equipment exceeds target levels.

Labeling Standards

Where interface identification is required (e.g., power, data, fluid lines), labels follow SSP 57000 Appendix O conventions for visibility, gloved operation, and hazard mitigation. High-contrast fonts and durable adhesives were selected to withstand long-duration exposure and ensure clear labeling of rack utilities, interfaces, and safety-critical points.

3 Trade Studies and Testing

3.1 Material and Rail Trade Study

3.1.1 Material Trade Study – Andrew Dolecki

For the materials trade study, we sought to find a material with high tensile strength but low density. Composite materials offer the highest tensile strength for very low density, but they experience significant strength degradation when machined. Therefore, due to machine-ability constraints, we ruled out the use of composites.

After ruling out composites, we focused on alloys—particularly aluminum alloys—and found that they offer a favorable tensile strength-to-density ratio. Among them, Aluminum 7075-T6 stood out as having the highest tensile strength-to-density ratio of the aluminum alloys considered. One downside of Aluminum 7075-T6 is that it is not weldable, so we plan to assemble the rack using fasteners instead.

Although we plan to manufacture our own rails, the material data shown in Figure 22 provides a useful reference for material selection.

Materials	Ultimate Yield Strength (MPa)	Tensile Strength (MPa)	Density (Mg/m^3)	Elastic Modulus (GPa)	Shear Modulus (GPa)
Aluminum 6061 T-6	260	240	2.71	72	27
Aluminum 2024 T-4	448	296	2.77	72	27
Aluminum 7075 T-6	593	538	2.77	72	27
Steel 440C A	807	462	7.92	190	73
Titanium Annealed	1070	930	4.63	114	43

Figure 22: Material Properties for Trade Study Comparison

3.1.2 Rail Trade Study – Andrew Dolecki

For the rail selection, we first considered whether we wanted to use static rails or telescoping rails. We decided to use telescoping rails so that astronauts would have access to payloads [**LSM-6**]. There are two types of telescoping rails: those with a drawer release, and those without. The drawer release allows the payload to be removed from the shelf directly on the rail, but this comes at the cost of significantly reduced load capacity. On McMaster, the 24” stainless steel rails with a button release can hold a payload of 105 lbs. In comparison, the 24” stainless steel rails without a drawer release can hold 475 lbs. Due to this difference in strength, our team decided to use rails without a drawer release. If the payload needs to be removed from the rack, it can be lifted off the platform it rests on using a separate mechanism. This approach allows the rack to retain its strength without sacrificing functionality.

Although we plan to manufacture our own rails, which will have different strength characteristics, these specifications from McMaster serve as a useful reference during the design and manufacturing process.

3.2 Structural Analysis and Optimization

3.2.1 Optimization of Member Cross-Section Geometry – Grace Johnson

Vertical Members

Multiple iterations of optimization for the vertical members of the rack frame were conducted in order to conserve material mass, and therefore cost, while ensuring the structure would be able to withstand axial buckling loads. See Appendix B for information on the first approach to this optimization. Material properties of Al7075-T6 were taken from *Mechanics II: Mechanics of Materials* by James Dally, Robert Bonenberger, and William Fourney. A square cross-section was assumed with constant wall thickness for symmetry and ease of manufacturing. However, a yield safety factor of 1.25 and ultimate safety factor of 1.4 were used according to NASA proto flight specifications (NASA Johnson Space Center, 2014). Critical stress due to Euler buckling was calculated using equation (34) for various combinations of outer length and wall thickness dimensions.

$$\sigma_{cr} = \frac{\pi^2 EI}{AL^2} \tag{34}$$

In this equation, E is the Young's modulus, I and A are the area moment of inertia and cross-sectional area, respectively, for each combination of dimensions, and L is the effective length of the member. For this analysis, fixed-fixed end conditions were used for the buckling column. Matlab code for this process can be found in Appendix C. Additionally, predicted stress of each member during 6g axial launch loading was calculated. This value was found using an assumed maximum mass at launch of 375 kg [MPA-5] and an assumed even distribution of load across all four vertical members. Chosen geometry exhibited a predicted critical stress due to buckling closest to but still greater than the predicted stress experienced under 6g axial launch loading. These stress values were then confirmed to be well under the material constraints for yield and ultimate strength. Using this approach, the cross sections of vertical members in the rack frame had an outer length of 11.8 mm and wall thickness of 3.50 mm. This would lead to a yield margin of safety of 12.9 and ultimate margin of safety of 16.1. Additionally, outer corners of all members are filleted with a radius of 3.00 mm in accordance with NASA STD 3001.

Horizontal Members

Optimization of the cross-sectional geometry of the horizontal members of the rack was conducted to conserve material mass, and therefore cost, while ensuring the structure would be able to withstand maximum payload mass under 6g launch loading conditions. Material properties of Al7075-T6 were taken from *Mechanics II: Mechanics of Materials* by James Dally, Robert Bonenberger, and William Fourney. A square cross-section was assumed with constant wall thickness for symmetry and ease of manufacturing. Additionally, a yield safety factor of 1.25 and ultimate safety factor of 1.4 were used according to NASA proto flight specifications (NASA Johnson Space Center, 2014). According to [LSM-8], the maximum payload mass that these horizontal members would need to support is 80 kg, with this loading assumed evenly distributed between two members. Therefore, each horizontal member was modeled as a uniform beam under an evenly-distributed 40 kg at 6g launch loading. Critical stress due to beam loading was calculated using equation (35) for

various combinations of outer length and wall thickness dimensions.

$$\sigma_{max} = \frac{Mc}{I} \tag{35}$$

In this equation, M is the maximum internal bending moment, c is half of the outer length, and I is the area moment of inertia. Matlab code for this process can be found in Appendix C. Chosen geometry exhibited a predicted critical stress due to beam bending under 6g launch loading closest to but still less than the limiting material constraints for yield and ultimate strength. Using this process, the cross sections of horizontal members in the rack frame had an outer length of 28.6 mm and wall thickness of 4.30 mm. This would lead to a yield margin of safety of 0.589 and ultimate margin of safety of 0.961. Additionally, outer corners of all members are filleted with a radius of 3.00 mm in accordance with NASA STD 3001.

3.2.2 Finite Element Analysis and Load Cases – Muhammad Chaudhry

Load Case A

Load Case A simulates the case where the rack is bolted to the floor of the launch vehicle and attached to an adjacent interior wall. The fixed faces are shown in Figure 23. According to the Falcon 9 user manual pictured in Figure 24 (SpaceX, 2021), payloads may experience launch loads up to 6g in the axial direction and 0.5g in the lateral direction. In this model, 0.5g is applied to the front face, one side of the rack, and one side of the horizontal members as seen in Figure 23. Per fine element analysis through SolidWorks, the maximum stress is 268.1 MPa seen in Figure 25, as well as a close up view in Figure 26. As well as a maximum displacement of 22.2 mm, seen in Figure 27. Additionally to help visualize where the deformation is occurring Figures 28 and 29 both exaggerate the stress and displacement plots and are scaled by 8.6x.

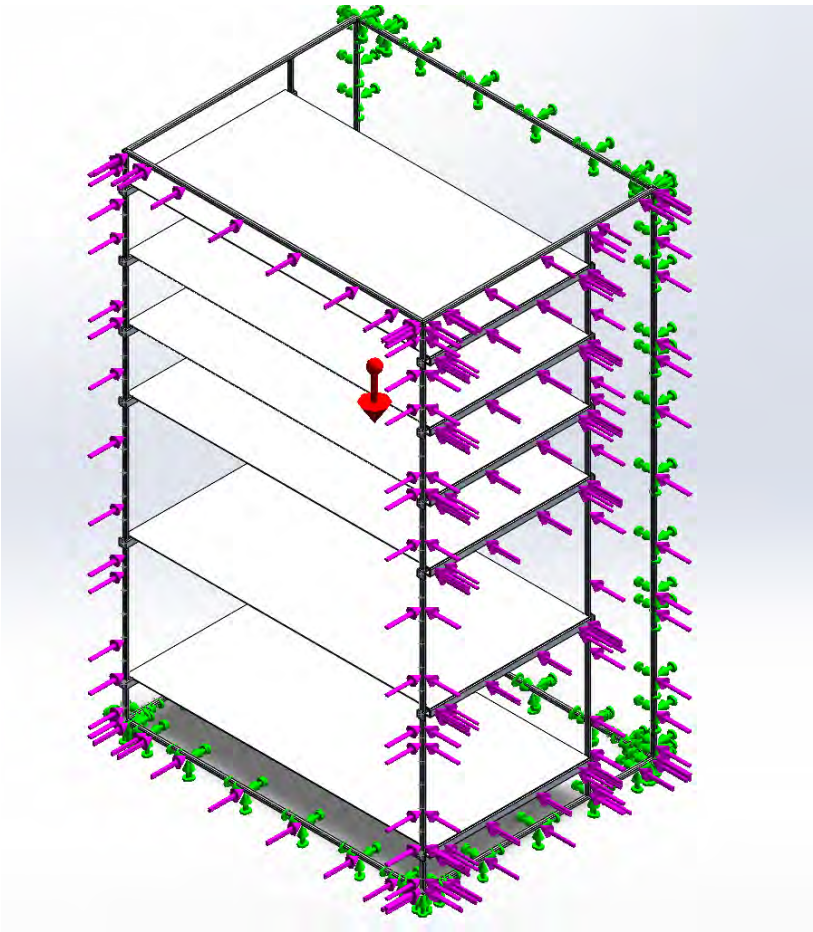

Figure 23: Load Case A Model

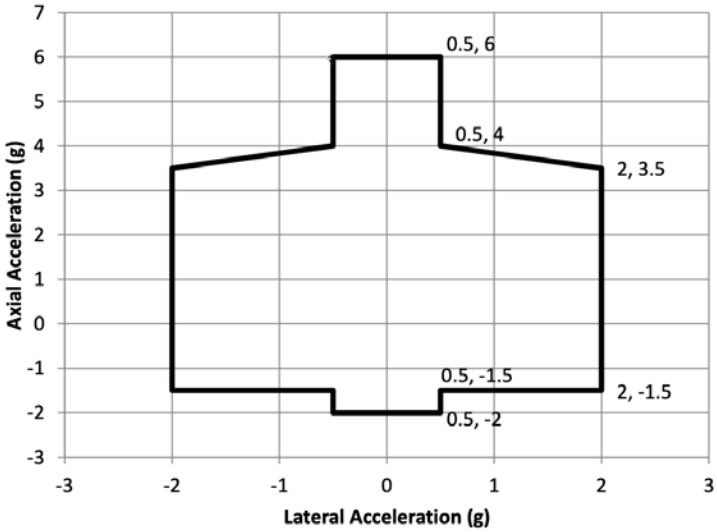

Figure 24: Falcon 9 User Manual - Axial and Lateral Loads at Launch

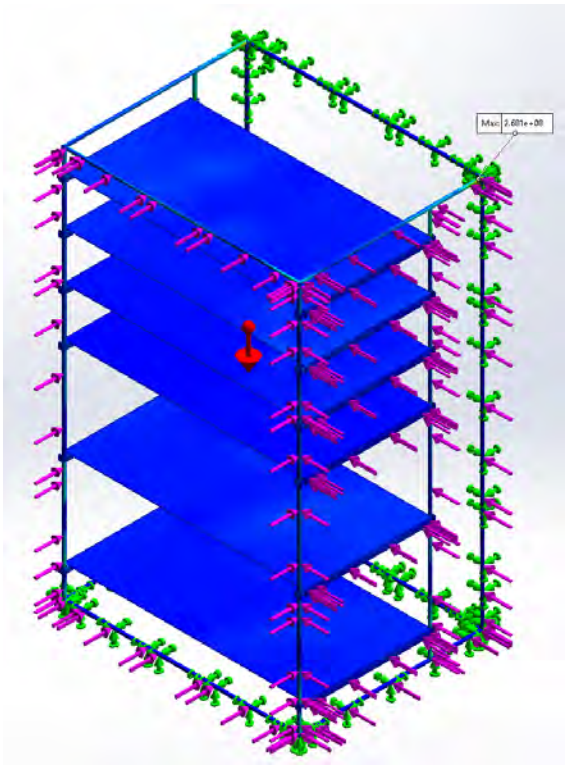

Figure 25: Stress Plot of Load Case A

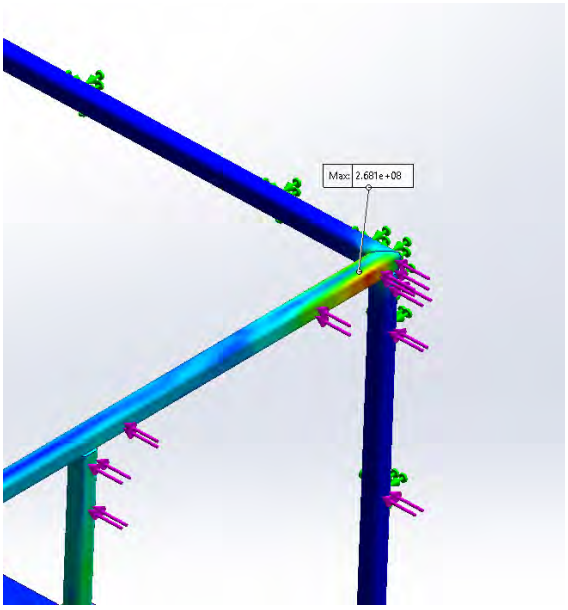

Figure 26: Zoomed View of Maximum Stress Region

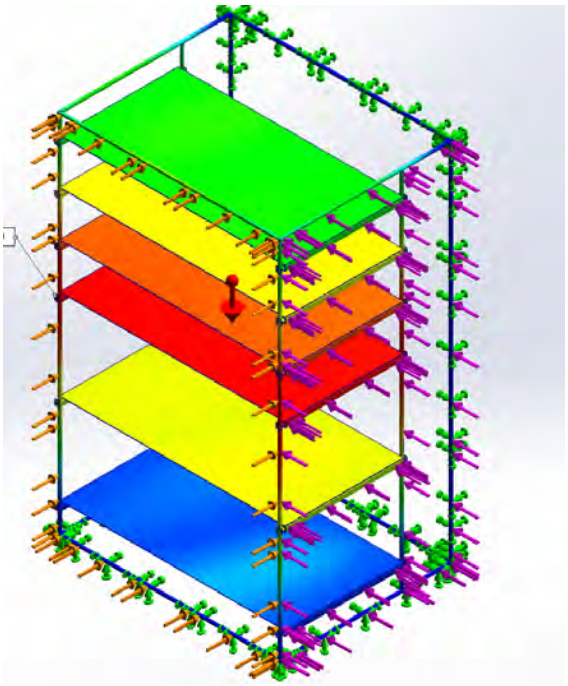

Figure 27: Deformation Plot of Load Case A

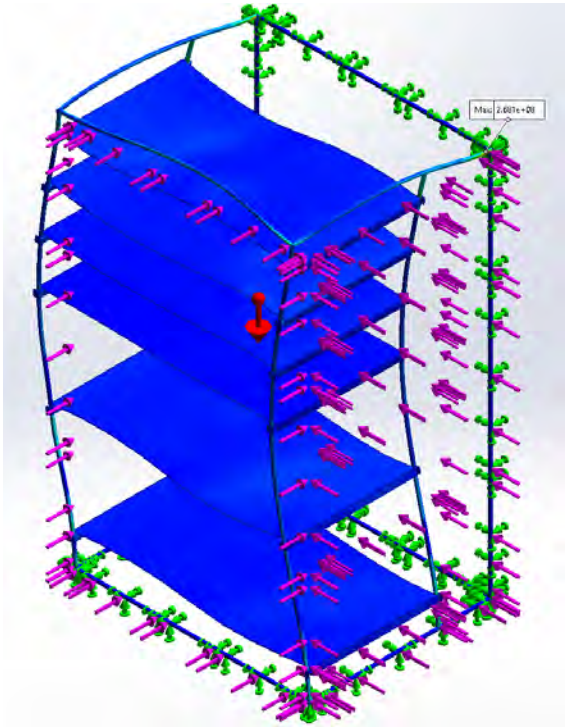

Figure 28: Exaggerated Stress Plot

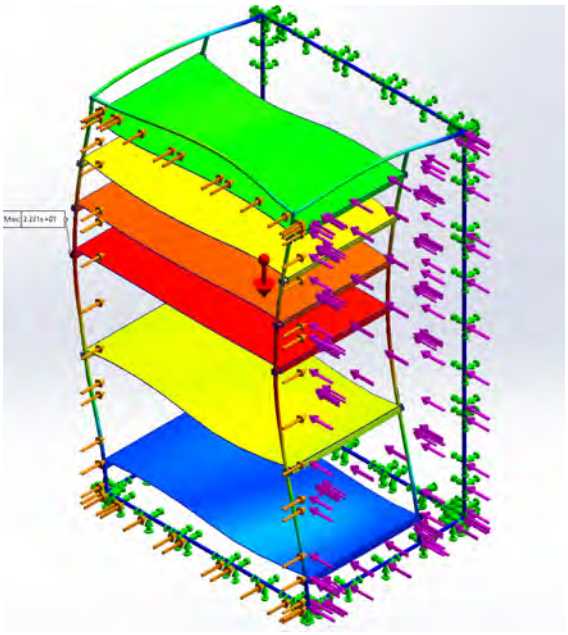

Figure 29: Exaggerated Deformation Plot

Load Case B

Load Case B uses the same fixed constraints as Load Case A. The applied loading also consists of the same 6g axial and 0.5g lateral; however, the lateral load in this case is distributed across all three side faces of the rack, shown in Figure 30. This allows us to study a more uniformly distributed lateral loading condition. The results show a maximum stress of 108.2 MPa as seen in Figure 31 and Figure 32. As well as a maximum displacement of 10.4 mm seen in Figure 33. Additionally to help visualize where the deformation is occurring Figures 34 and 35 both exaggerate the stress and displacement plots and are scaled by 19.4x.

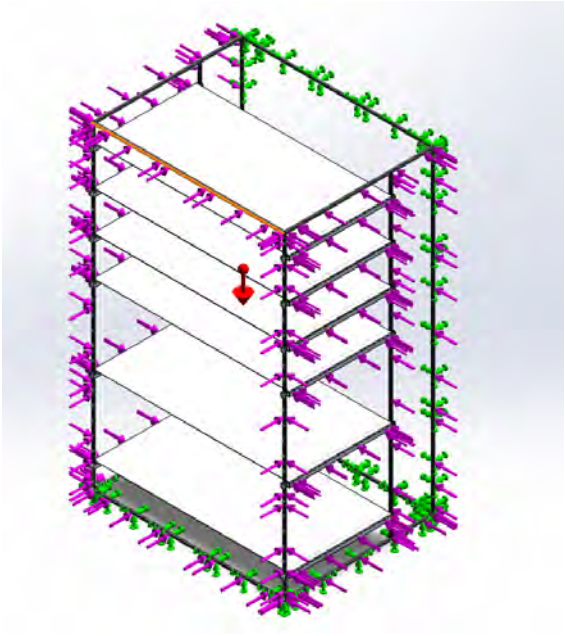

Figure 30: Load Case B Model

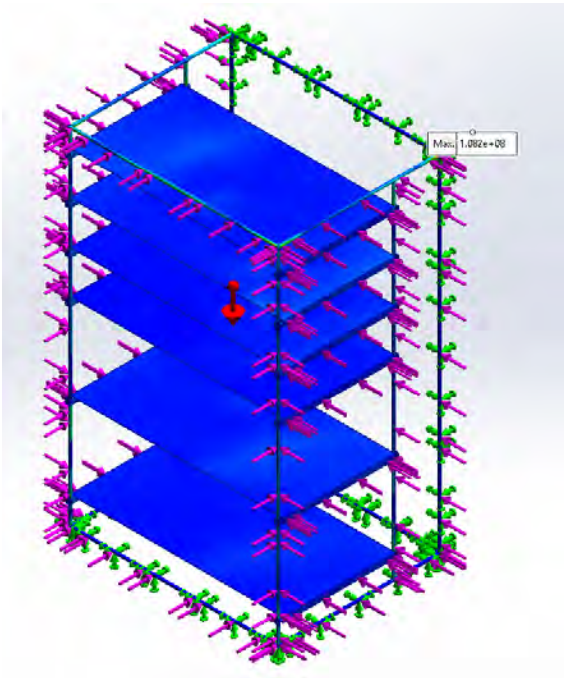

Figure 31: Stress Plot of Load Case B

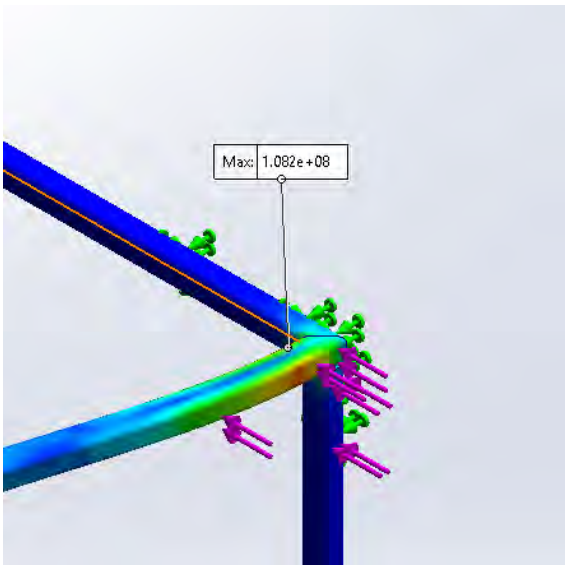

Figure 32: Zoomed View of Maximum Stress Region

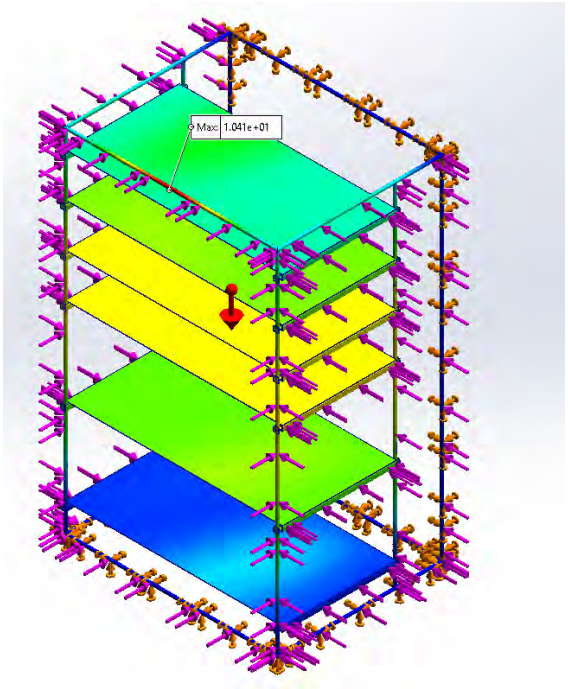

Figure 33: Deformation Plot of Load Case B

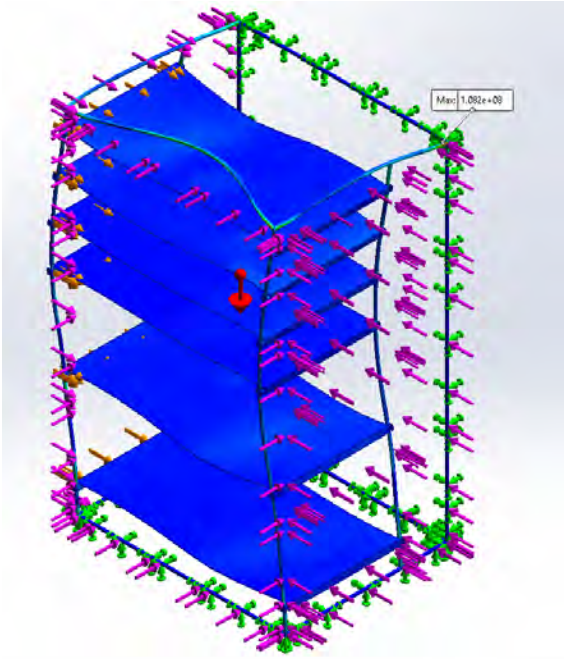

Figure 34: Exaggerated Stress Plot

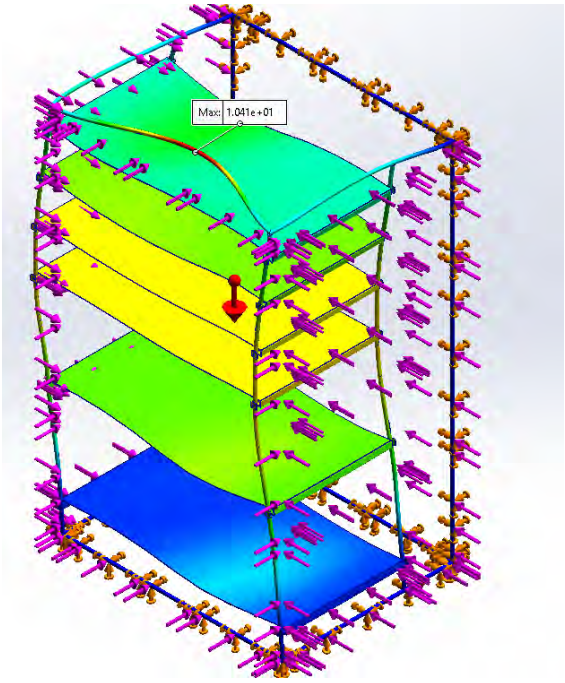

Figure 35: Exaggerated Deformation Plot

Load Case C

Load Case C is based on another critical loading condition identified in the Falcon 9 user manual, which is 2g lateral and 3.5g axial per Figure 24. Lateral load is applied to the front face and one side, exactly how load Case A is set up. The total lateral force on front face and side face

is 7,357 N, derived from a 375 kg total mass subjected to 2g lateral acceleration (375 kg x 2 x 9.81 m/s^2). Additionally, the horizontal member experiences 584.2 N, based on a 29.78 kg mass at 2g. The stress plot shows a maximum of 1057 MPa seen in Figure 36 and Figure 37. As well as the displacement reaching a maximum of 89 mm, seen in Figure 38. Additionally to help visualize where the deformation is occurring Figures 39 and 40 both exaggerate the stress and displacement plots and are scaled by 2.2x.

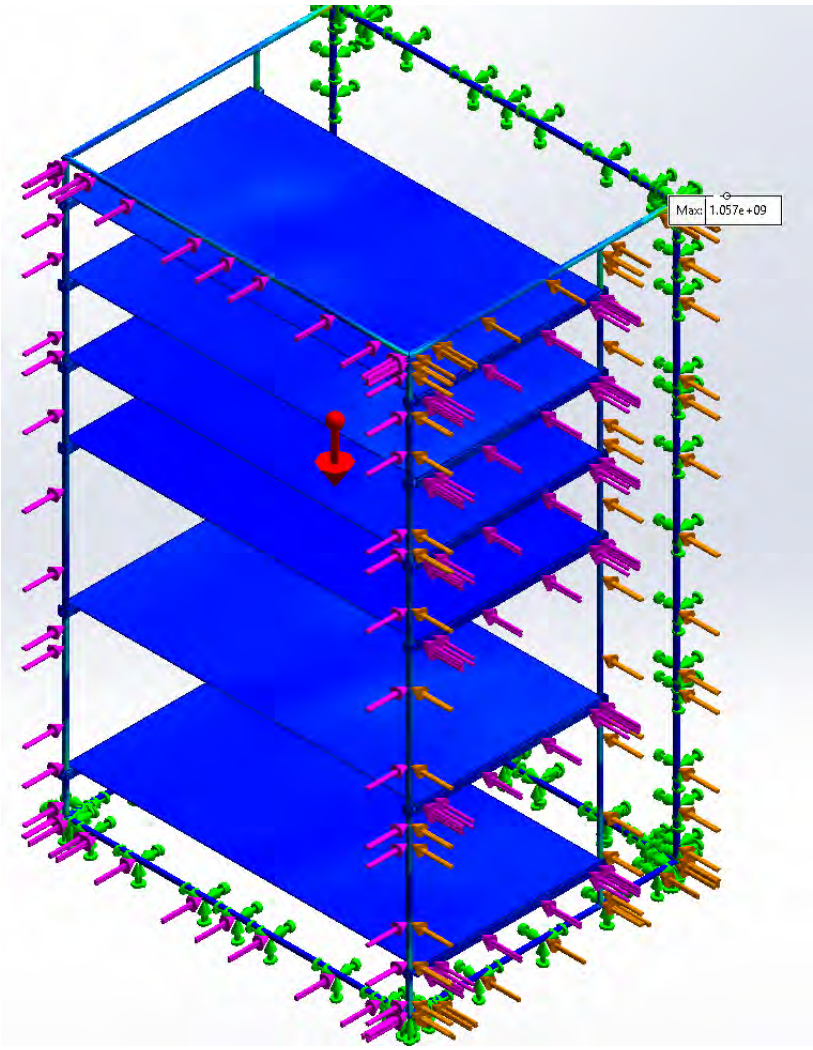

Figure 36: Stress Plot of Load Case C

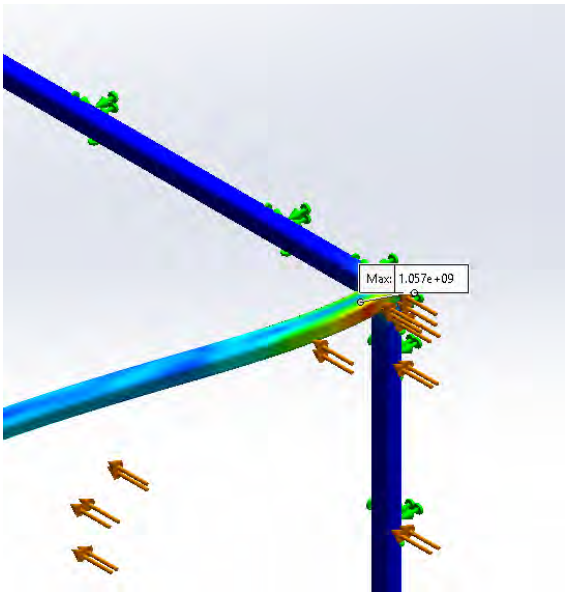

Figure 37: Zoomed View of Maximum Stress Region

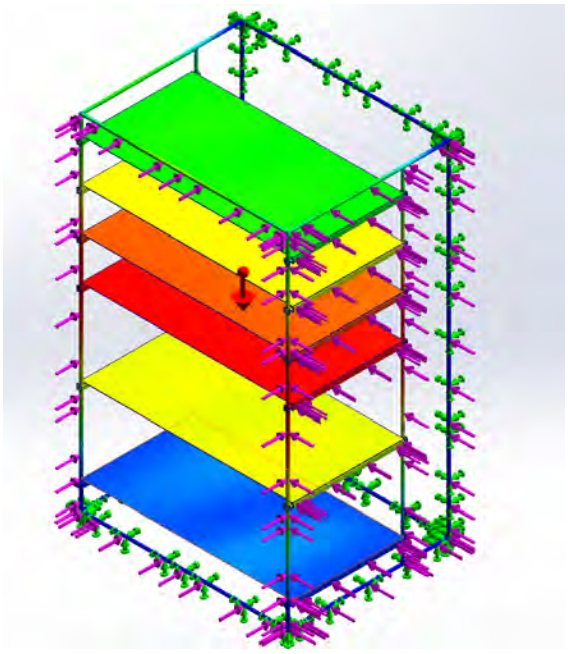

Figure 38: Deformation Plot of Load Case C

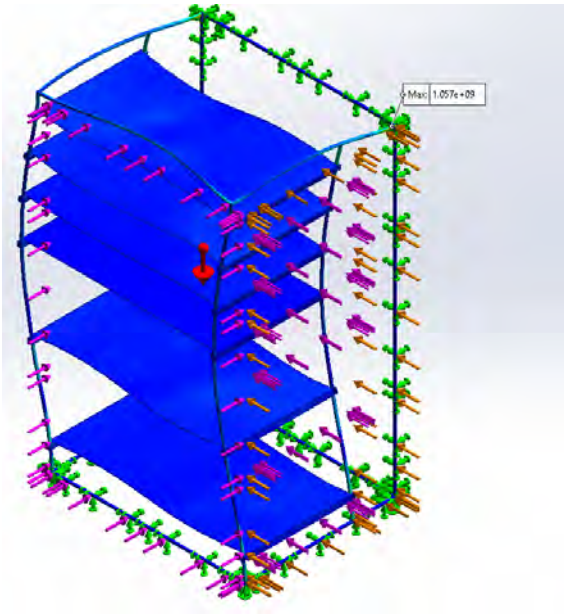

Figure 39: Exaggerated Stress Plot

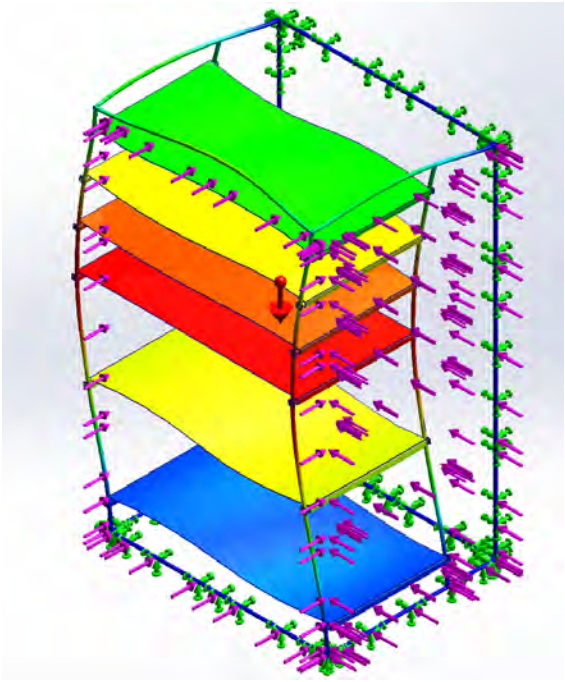

Figure 40: Exaggerated Deformation Plot

Load Case D

Load Case D also looks at 2g lateral and 3.5g axial, but like Load Case B, the lateral loads are applied to all 3 faces, as seen in Figure 30. From this set up the resulting maximum stress is 427.4 MPa, per the stress plots seen in Figure 41 and 42. With a maximum displacement of 41.9 mm,

via Figure 43. Additionally to help visualize where the deformation is occurring Figures 44 and 45 both exaggerate the stress and displacement plots and are scaled by 4.8x.

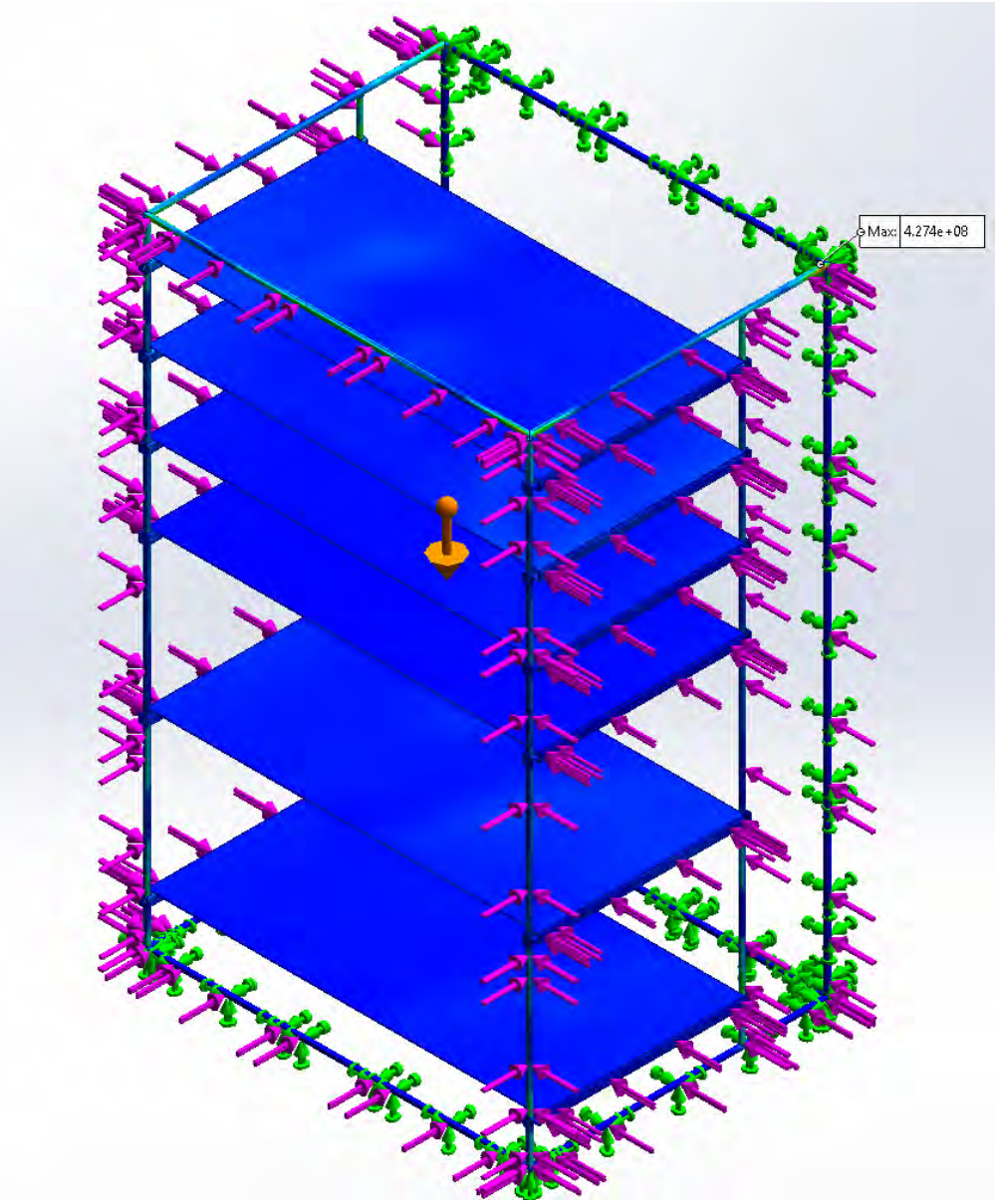

Figure 41: Stress Plot of Load Case D

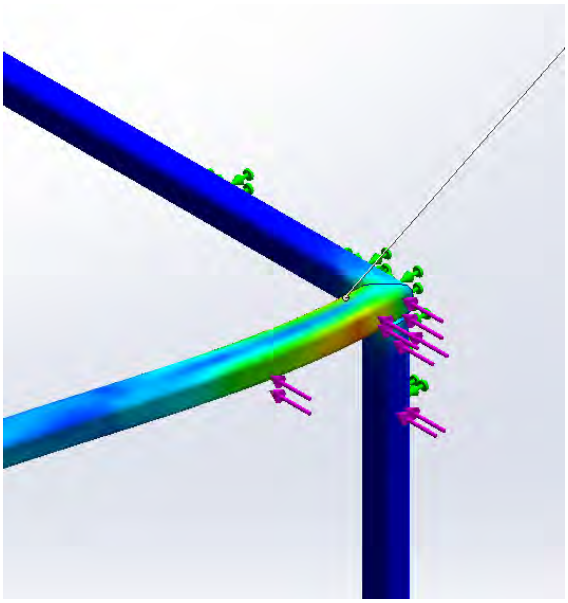

Figure 42: Zoomed View of Maximum Stress Region

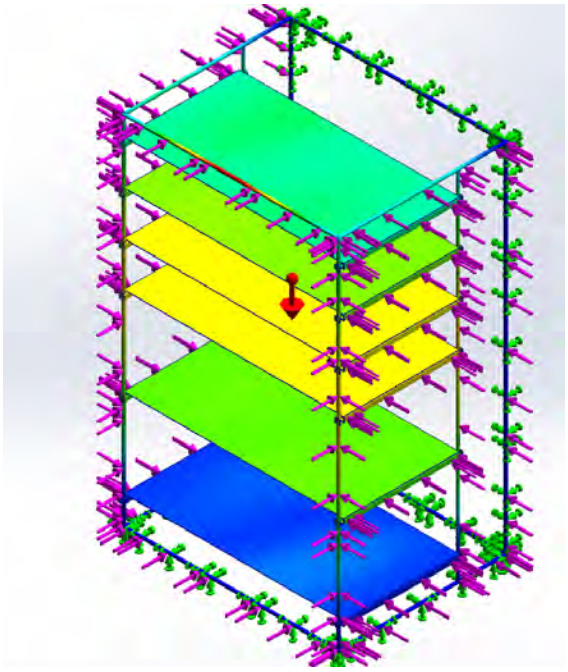

Figure 43: Deformation Plot of Load Case D

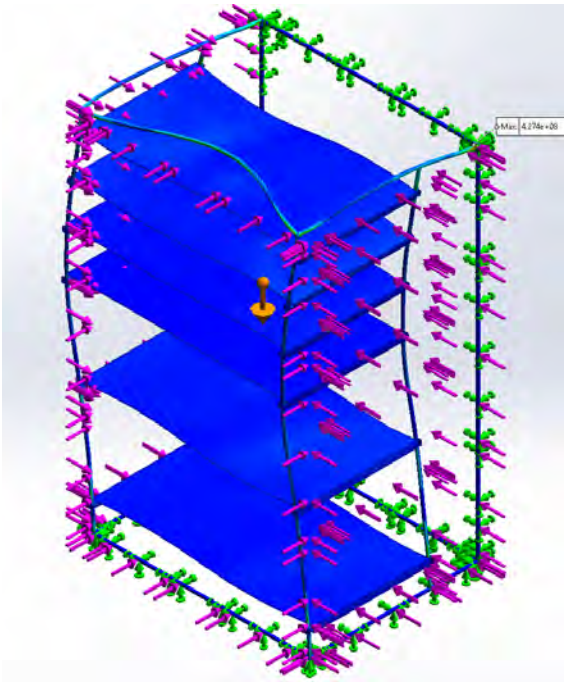

Figure 44: Exaggerated Stress Plot

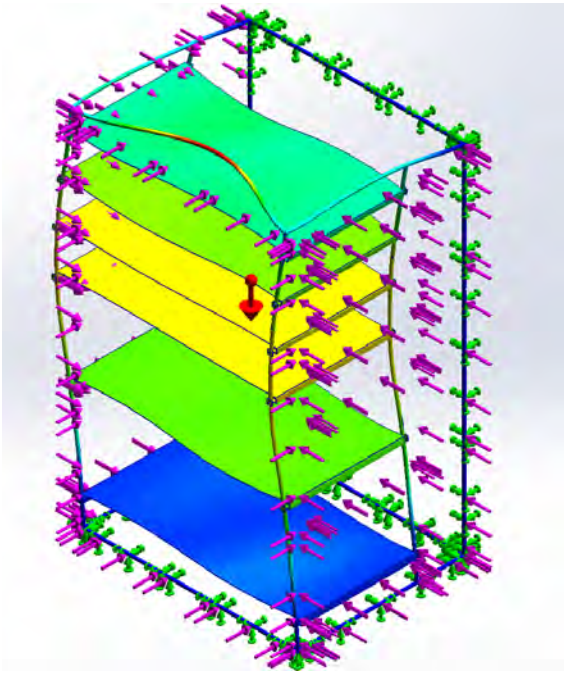

Figure 45: Exaggerated Deformation Plot

Discussion on Vibration Analysis

When designing a payload for Falcon 9, the hardware must survive sinusoidal accelerations up to approximately 0.9g across various frequencies, without safety margins applied, per Figure 46 (SpaceX, 2021). Our team began developing models to understand the behavior of the rack under

this frequency range. The initial model was similar to Figure 23, where only the rack frame was included, and the bottom was fixed. Based on this model, we observed bending and torsion in the vertical members. However, because the model did not include the rails/horizontal members, we believe it is not fully accurate; the actual rack would be stiffer, which would help mitigate vibrations.

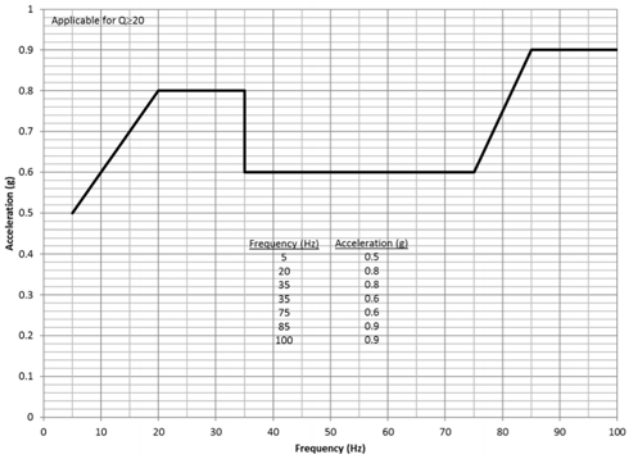

Figure 46: Falcon 9 User Manual - Axial Sine Environment

Conclusion

The load cases analyzed only represent a subset of the many possible load combinations the rack may experience during launch. We acknowledge that this study does not contain all potential scenarios, and additional cases may need to be studied to ensure safety and completeness.
From Load Cases A and B, which were defined by 6g axial and 0.5g lateral, we saw stress values that remain below the yield and ultimate stress limits of approximately 400-500 MPa established in Section 3.2.1. These results indicate that the current design can withstand these conditions during launch.

However, Load Case C, which introduced a higher lateral acceleration of 2g combined with 3.5g axial, resulted in a maximum stress of 1057 MPa. This value greatly exceeds the allowable yield and ultimate stress discussed above, indicating a critical failure. The maximum stress occurred in the location shown in Figure 37, which aligns with our expectations based on the loading direction and structural layout. If we were to imagine a cantilevered beam, and instead of applying the load at the top surface we did it from the side we would expect it to break in the same area where Figure 37 based on properties of mechanics. With that, Load Case C, as well as the loading 2g lateral and 3.5g axial, become the driving load conditions of our design.

To address this, we propose reinforcing the identified areas with triangular gussets, similar to those seen in our 80/20 prototype. Adding the gussets would help distribute the lateral load more effectively into the vertical members and reduce the stress concentration in the specific region, increasing the overall structural integrity.

3.3 Dry Land Weight Testing

3.3.1 Purpose - Benjamin Leazer

To verify the MPA mass-related requirements, specifically, the maximum allowable mass of the rack prior to installation (MPA-5) and the corresponding liftable mass constraint for two individuals operating in lunar gravity (MPA-1), the initial approach involved reviewing prior analyses. A brief literature review was conducted to determine whether relevant research had already addressed these requirements.

This review identified NASA-STD-3001, Volume 2, Revision D, which lists a lifting strength maximum operational load of 93 N (21 lbs) under the "Other Ops" category for routine tasks performed in unsuited conditions (Appendix E) (NASA, 2023). Because MPA-1 is designed for two individuals, this value was extrapolated to a combined lifting load of 186 N (42 lbs).

Additionally, a paper from the Neutral Buoyancy Research Facility (NBRF), titled *"Developing an Integrated Logistics Infrastructure for Lunar Surface Habitats*," reported that the maximum lunar weight for a Suit-port Logistics Carrier, a payload intended for suited, EVA conditions, carried by two individuals was 314 N (70 lbs) (Akin, 2023). The significant discrepancy between the unsuited and suited lifting capacities, where the latter is more than 1.5 times the former, highlighted inconsistencies in existing data. As a result, it was determined that prior research would not provide a reliable basis for defining the necessary values for MPA-1 and MPA-5.

To address this, the team proposed conducting in-house testing to establish a more accurate maximum weight and corresponding mass for the rack. This approach would also enable control over the rack's dimensions, ensuring that requirement values were directly tied to the actual design and measurements of the rack.

3.3.2 Objective - Benjamin Leazer

The objectives of the dry land weight testing were closely aligned with the MPA mass requirements (MPA-1 and MPA-5). The primary objective was to determine the maximum feasible weight of the rack that can be carried by two individuals during a lunar mission. A secondary objective was to assess whether additional transport strategies might be necessary to move the rack through confined spaces, such as the 40" x 60" hatch (MPA-6), whose dimensions were provided by NASA Marshall during design reviews. This objective also aimed to evaluate whether the liftable weight constraint could be increased through the use of assistive devices, such as lifting straps.

The final objective was to determine whether the rack could be launched pre-loaded with all payloads installed, or if payloads would need to be integrated on the lunar surface. Based on the data collected during testing, where various apparent weights were applied to simulate lunar gravity and the corresponding mass was then extrapolated, the team aimed to define an appropriate mass limit for the rack prior to installation, as required by MPA-5. This would inform whether a fully loaded launch configuration is feasible, based on the maximum allowable payload mass of 80 kg determined by Crew Systems analysis (see Section 2.3.2).

3.3.3 Setup - Mason Eberle

Dry testing was conducted using a PVC carrying rack that had been used in previous research experiments. The structure provided a reasonable approximation of our preliminary design and was capable of supporting significant weight. It featured a frame with multiple cross members made from PVC. To simulate the expected payload mass, weights were securely strapped or molded onto the sides of the frame. When additional mass was required, weighted vests were also placed over the center of the rack to increase the overall load.

To simulate the physical constraints of transferring cargo into a habitat, a separate metal storage rack was repurposed to represent the hatch opening. The top of this rack was adjusted to match our planned hatch dimensions of 40x60 inches.

The course was set up on the top floor of the University of Maryland's NBRF. The layout consisted of two straight segments: an initial stretch of about 3 meters, followed by a turn, and a second segment of about 7 meters. The storage rack acting as the hatch was positioned at the midpoint of the course and stabilized on each side. All testing was performed indoors on a concrete floor, with a timer walking alongside the participants from start to finish to ensure accurate measurements.

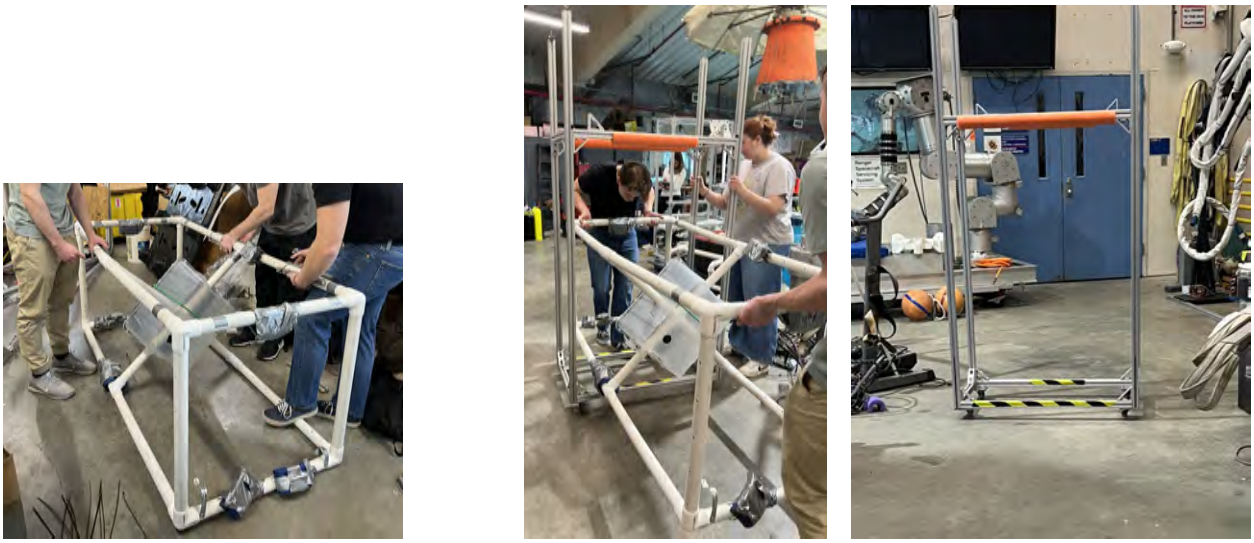

(a) Team members securing ballast onto the PVC test rack prior to next trail

(b) Carrying the weighted rack through the simulated hatch constraint during testing

(c) Static view of the repurposed metal storage rack representing the hatch dimensions

Figure 47: Dry testing payload rack and hatch simulation setup

3.3.4 Safety Procedure - Sofia Correia

Strict procedures were followed to ensure the safety and well-being of all participants. Prior to testing, subjects were informed that they could opt out of a trial or terminate the test at any time, for any reason.

Lifting heavy objects poses the risk of injury if not executed properly. To mitigate this risk, each subject observed a demonstration on safe lifting techniques, including posture, grip, and form. Instructions were also given on the proper use of the lifting straps. To prevent fatigue from affecting

results and posing a threat to the subjects proper lifting form, each participant was provided a minimum five-minute rest period between trials, and additional rest was taken as needed. All tests were conducted in a controlled environment, with ample space.

The mock lunar habitat hatch, constructed from 80/20 aluminum framing, introduced additional safety concerns due to the potential for impact or tripping. To mitigate these risks, preventative measures were taken. One team member was stationed on either side of the hatch to stabilize the structure as subjects moved the rack through the frame. A foam pool tube was cut and applied along the top of the hatch to cushion any accidental head contact. High-visibility caution tape was applied to the bottom edges of the hatch, which sat elevated from the ground, to reduce the risk of tripping while subjects were carrying the rack. The test area was also cleared of all non-essential personnel, and those observing remained alert for any signs of subject strain or instability during the trials.

3.3.5 Testing Procedure - Sofia Correia

Prior to each trial, the rack was positioned on its side to allow subjects to position themselves on either side where the top and bottom of the rack would be if it were in its upright orientation. The subjects were then instructed to lift and carry the rack along a 10 meter course. A mock hatch, simulating the 40 inch by 60 inch hatch present in the habitat, was positioned five meters into the course and required subjects to maneuver themselves and the rack through the opening. At the end of the course, the subjects placed the rack on the ground, marking the conclusion of the trial.

Once the subjects lifted the rack, the timer was started and was stopped once the rack was placed on the found at the end position. Subjects were permitted to set the rack down and take a rest or reposition themselves, however the timer continued. If a subject elected to terminate the trial, it was considered a failure and time was not recorded. Immediately following the conclusion of each trial, subject immediately filled out the NASA Task Load Index (TLX) form, as well as a question regarding their preferred hand position for lifting the rack at the current weight.

The testing sequence began with the male-male subject pair, and the rack weighted to the lightest load of 475 newtons (107 pounds). The subjects lifted the rack without the aid of lifting straps and completed the course. Following the male-male trial, the female-female and female-male pair completed the trial under the same test conditions. After the three subject groups completed the course without lifting aids, the lifting straps were introduced and the trials were repeated. New data was recorded for each configuration. Once testing at the lightest weight was complete for both strap and no-strap conditions, the process was repeated at increasing weights of 556 N (125 lbs), 689 N (155 lbs), 826 N (186 lbs), 929 N (209 lbs), and 1076 N (242 lbs). Weights were added symmetrically to the rack using a combination of moldable lead, lead blocks, diving weights, and weighted vests.

3.3.6 Assumptions - Mason Eberle

Several assumptions were made during the dry land weight testing to ensure the applicability of the results to future lunar or Martian missions. First, the test rack was loaded symmetrically with weights, purposefully maintaining the center of mass near the geometric center of the structure. It was assumed that the test rack's mass distribution was representative of the fully integrated

payload rack.

Second, the subject pool was intentionally varied in terms of gender, height, and body type, with male-male, female-female, and male-female pairs participating in all trials. By incorporating a variety of physical characteristics, the team assumes that the results are representative of the astronaut crews, who will also vary in stature and strength.

Lastly, while translating the rack through the simulated habitat hatch, participants were required to step over a horizontal bar positioned approximately 10 cm above the ground. This reflects the threshold present in hatchways between a launch vehicle and a habitat. The assumption is that this obstacle accurately simulates the constraints astronauts will face while transferring the rack in lunar or Martian environments.

3.3.7 Data Collection and Results - Ava Ward

Data collected during dry testing included both objective and subjective metrics to evaluate the feasibility of two astronauts carrying a model rack under lunar gravity conditions. The objective data focused on the duration of each task from start to finish. Trials were conducted with and without lifting straps, and comparisons were made across three different subject pairings: male-male, female-female, and male-female. These combinations were tested to ensure that the rack's maximum feasible weight could be transported by any astronaut pairing. As expected, an increase in weight led to a slight increase in task duration. While most groups completed the tasks in comparable times, the female-female pairing exhibited a substantial increase in completion time at the highest weight when no lifting straps were used (Figure 48). This discrepancy was mitigated when lifting straps were introduced, as demonstrated by the reduced time variability across all test groups (Figure 49).

Subjective data were collected using NASA's TLX, which assesses mental, physical, and temporal demands, as well as effort, perceived performance, and frustration. Test subjects completed the TLX form immediately after each trial, rating each category on a scale from 0 (least demanding/most successful) to 10 (most demanding/least successful). Although these values are inherently subjective, consistent trends were observed. In general, TLX scores increased with heavier loads (Figure 50), while the use of lifting straps consistently resulted in lower TLX ratings for a given weight and test group (Figures 50 and 51).

Integrating both the objective time measurements and subjective TLX assessments, the team identified 827 N (186 lbs) as the maximum feasible weight for two astronauts to carry. This determination reflects a balance between operational difficulty and repeatability; while the task is challenging, it is not prohibitively strenuous. It is important to note that the time required to install lifting straps was excluded from this phase of data collection but was accounted for in subsequent testing.

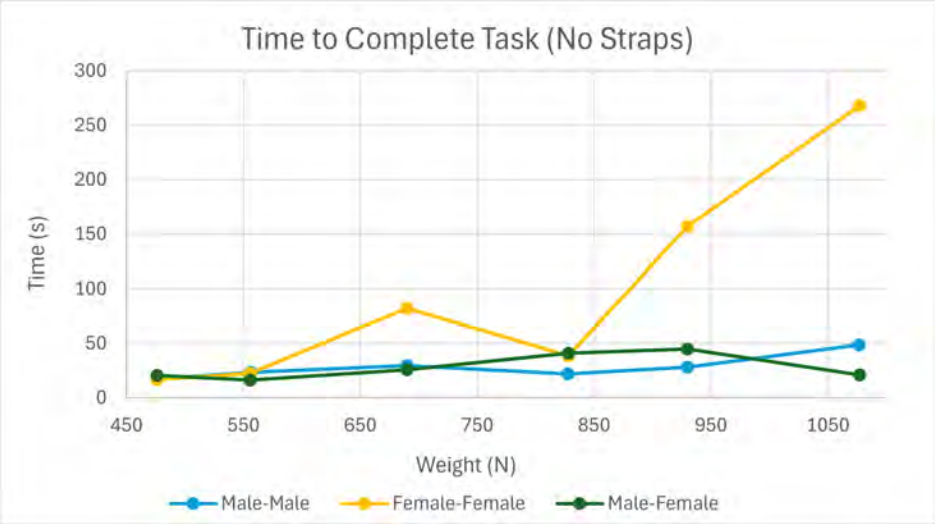

Figure 48: Total Time to Complete Dry Land Rack Movement Without Straps for Different Test Groups

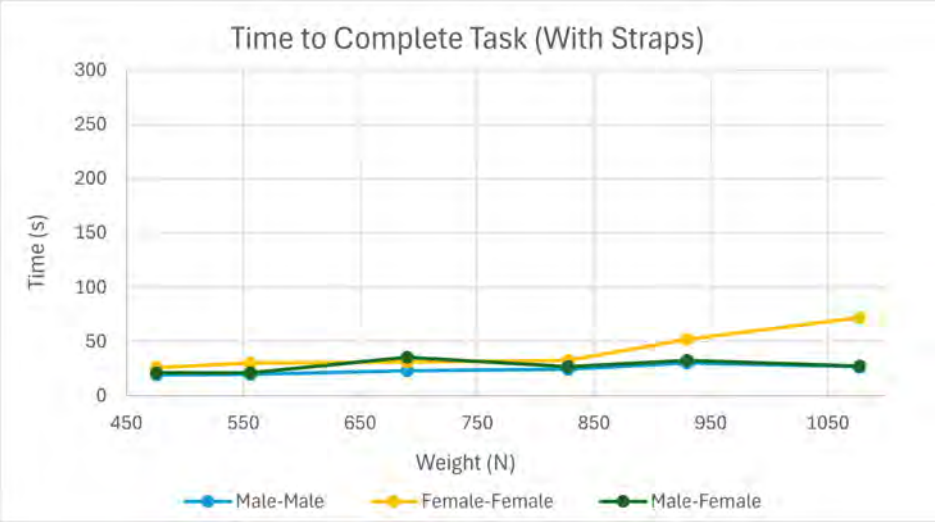

Figure 49: Total Time to Complete Dry Land Rack Movement With Straps for Different Test Groups

Figure 50: Dry Land Rack Movement TLX Results Averaged Across all Test Groups for Various Weights (Straps vs No Straps)

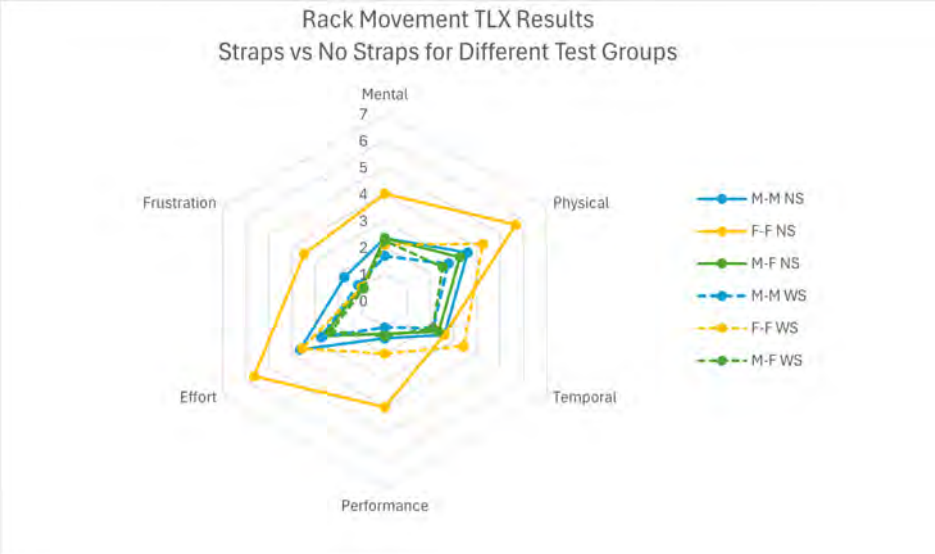

Figure 51: Dry Land Rack Movement TLX Results Averaged Across all Weights for Various Test Groups (Straps vs No Straps)

3.4 Underwater Mass Testing

3.4.1 Purpose - Benjamin Leazer

While dry land weight testing proved useful to evaluate a large range of apparent weights, it did not adequately capture the significant influence of lunar gravity on the test subjects' ability to carry the rack. Specifically, dry testing could not simulate the distinction between weight and inertial mass. In these tests, the rack was weighted to match its apparent weight under lunar gravity; however, due to Earth's gravity, it only possessed approximately one-sixth of the inertial

mass it would have on the Moon.

Because inertial mass is independent from gravitational effects, and the team was assessing the maximum weight two individuals could lift, the dry testing setup could not accurately represent how the rack would behave on the lunar surface. Furthermore, the dry land testing served as a preliminary assessment and focused exclusively on transporting the rack through a hatch. It did not incorporate other critical actions such as rotating and positioning the rack at its end location, which are essential tasks required for unloading the rack from a lander and installing it into a volume-constrained lunar habitat.

To address these limitations, the team conducted underwater testing at the NBRF in the Space Systems Laboratory (SSL). This environment allowed for the simultaneous simulation of both lunar apparent weight and the correct inertial mass by properly ballasting the rack. In addition, scientific divers could also be ballasted to their lunar-equivalent body weights, offering a more realistic approximation of how astronauts would interact with their environment. This setup enabled a more accurate assessment of lifting, maneuvering, and placement capabilities under simulated lunar conditions.

Unlike dry testing, the underwater testing protocol was expanded to include rotations, placements, and orientation of the rack, thereby increasing the fidelity of the assessment in replicating operations within a limited-space environment. Given that the dry land testing underestimated the impact of inertial mass on lifting capabilities and maneuverability, the team selected the previously determined maximum feasible rack mass of 510 kg as the upper limit for underwater trials.

3.4.2 Objective - Benjamin Leazer

The objectives of the underwater mass testing were directly informed by the findings from the dry land weight testing. The primary objective was to refine the maximum feasible weight of the rack that can be safely transported and installed in a lunar surface habitat. In this additional round of testing, the team evaluated a narrower range of weights, selected based on the results of the initial dry tests, while also aiming to more accurately model the effects of lunar gravity.

The second objective was to assess whether lifting methods or assistive devices remained effective and practical within a constrained environment. Dry land testing had demonstrated the utility of lifting straps; the underwater testing aimed to determine whether such devices would remain viable when maneuvering the rack through tight clearances, particularly with only five inches of margin when passing through the hatch due to the dimensions of the test rack.

The final objective was to evaluate whether additional features or considerations would be necessary to successfully position the rack within a limited-space environment. The included determining whether floor-mounted sliders or similar aids would be required to place the rack accurately in its final location.

3.4.3 Ballast Process - Benjamin Leazer & Mason Eberle

Ballasting is the process of attaching additional materials to an underwater test model to simulate both the apparent weight and inertial mass of a target object—in this case, the test model rack. It requires calculations to determine the appropriate proportions of ballast components, which in the team's case, were weights and containers. Ballasting is essential in underwater testing due

to the influence of buoyant force on test models, which is not present in dry land testing. This force is dependent on the volume of water displaced by the object, and when fully submerged, it is strongly affected by the density and shape of the materials used.

Similar to that of dry testing, for underwater testing, the design variable was lunar apparent weight, as it directly informs the MPA mass-related requirements. To achieve specific apparent weights underwater, the team needed to add calculated amounts of ballast weight to the rack to account for buoyancy. The test plan included four lunar apparent weight conditions, each tested with and without lifting straps, resulting in a total of eight trials. Since inertial mass is directly proportional to apparent weight, each condition also required a different corresponding inertial mass.

Once the apparent weights and associated inertial masses for each trial were defined, the team calculated the necessary ballast. The ballast materials consisted of three primary components: the 80/20 test rack frame, lead weights and plastic containers. The test rack, built by the LSM team, was made of 80/20 6061-T6 aluminum and reflected the bulkier double rack design (1.16 m x 1.91 m x 0.90 m) to simulate the most challenging handling conditions.

After fabrication, a crane scale was used to obtain experimental measurements of both the dry and submerged weights of the rack, which served as the basis for ballast calculations. The first ballast component added was lead weight to achieve the target apparent weights. Lead was selected due to its high density and low displacement as well as its prevalence within NBRF. With a specific gravity of 11.35, lead's effective weight underwater is reduced by about 10%, meaning the team had to increase the total mass of lead by that amount to meet apparent weight targets.

The second component, plastic containers, was used to simulate additional inertial mass. While lead weights could achieve apparent weight, it did not fully replicate the corresponding inertia experienced on the lunar surface. As a common practice in underwater simulated gravity testing, adding inertial mass is achieved by "designing the physical envelope of the object to enclose the appropriate amount of water" (Akin, 2025). To address this, the team used plastic containers designed to capture water. The water enclosed within the fixed volume containers increases the inertial mass of the rack as the captured water must then also be accelerated or decelerated along with the rack. The containers were drilled with holes to allow water to enter and were made of plastic, which has a relative density near 1.0. As such, they were considered neutrally buoyant, contributing inertial mass without affecting weight. The amount of water required to model the missing inertial mass was calculated based on the dry weight of the rack and the attached lead weights. Since 1 liter of water has a mass of approximately 1 kg, volume-to-mass conversion was straightforward. However, conversions were later adjusted to gallons to match commercially available container sizes.

Mass Testing and Relevant Calculations								
Mass Test	Testing Inertial Mass [kg]	Lunar Apparent Weight [lbs]	Lunar Apparent Weight [N]	Underwater Weight Required [N]	Lead Weight Required [N]	Lead Weight Required [lbs]	Lead Mass Required [kg]	Water Capture Required [kg]
4	285	104.8	466.0	207.9	226.2	50.9	23.1	218.1
3	345	126.8	564.1	306.0	333.0	74.9	33.9	267.3
2	400	147.0	654.0	395.9	430.8	96.9	43.9	312.3
1	458	168.3	748.8	490.7	534.0	120.1	54.4	359.8

Actual Structure Weight [N]	Underwater Structure Weight [N]
429.6	258.1

Figure 52: Ballast Calculations

The heaviest intended trial was based on the final feasible mass of 510 kg, derived from dry land testing. However, this goal could not be fully realized for two reasons. First, the 80/20 test rack was lighter than expected once constructed. The initial mass estimate, calculated from aluminum density and an 80/20 parts lists composed by LSM, overestimated the rack's actual weight. Second, the team received an incorrect container size in their test materials order. Although a replacement was used, it was smaller than the intended volume, which reduced the total amount of water (and thus inertial mass) that could be added. Therefore, as seen in Figure 52, the heaviest trial tested was 168.3 N.

To streamline testing, the rack was pre-loaded with all ballast (lead weights and plastic containers), allowing the divers to only remove components during testing rather than add them underwater. This approach significantly reduced the time and complexity of the testing. To incorporate all four lunar apparent weight conditions, the team designed a modular ballast configuration, which allowed for components to be detached systematically between trials to lower both the weight and inertial mass.

(a) Permanent Ballast

(b) Removable Ballast

(c) Ratchet Straps

Figure 53: Front, Back, & Side View of Test Model Rack

The lightest weight trial required 226.2 N of lead weights and 218.1 kg of captured water, as detailed in Figure 52. These materials remained on the rack at all times, as they were part of the final (lowest weight) condition. Three plastic containers and two lead weights, highlighted in Figure 53a, were permanently affixed to the rack structure using two to four metal hose clamps for secure attachment.

Containers intended to be easily removed after each trial were secured with one to two ratchet straps for quick-release functionality. Each container was labeled according to the removal order, with weights housed inside, so that both inertial mass and weight components could be removed simultaneously to prepare for the next trial. Throughout this process, the team attempted to ensure the symmetrical placement of all ballast components to maintain an even distribution of both inertial mass and apparent weight, taking into account the sequential removal of ballast during testing.

3.4.4 Setup - Mason Eberle

Underwater testing was conducted in the NBRF. The test utilized our custom built rack, which was designed to match the exact dimensions required and ballasted appropriately to simulate both the symmetrical weight distribution and inertial mass expected in lunar conditions.

To replicate the confined spatial environment astronauts would experience inside a lunar habitat, previously used racks from earlier NBRF tests were repurposed to create the boundaries of the course. A simulated hatch was constructed using two additional old racks, with the crossbars adjusted to a height of 60 inches. A corrugated plastic sheet was then floated between these racks to represent the overhead clearance of the actual hatchway.

The full course layout (Figure 54) was arranged on the bottom of the neutral buoyancy tank. At the starting point of the course, the test rack was positioned between the two permanent racks to simulate the restricted maneuvering space of a habitat interior. The entrance to the simulated hatch was positioned 5.5 meters from the starting point, marking the midpoint of the course. The end of the course was located another 5.5 meters beyond the hatch, where the test rack would be positioned between two additional permanent racks. Several cameras were placed around the course to provide full visual coverage of the test.

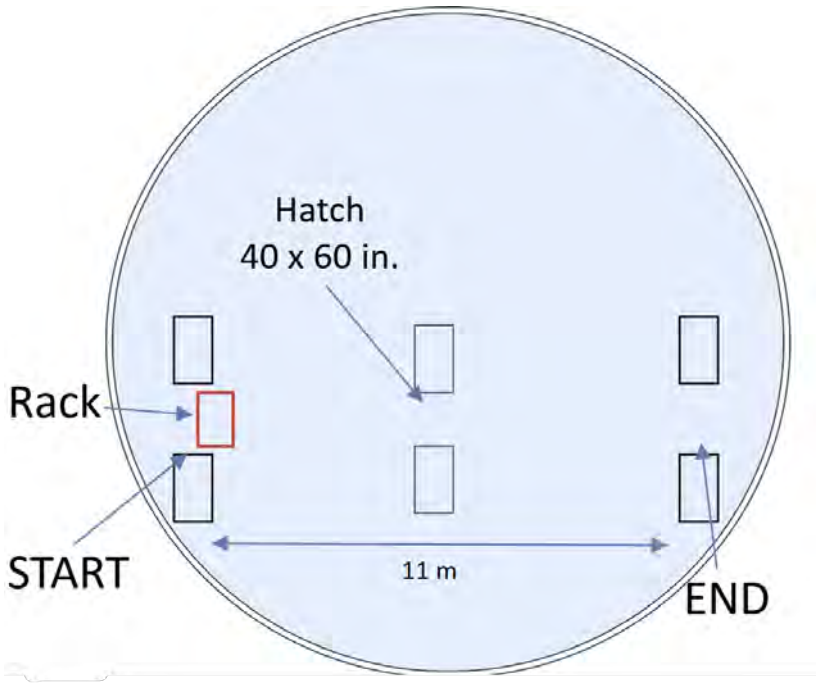

Figure 54: Top view: NBRF underwater testing course layout

3.4.5 Safety Procedures - Sofia Correia

Given the increased risks that accompany underwater testing, strict safety protocols were implemented to ensure the well-being of all participants. As with all testing involving human subjects, participants retained the right to terminate a trial or withdraw from testing at any point and for any reason.

Prior to entering the water, test subjects received a comprehensive briefing regarding the procedure and associated safety measures. To simulate lunar gravity, subjects were ballasted using lead weights, which were easily removable in case of an emergency. Unlike standard SCUBA diving, subjects did not carry their air tanks on their back; instead, air was supplied through an umbilical. This setup introduced unique risks that required additional supervision.

To mitigate these risks, a team of five additional divers were present in the tank, with at least one diver in close proximity to each subject at all times. These divers were responsible for monitoring air supply, alerting subjects when the tank pressure approached the predetermined threshold requiring replacement, and providing an emergency air supply should it be needed. The supplementary divers also managed the air and communication lines to prevent entanglement in the test structure or equipment. Care was taken to avoid scenarios where the lines could become caught in the aluminum frame of the hatch, or pose a tripping hazard during the simulated rack transport.

Rather than reusing the dry testing mock hatch as was originally planned, modifications were made to improve subject safety in the underwater environment. The final structure consisted of two parallel aluminum frameworks, 40 inches apart, with corrugated plastic bridging the top. This design allowed subjects to walk across a flat surface, eliminating the risk posed by the raised base of the dry-test hatch. The corrugated plastic ceiling provided a softer impact in the event the

subjects' head came in contact with the mock hatch, minimizing the risk of injury during trial execution.

Throughout the testing, diver safety remained the highest priority. While support divers contributed to trial documentation and data collection, their primary role was to observe, assist, and intervene immediately if any subject appeared distressed or unsafe.

3.4.6 Testing Procedure - Benjamin Leazer

The underwater procedure consisted of two main phases: test resetting and test execution. The resetting phase focused on the preparatory steps necessary to ensure that each trial could be conducted smoothly and efficiently.

A total of eight discrete trials were conducted: two at each apparent weight level, one without lifting straps and one with straps. Testing began with the heaviest apparent weight in the no-strap configuration. Following the completion of each no-strap trial, scientific divers repeated the trial using lifting straps for rack transport. Once both trials at a given apparent weight were complete, the rack was adjusted by support divers to reduce its weight and mass to the next test level. This was accomplished by removing labeled ratchet straps and their corresponding containers (including the internal weights). After completing these steps and recording the necessary data, the test course, equipment, and support and safety diver location were reset in preparation for the next trial.

Once the reset was complete, the divers prepared for the next trials. Before starting the timed portion, the rack was positioned vertically at the designated (reversible) start/end point. Two scientific divers assumed starting positions in front of the rack, with their backs to the rest of the course. Upon verbal confirmation from both divers, the trial began and the timer was started.

The two scientific divers grasped the sides or top bar of the rack and rotated it downward so that its long axis was horizontal. They then rotated the rack again onto its side to achieve the proper orientation for passing through the hatch. The divers repositioned themselves on either side of the rack along the long axis and determined who would walk forwards and who would walk backward during transport. If the trial involved lifting straps, the divers prepared them by threading the straps through the rack framework. At this point, the time to complete the "setup" phase was recorded.

The scientific divers then lifted the rack, either directly by the frame or using lifting straps, and began translating it forward along the test course. After moving the rack approximately 6 m, the divers navigated the rack through a simulated hatch. During this stage, support divers recorded the number of times the rack contacted the hatch structure. Once through, the divers transported the rack an additional 6 m toward the end location. After setting down the rack, the "transport" time was recorded. Lifting straps, if used, were removed at this stage.

Next, the divers rotated the rack 180 degrees to ensure it was correctly oriented for final placement. The front of the rack was then tipped face-down, and the divers aligned it between two fixed structures at the end location. Once aligned, the rack was tipped upright, returning it to its original vertical orientation. The time required to complete the "installation" phase was then recorded.

If at any point during a trial the scientific divers felt the rack was too heavy to safely manage, they were instructed to designate that trial as a failure. Immediately following each trial, whether

completed or failed, both divers completed a NASA TLX questionnaire to assess perceived workload. The course and rack were then reset as described for the next trial.

3.4.7 Assumptions - Mason Eberle

Several assumptions were made during underwater testing to ensure that the results are applicable to future lunar missions. First, the test rack was loaded symmetrically with weights to simulate the distribution astronauts would experience in lunar gravity. Additionally, the divers were weighted to approximate how astronauts would move on the Moon's surface. It is assumed that the feel and handling of the rack underwater, considering both resistance and inertia, reasonably replicate how the rack would feel when maneuvered in lunar gravity.

The two divers selected for testing had extensive experience in neutral buoyancy environments. It is assumed that future astronauts will undergo similar or more rigorous training in preparation for their missions. Therefore, it is reasonable to expect that they will be equally or more capable of maneuvering the rack, supporting the validity of the selected maximum mass.

During the test, the divers were required to step over a 4.5 cm high bar underwater. This was assumed to represent the kind of obstacle astronauts may encounter when transitioning from the launch vehicle to the habitat. Furthermore, the floor of the neutral buoyancy tank was uneven. In contrast, it is assumed that the habitat interior on the Moon will be flat, which would make maneuvering the rack easier than in testing. However, the uneven floor may also provide insight into the rack's performance on the actual lunar surface, where terrain is not always flat.

3.4.8 Data Collection and Results - Ava Ward

The underwater testing phase mirrored the dry land trials in its use of both NASA TLX workload assessments and time-based task measurements, but with added detail. In addition to total task duration, the underwater trials recorded the time required to complete each of three task stages: setting the rack down, moving it through a hatch, and positioning it on the opposite side (Figures 55, 56, and 57). Furthermore, the number of rack collisions with either the hatch or the pool floor was tracked to quantify operational difficulty (Figure 58).

Unlike dry land testing, where trials progressed from lightest to heaviest weights and demonstrated a performance learning curve over time, the underwater tests were conducted in reverse order, from heaviest to lightest mass, which also revealed a learning effect. Subjective workload, measured via the NASA TLX, increased with mass in both strapped and unstrapped conditions (Figures 59 and 60). The use of lifting straps consistently lowered TLX ratings at equivalent mass levels, confirming their benefit in mitigating perceived task difficulty. Another key observation was that the diver positioned to carry the rack backward reported higher TLX scores than their forward-facing counterpart, regardless of mass or strap use (Figure 61). This discrepancy likely reflects the reduced visibility and control when operating in reverse.

While the overall mass did not significantly affect total trial time, the trial involving the heaviest mass did result in a noticeable increase in completion time (Figures 56 and 57). However, this was also the diver's first trial, suggesting that inexperience, rather than mass alone, may have contributed to the delay. Across all stages, lifting straps neither substantially increased nor decreased total transport time, though they did lengthen the initial setup phase, which included the time

required to attach the straps to the rack (Figure 55).

A final trend observed was a greater number of rack collisions in trials without straps, particularly at higher weights, indicating reduced control and increased task complexity (Figure 58). Based on these findings, and considering the simulated inertial effects present during underwater testing, the revised recommended maximum mass for astronaut rack transport is 375 kg (138 lbs). Additionally, the use of a lifting tool, such as straps, is recommended, as it reduces workload perception without substantially increasing task duration.

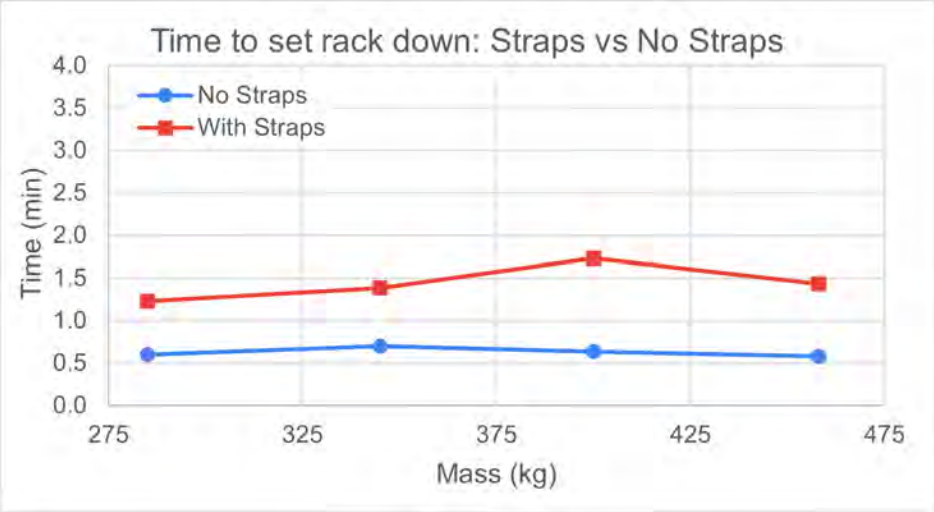

Figure 55: Time it Took Divers to Set Rack Down in Underwater Testing (Start of Trial)

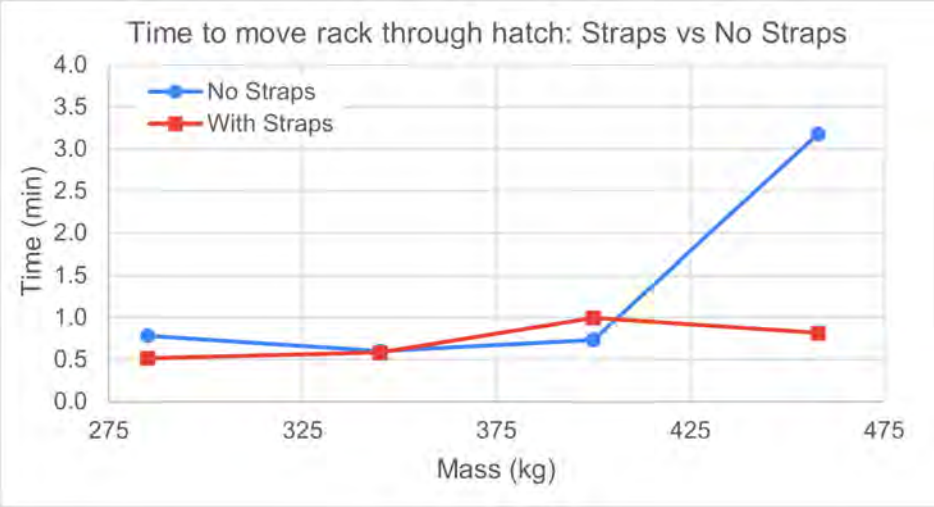

Figure 56: Time it Took Divers to Transport Rack Through Hatch in Underwater Testing (Middle of Trial)

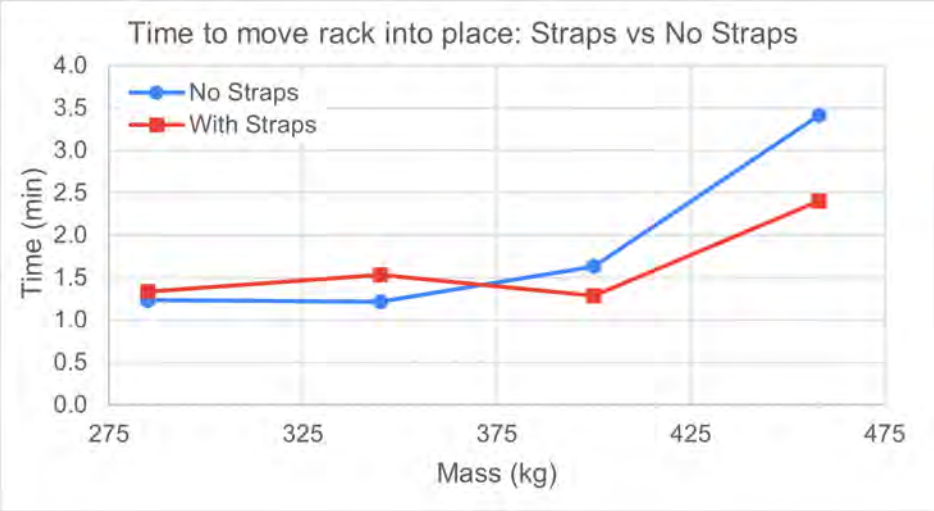

Figure 57: Time it Took Divers to Set Rack into Place in Underwater Testing (End of Trial)

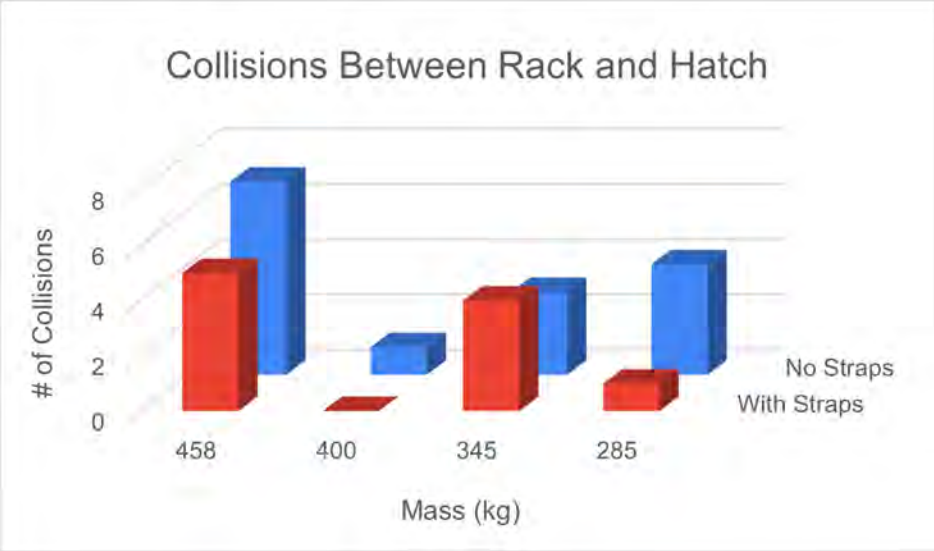

Figure 58: Number of Rack Collisions During Underwater Testing (Straps vs No Straps)

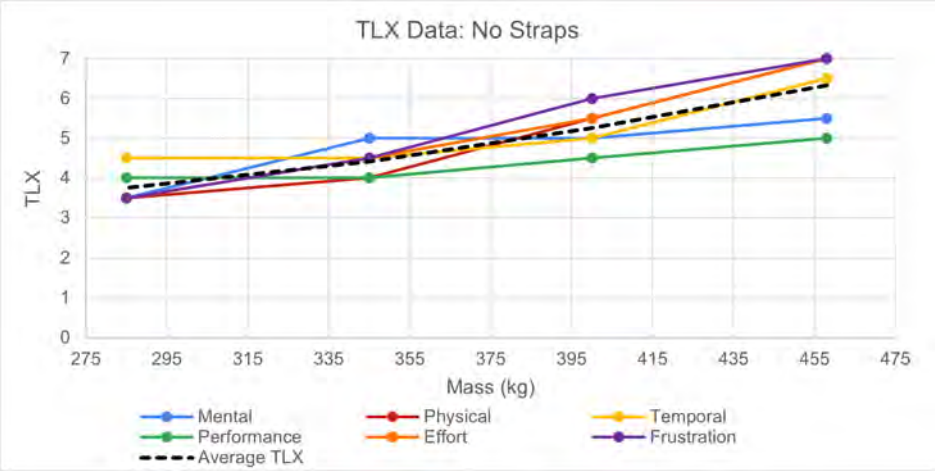

Figure 59: Underwater Testing TLX Data for Trials Without Straps

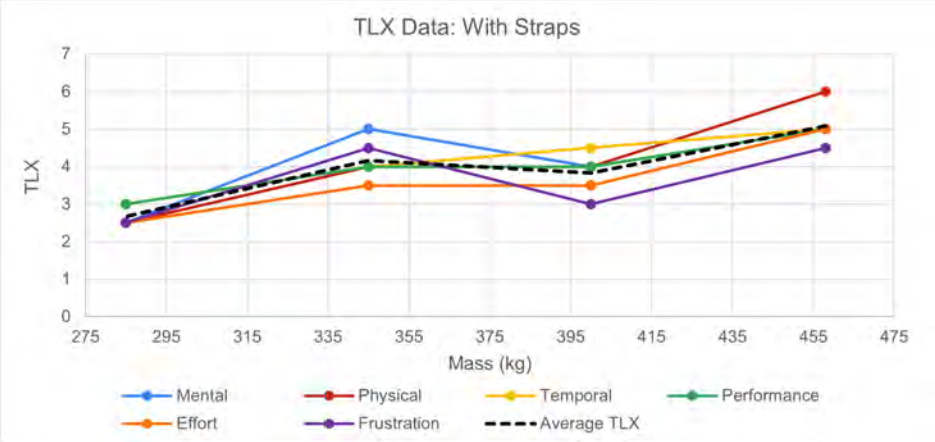

Figure 60: Underwater Testing TLX Data for Trials With Straps

Figure 61: Underwater Testing Average TLX Data for Test Subjects Facing Backwards and Forwards (Straps vs No Straps)

3.5 Underwater Payload Testing

3.5.1 Purpose - Avery Lowe

As established in 3.4.8, to minimize the requirement of crew members to install payloads in the habitat, our rack will be launched partially loaded with payloads. However, crew members will still have to perform some installation as well as routine removal and replacement of different ORU's for maintenance and troubleshooting purposes. With this established, a payload installation feasibility test was proposed to ensure that our rack design was suitable for such tasks.

Payloads that occupy a standardized payload rack can vary significantly in terms of size and weight depending on the function of the payload. The payload rack has 6 different possible installation platforms at varying heights, each introducing its own ergonomic challenges. To capture a more accurate payload to rack connection effort, ECLSS systems were analyzed as these systems often have a much more exhaustive list of connections that need to be made.

Therefore, the crew members' installation effort can be defined by three key factors.

1. The size of the payload,
2. The position of the payload in the rack,
3. The number of connections between the payload and the rack.

As mentioned before in Section 3.4, testing underwater with the help of NBRF, we can more accurately represent the effects of partial gravity on the installation effort from the crew. As simply reducing the mass of the payloads by 1/6 and doing a dry land test can give a good representation of the overall crew member motion it fails to account for the inertial mass effects of moving the payloads around. Thus, underwater testing where both payloads and crew are ballasted for lunar gravity, provides a more accurate representation.

3.5.2 Objective and Scope - Avery Lowe

The objective of this payload test is to answer the question, how does the number of connections and payload size affect outfitting time on a rack with multiple height levels? To answer this question, we need to determine the functional relationship between the outfitting time and the payload characteristics such as the payloads size and mass, the number of connections, and the shelf height. Determining this relationship would allow us to better understand how the crew should manage the payloads, as well as determine the best possible placement of payloads that could prove to be challenging to maneuver.

The scope of this test was lessened to allow for the testing subjects to complete the test in the allotted time we had at the NBRF. This meant that we would not test in microgravity or Martian gravity and only test in lunar gravity. The test was to include two payloads varying in size, both representative of ECLSS systems. The larger payload represents the distillation assembly with an approximate mass of 75kg, while the smaller payload represents the common cabin air assembly with an approximate mass of 30kg. Future testing could expand to include additional payloads, gravity environments, and connection complexities.

3.5.3 Assumptions - Avery Lowe

There were several assumptions we made going into this test that helped streamline the testing environment to allow us to collect data on more trials. The largest assumption we made was that the mock connections we made accurately reflected real ECLSS connection effort. This assumption was made of necessity, even though it may not be an entirely correct assumption. Real ECLSS systems generally will have sealing, torque locking mechanisms, and confirmation steps that we are unable to simulate in the underwater environment. We are also not able to test live payloads with dynamic fluid or airflow which would be seen in a real system. The next assumption we made was that the payload weight and size approximations are representative of real systems, and that installation effort for other systems can be represented as a linear curve fit between the two chosen systems, is assumption can be extended to say that each connection on an ECLSS system takes roughly an equal amount of time. This assumption was made due to the limitations of the time constraints for the development of the mock payloads, as well as the lack of exact dimensions of other payloads. Other assumptions we made include that the shelf heights accurately simulate the ergonomic challenges and that underwater testing accurately simulates different gravity environments.

3.5.4 Setup - Avery Lowe

payload testing was conducted at the NBRF within SSL. This test required the construction of three major components:

1. Shelves to hold the payloads
2. Mock payloads
3. Connection boards for interfacing between the rack and payload

Note: The construction of these components occurred in a laboratory in the United States. Therefore, the primary units in this section will be in imperial units.

Shelf Construction:

The Earth-model frame, originally built by LSM and used in previous MPA testing, was modified to include three shelf platforms, each spaced 24" apart. The shelves were constructed from Starboard material, measuring 41" x 24", and designed to fit snugly between the frame rails. Each shelf was secured to the rails using six-4" wood screws (three per rail).

To facilitate payload installation, each shelf was modified with two sets of four tapped ¼-20 holes, aligning with corresponding holes on the mock payloads. This allowed the payloads to be bolted securely in place during testing. Additionally, the outline of each payload's position was marked on the shelves to streamline installation for test subjects.

Mock Payload Construction:

The mock payloads were constructed by modifying small and extra-large PVC cargo bags. The small payload (16"x14"x11") represented the CCAA, while the large payload (30"x16.5".18") represented the DA. The PVC material was assumed neutrally buoyant, and holes were drilled to allow water to fill the interior, adjusting buoyancy as needed.

To simulate lunar gravity conditions, the payloads were ballasted to the required inertial mass following MPA's underwater ballasting procedure (Fig. 63). The large payload required 30 lbs of

Figure 62: 3 Shelves Installed in Earth Frame

Payload Testing and Relevant Calculations (LUNAR)							
Testing Inertial Mass [kg]	Lunar Apparent Weight [lbs]	Lunar Apparent Weight [N]	Lead Weight Required [N]	Lead Weight Required [lbs]	Lead Mass Required [kg]	Water Capture Required [kg]	Gallons Required (gal)
75	27.57	122.63	133.44	30.00	13.60	61.40	16.22
30	11.03	49.05	53.38	12.00	5.44	24.56	6.49

Figure 63: Underwater Payload Ballast Table

added weight and approximately 16 gallons of captured water, while the small payload required 12 lbs and roughly 6 gallons.

- Additional Mass: Dive weights (2 lb and 4 lb increments) were evenly distributed across the PVC frame using zip ties to avoid significant shifts in the center of gravity.
- Captured Water Volume: Three 5-gallon water jugs were used for the large payload, and one 5-gallon jug for the small payload. Though this did not provide the exact required volume, the remaining water displacement was assumed to be accounted for by the water inside the PVC frame

Connection Board Construction:

The final components constructed for this test were the mock connection boards. Due to time and material constraints, only a single set was fabricated —one for the payload and one for the rack—requiring the boards to be transferred between payloads as needed during testing. The connections were simulated as follows:

- Data/Power Connections: Ethernet cables were used instead of ISS-standard barrel connectors. While not identical, their quick-connect functionality was deemed representative for test purposes.
- Fluid Connections: Quick-connect hose fittings were used, with male connectors on the payload side and female connectors (attached to extendable hoses) on the rack side.
- Airflow Connections: PVC ducting was installed on the rack connection board, sliding over a barbed, 3D-printed socket on the payload side to ensure a secure fit.

3.5.5 Procedure - Avery Lowe & Allison Rahr

Prior to testing, the subject will be familiarized with the types of payload connection (data, power, fluid and airflow), as well as the three installation levels of the rack. The first run through of the test will be with the connection board secured to the large payload. The test will start with the timer starting as the subject extends the top shelf from the rack using the rail system. The subject then lifts the payload, aligns it with the marked outline on the shelf, and secures it using bolts, initiating thread engagement without full tightening. Once the last bolt is started, the timer records the mechanical connection time as a standalone metric. Next, the subject connects only

Figure 64: Small Payload with Connection Board

Figure 65: Rack Connection Board

the Ethernet cables (simulating data/power) before sliding the shelf back into the rack, at which point the timer stops to record the total payload installation time.

For removal, a second timer starts when the subject places their hand on the shelf. The subject first disconnects the wires, then removes the bolts (placing them on an unused shelf to prevent loss), and finally extracts the payload and sets it on the ground. The timer stops upon payload placement, yielding the *removal time*. After each trial, the subject provides subjective workload feedback via the NASA TLX questionnaire.

The procedure repeats for two additional connection configurations:

1. Trial 2: Connects both data/power lines *and* both fluid quick-disconnects (4 total connections).

2. Trial 3: Connects all 6 simulated interfaces (data, power, 2 fluid, 2 airflow).

After completing all three trials on one shelf level, an assistant transfers the rack's connection board to the middle shelf, and the subject repeats the entire process for the remaining levels. Once all levels are tested with the first payload, the payload connection board is swapped to the second smaller payload, and the full procedure is repeated across all rack heights.

The dry-land run-through took place the night before the underwater testing and served primarily to establish baseline data and refine testing procedures. The data collected was how long it took for the subject to make the mechanical connections, the total installation time, and the total disconnect time, much like the underwater testing; however, due to the secondary nature of this testing, TLX data was not included. This run-through allowed us to adjust our testing procedures in preparation for the underwater testing; most notably, the dry-land testing required the subject to hand-tighten the bolts to complete the mechanical connection. This was done to more accurately simulate an actual installation procedure, which would require securing the payload to the shelf. However, due to limited time for the underwater testing and to combat the difficulties of working underwater, this was adjusted to simply placing the bolts within the holes and slightly tightening them – it was left to the test subject's discretion to decide what this meant. This was also where we determined the official start and end criteria for each trial - we decided that, in order to compare how easy or difficult it was to slide out the shelves at different heights, the test should start when the shelf was pulled out and end when it was returned to its original position.

3.5.6 Results - Colin Keller & Allison Rahr

The task load index data shown was done on a scale from 0-7 with zero being the worst and seven being the best. This will be referred to as "TLX" in this section.

Beginning with the highest shelf in our rack, this shelf height seemed to require the most effort, while also causing a fair amount of frustration. Although performance does not appear poor on paper, this shelf height has been deemed quite difficult to work with.

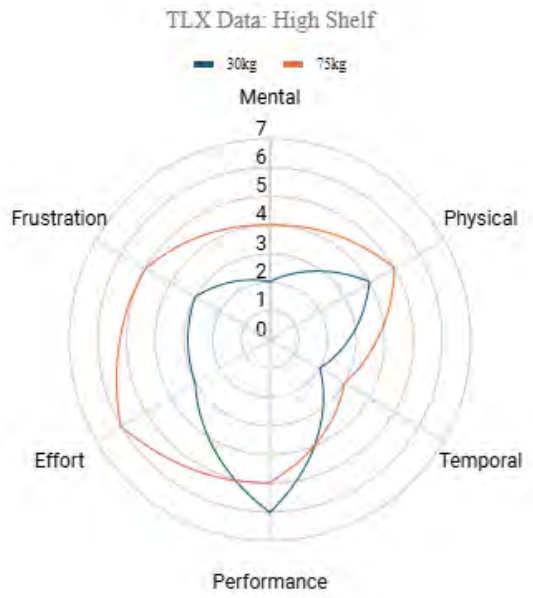

Figure 66: High Shelf Single Subject TLX Data

Shelf Height:	Payload Size:				
High	Large			Small	
Number of Connections:	Mechanical Connection Time	Total Installation Time	Total Disconnect Time	Mechanical Connection Time	Total Insta
2	0:48	1:14	1:11	0:53	1:
4	1:19	3:00		0:43	1:
6	1:00	1:54		0:43	1:

Figure 67: Underwater Testing High Shelf Data

Our subject stated that they had a difficult time getting the payload to this height. For starters, the larger payload was found to be immensely heavy and required quite the amount of effort to lift from ground height to the top shelf. The time taken for the 2, 4, and 6 connections made was the longest at this shelf height, averaging 121.7 seconds for the large payload. The smaller payload took an average of 76 seconds similarly. Once the payload was at this height, it was not entirely difficult to conduct these tests and make mock connections. The subject was able to move around the payload easily, had ample room, and was not caught in any extremely awkward positions that were necessary to complete the given tasks.

Now, on to the middle shelf. This shelf was found to be the preferred shelf. Low frustration levels, high performance, low effort, and minimal mental strain made this shelf the easiest to work with by far.

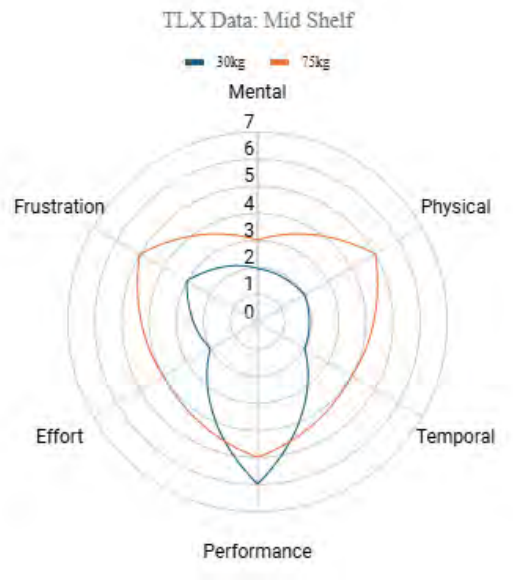

Figure 68: Middle Shelf Single Subject TLX Data

Shelf Height:	Payload Size:					
Middle	Large			Small		
Number of Connections:	Mechanical Connection Time	Total Installation Time	Total Disconnect Time	Mechanical Connection Time	Total Installation Time	Total Disconnect Time
2	1:01	1:28	0:59	0:39	0:44	
4	0:55	1:25	0:58	0:38	0:48	
6	0:53	1:34		0:32	0:58	

Figure 69: Underwater Testing Middle Shelf Data

Our subject was able to maneuver quite well when working on this shelf compared to the highest shelf. The average times for the 2, 4, and 6 connections made for the large and small payloads were 89 and 50 seconds, respectively. Right away, it is quite clear that this shelf took significantly less time to complete the required connections than the highest shelf. Granted, this could be due to a slight learning curve, but nonetheless it is still a noticeable difference. It is important to note that it still required a decent amount of physical strain to get the large payload to this height, but the amount of physical strain decreased with each subsequent level on the rack.

Finally, we have our bottom shelf. Although you may think that this shelf height would be the easiest, it turns out that was not the case. At this height, our subject found that it was easier than the highest shelf, but harder than the mid shelf, as for some connections or maneuvers, they had to lay down or balance on their elbows to complete tasks. The two trials on the lower shelf showed similar frustration in both payload sizes and exhibited the lowest performance metrics.

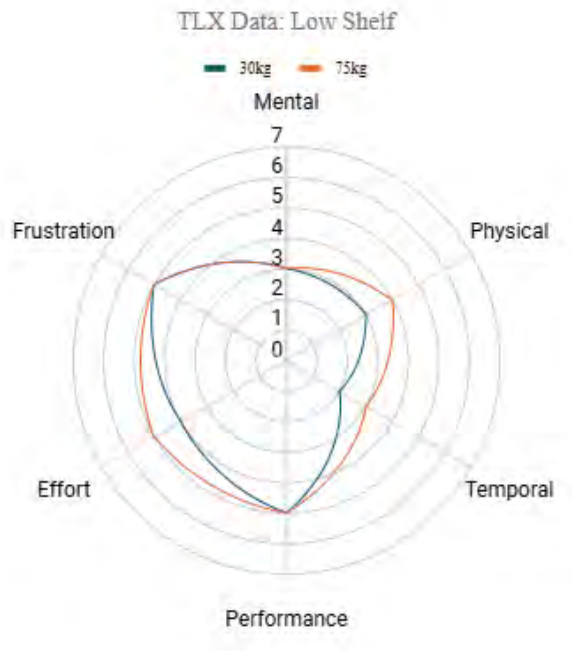

Figure 70: Low Shelf Single Subject TLX Data

Shelf Height:	Payload Size:					
Low	Large			Small		
Number of Connections:	Mechanical Connection Time	Total Installation Time	Total Disconnect Time	Mechanical Connection Time	Total Installation Time	Total Disconnect Time
2	1:14	1:25		0:44	0:51	
4	1:02	1:45		0:38	0:50	
6	1:14	1:46		0:37	0:54	

Figure 71: Underwater Testing Low Shelf Data

As for the average times for the 2, 4, and 6 connections made for the large and small payloads, they came out to 98.7 and 51.7 seconds, respectively. With this being the third shelf height to be tested, and a learning curve in mind, it is apparent from this data that this shelf was far from the most ideal.

There are several key takeaways from our simulated data. To start, there was not a significant difference between the number of connections made and the time taken for the complete installation of either payload(s). The driving factor for the total installation time happens to be the actual payload size. Furthermore, the middle shelf provided the best access for payload maintenance, had the best performance metrics, and had the fastest average time for connections made on the payloads.

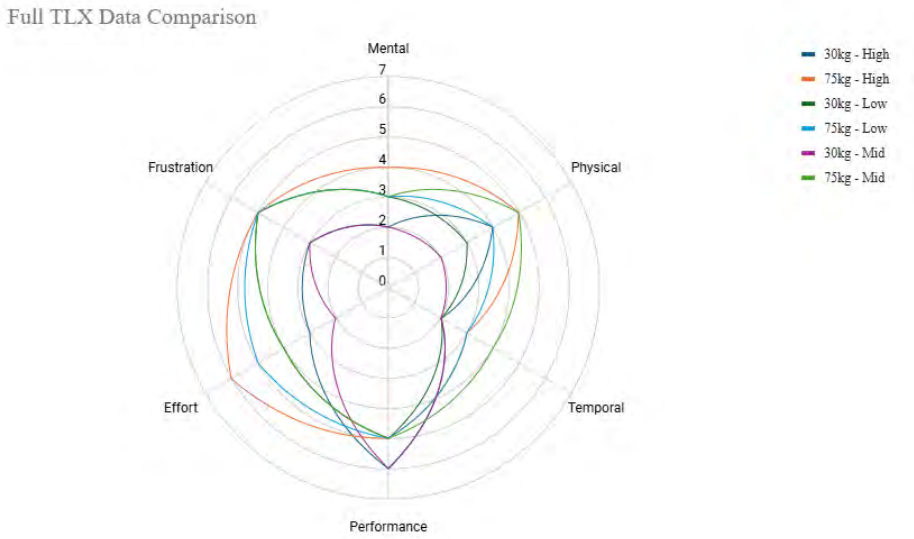

Figure 72: Full TLX Data Comparison

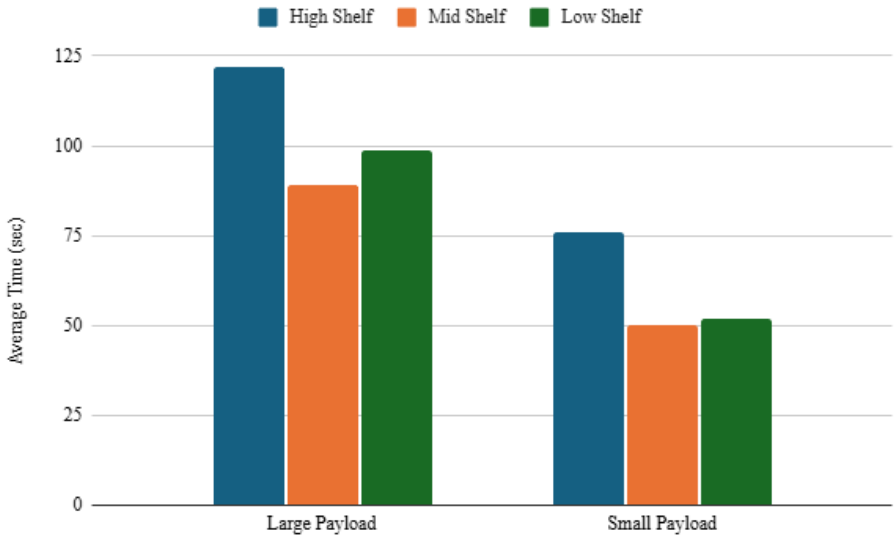

Figure 73: Average Connection Time vs Shelf Height

The results of the dry-land run-through indicated that, predictably, the smaller payload was much easier to maneuver than the larger one. The average time it took for the test subject to lift the payload and complete the mechanical connections across 9 trials each at all shelf heights was 90 seconds for the larger payload, compared to 59.2 seconds for the smaller payload. It's possible that the learning curve may be factoring into this difference, given that the subject performed the trials with the larger payload first; they may have taken some time to adjust to maneuvering the larger payload, which would have made the smaller, lighter payload comparably easier. However, the subject's first trial on a new shelf height was generally noticeably longer than the other two trials at that height with that size payload. Furthermore, times for mechanical connections were not

unanimously shorter for the smaller payload, indicating that the learning curve was only noticeably observable on a small scale (at the start of each new shelf height/payload size trial), not across all trials.

Shelf Height:	Payload Size:					
High	Large			Small		
Number of Connections:	Mechanical Connection Time	Total Installation Time	Total Disconnect Time	Mechanical Connection Time	Total Installation Time	Total Disconnect Time
2	1:54	2:05	0:46	1:17	1:26	0:47
4	1:26	2:13	1:09	0:57	1:18	0:43
6	1:27	2:08	1:12	0:53	1:27	0:45

Figure 74: Dry-land Testing High Shelf Data

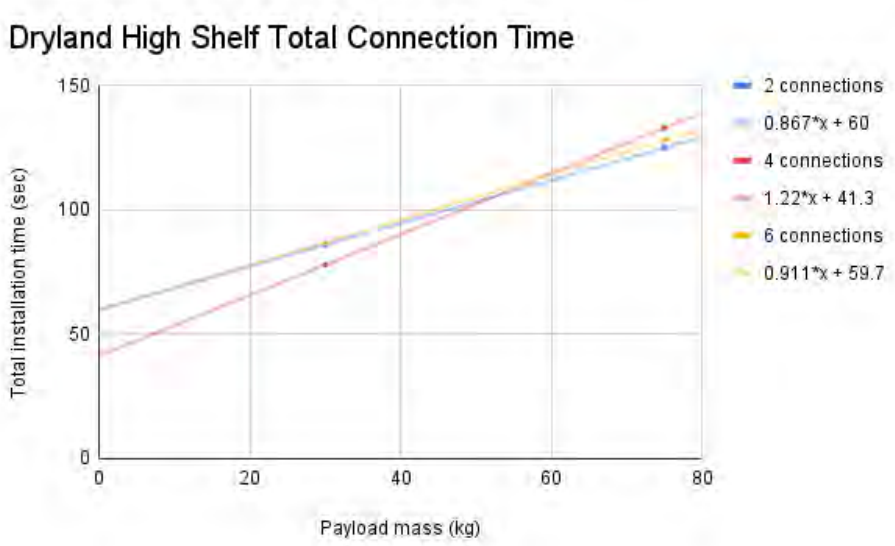

Figure 75: Dry-land Testing High Shelf Total Installation Time

When the dry-land run-through moved to the middle shelf, both the time to make the mechanical connections and the time to complete the installation decreased. The middle shelf had the fastest average total installation time for both payloads, with 105 seconds for the larger payload and 72 seconds for the smaller payload.

Shelf Height:	Payload Size:					
Middle	Large			Small		
Number of Connections:	Mechanical Connection Time	Total Installation Time	Total Disconnect Time	Mechanical Connection Time	Total Installation Time	Total Disconnect Time
2	1:20	1:32	0:49	1:01	1:08	0:28
4	1:14	1:34	1:14	0:54	1:11	0:28
6	1:35	2:10	1:11	0:47	1:18	0:36

Figure 76: Dry-land Testing Middle Shelf Data

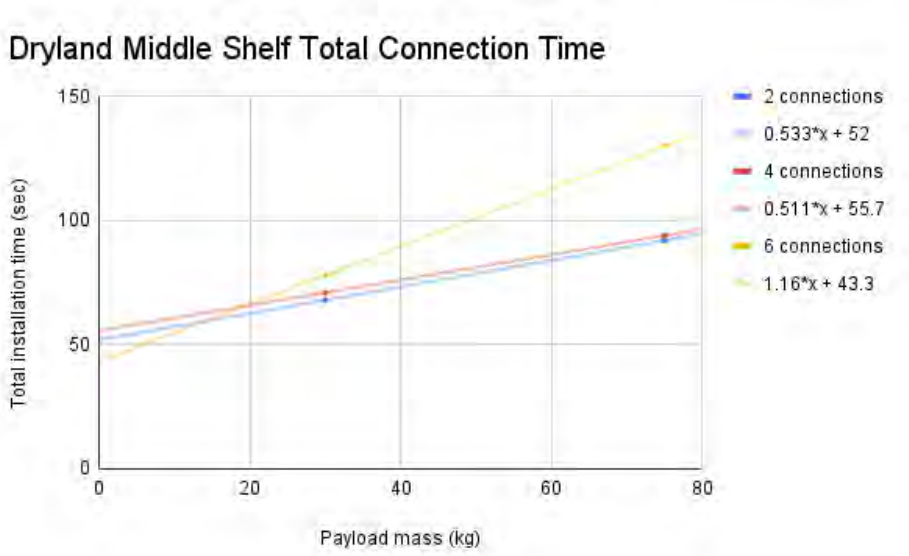

Figure 77: Dry-land Testing Middle Shelf Total Installation Time

On the lowest shelf, times were comparable to those for the highest shelf. Though it required less effort for the subject to move the payload onto the shelf, it was more inconvenient to reach the connections, which made the total time longer.

Shelf Height:	Payload Size:					
Low	Large			Small		
Number of Connections:	Mechanical Connection Time	Total Installation Time	Total Disconnect Time	Mechanical Connection Time	Total Installation Time	Total Disconnect Time
2	1:48	2:04	43.7	0:55	1:02	0:23
4	1:40	1:54	43.1	0:55	1:11	0:31
6	1:08	1:33	43.7	1:14	1:38	0:29

Figure 78: Dry-land Testing Low Shelf Data

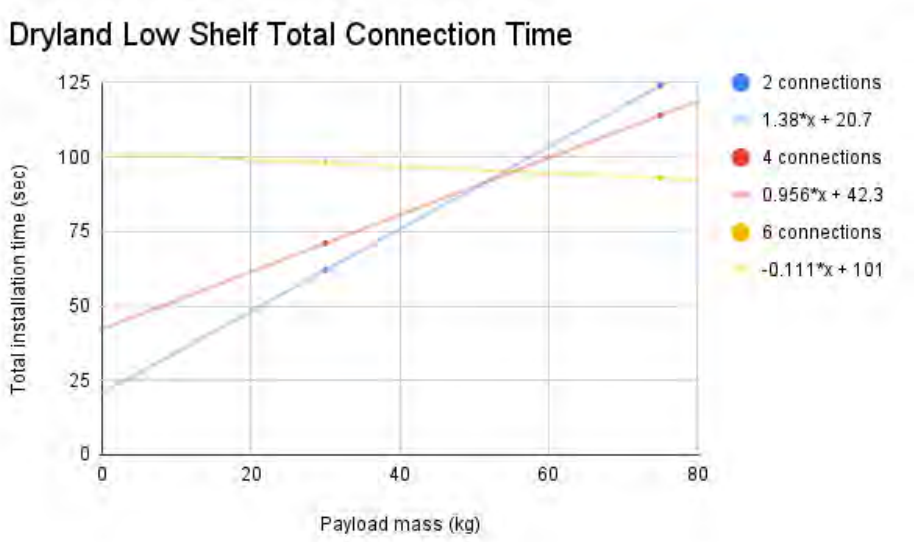

Figure 79: Dry-land Testing Low Shelf Total Installation Time

3.5.7 Analysis and Conclusions - Allison Rahr

Unfortunately, due to technical difficulties during the underwater testing, we were unable to collect consistent data for disconnect times. We were depending on underwater cameras to record these trials, as communication between the diver and the surface was difficult and we were constrained by time, but the cameras prioritized recording installation and, as such, often were not turned on to observe the removal process. Please note that while the values we were able to collect for disconnect times are included in the raw data tables for the sake of completeness, they are no graphical representations due to lack of data points.

The underwater testing was hindered by communication issues. It was often difficult for people on the deck to hear and understand the diver, and vice versa. For this reason, TLX data was not collected until *after* all of the trials had been completed and the diver had exited the water, not immediately after each trial. We recognize that this could skew the results, given that there is a possibility that he was unconsciously comparing the trials and/or mixing them up. In order to reduce the likelihood of this happening and avoid confusion, this is also the reason that TLX data was only collected for trials that used the maximum number of connections (6), with the assumption being that trials with all 6 connections would provide a more complete insight than just 2 or 4.

There were also mechanical issues present - several of the shelves only had 3 holes drilled for the mechanical connections, not 4. Though this did not cause direct problems during the underwater testing, and was at least consistent with the dry-land run-through, we do recognize that this could, however minutely, affect the timing and/or TLX data.

The components used to simulate the data/power, fluid, and airflow connections were also suboptimal for this test, mainly due to their length. We were limited in our available supplies, and while these materials were, in our opinion, adequate to mimic different connection types and difficulties, the actual cables/hoses/ducts were long enough to be inconvenient for the trials. Their

length made it easy for them to get in the way of the shelves sliding in and out and get stuck behind the shelves. There was more than once instance of the diver struggling with the connections being unwieldy, which meant that certain trials took longer while he fixed them.

Similarly, the mock payloads also had design flaws. The attached water jugs were not secured well enough, specifically in the larger payload, and it was common for the diver to accidentally knock them askew when carrying out the trials. When this happened, the diver would often stop mid-trial to fix them, presumably thinking that it would be faster to just fix the issue immediately than have to do redo the entire trial on limited time. However, this did noticeably affect the time in certain trials when he had to stop. There were other structural issues with the mock payloads, including the larger payload's PVC pipes coming apart at one of the corners during one trial, and the payload panel's Ethernet outlet coming loose, the latter of which was not immediately fixed but continued to be a hindrance during multiple trials. We were not aware of these issues during the testing, though the Ethernet outlet was fixed on the surface during the switch between the larger and smaller payloads.

Overall, we were satisfied with our models for both the payloads and their connection points, especially given the limited time and materials we had to produce them. The mock payloads themselves were, in terms of weight and volume, adequately representative of the life support systems they were designed after, and the mock connections provided a spread of different types of interfaces that may be required between the rack and the payload, which allowed us to test the maneuverability and serviceability of these payloads. We also feel that our testing procedure was well-designed and collected useful data. Nonetheless, there were some glaring issues in both the hardware and the testing process that we acknowledge may have skewed our results, especially given that only one trial was conducted for each set of variables.

The diver indicated via TLX data and interview that the highest shelf was the most difficult to install the payload. He rated it a 6 out of 7 on the TLX Effort metric, indicating that he felt it took a significant amount of work to complete the trial. He noted in the interview that, especially with the larger, heavier payload, it was hard not to slam it down on the shelf. The diver also noted that, on the higher shelf, it was more difficult to see both the guiding marks for the mechanical installation as well as the connection ports. With this in mind, we recommend that higher shelf heights are not used for especially fragile payloads and/or ones that require frequent maintenance, as repeated removal and re-installation would be difficult and could cause damage if the astronaut is not extremely careful. His Frustration as well as his Effort metrics did significantly decrease when this trial was executed with the smaller payload, indicating that a top shelf could be a good placement for a lighter, more easily maneuverable payload. While we still wouldn't recommend it for regularly accessed payloads, reducing the weight would eliminate many of the concerns we have regarding the high shelf. The timing data also supports this, with the average total connection time decreasing by approximately 45 seconds with the smaller payload. It is important to note that there is an outlier in the collected times for the larger payload, stemming from the hardware issues discussed above; however, even when this value is removed, there is still a difference of 18 seconds between the two payloads, indicating that the smaller payload is, predictably, easier to install.

The middle shelf was found to be the most convenient shelf for installation and removal of the payloads. At this height, the diver did not have to work as hard to lift the payloads as he did for the higher shelf, and he described it as being much easier to see where the payload was supposed

to go and the mock connections. Our recommendation is that this shelf would be best suited for payloads that require routine removal and re-installation. In general, our assessment is that, for payloads that fit this criteria, the smaller the better, regardless of shelf height; however, we recognize that this will not always be feasible. In that scenario, the middle shelf would be optimal for those payloads since it is easier for the astronaut to lift and maneuver the payload than on the top shelf. Of the 3 shelves, the diver gave the middle shelf a lower Effort score than the other two in regards to the large payload trial, supporting this hypothesis.

The diver admitted that the lower shelf was by far the easiest to lift the payload onto, understandably, but noted that it was inconvenient to have to lean down to secure it and make the connections. He indicated that not having to work as hard to move the payload wasn't worth the added effort that came with completing the connections at this height. Notably, this was the only shelf height where the diver gave the same Frustration score for both payload sizes. Our recommendation is that a lower shelf would be optimal for a heavier payload that does not require frequent removal and re-installation. If the payload is difficult to move or has fragile parts, keeping it on a lower shelf would remove some of the risks of installation, both to the payload and the astronaut; however, since it has been established that making the connections at this level is inconvenient, this shelf would be best suited for a payload that would remain installed most of the time.

Though we were not able to collect enough data about disconnect times during the underwater testing to provide a thorough analysis, from what few data points we have as well as our experience with the dry-land run-through, we can comfortably say that it usually took less time for the subject to remove the payload and install it. There weren't any significant complications relating to disconnection in particular, and the installation process was generally more difficult and time-consuming. The astronaut should, however, be careful not to drop the payload or slam it down on the ground during removal, especially when dealing with a higher or middle shelf.

While the subjects expressed frustration as well as preferences for different shelf heights, it is important to note that there was no trial, either during the dryland run-through or the underwater testing, where the subject was physically unable to complete the task. In theory, either size payload could comfortably be stored on any shelf height and, if necessary, be removed and replaced with minimal inconvenience; these are simply recommendations for the safety of the astronaut and the integrity of the payload based on our data.

3.6 Corridor and Corner Testing

3.6.1 Purpose - Benjamin Leazer

During an early design review, NASA Marshall reviewers expressed their interest in how the dimensions of the rack might influence habitat layout decisions (MPA-10). Additionally, NASA-STD-3001, Vol. 2, Rev. D states that the habitat "shall provide intravehicular activity (IVA) translation paths that allow for safe and unencumbered movement of suited and unsuited crew and equipment" (V2 8013 – requirement code) (NASA, 2023). The standard further notes that the dimensions of such pathways should be informed by a comprehensive task analysis. Although conducting a full task analysis was beyond the scope of this project—since the team was not responsible for habitat design—it was still appropriate for the team to investigate the minimum corridor width necessary to maneuver the rack.

Initially, the team attempted to address this requirement through simulation. However, it became evident that while simulations can be useful in estimating global minimum constraints, they fail to capture the human factors involved in physically maneuvering a rack through a confined corridor or around a corner.

3.6.2 Objective - Sofia Correia

During both rack installation and end-of-life operations, astronauts will be required to transport the rack through the habitat. This includes maneuvering through corridors and around corners, which presents spatial and ergonomic challenges. The solicitation document provided to the team included three conceptual habitats; however, these references contained limited dimensions.

Since the rack design had already been finalized, the objective of the corner and corridor testing was to determine the minimum corridor width required to safely accommodate the rack as it is carried by two astronauts, one positioned on either side. The primary constraint driving the minimum width was the ability to navigate a 90-degree corner without compromising the safety of the astronauts or integrity of the habitat walls. The goal was to identify a corridor width that allows the maneuver without risk of collision with the walls of the corridor.

3.6.3 Simulation - Benjamin Leazer

A simulation was conducted in Matlab to estimate the absolute minimum corridor width required for the rack to successfully navigate a 90-degree turn (MPA-11). As mentioned previously, while simulation was a useful tool for identifying an appropriate minimum width, it could not account for the human factors associated with maneuvering the rack, thereby underscoring the need for physical testing to validate feasibility. The two-dimensional simulation was broken into three discrete phases: (1) the rack translated through a horizontal corridor, (2) the rack pivoted in a circular arc about the inner corner of a 90-degree turn, and (3) the rack continued through a vertical corridor with an equivalent width as the initial horizontal segment.

Two rack orientations were analyzed, both of which utilized the double rack design. The first represented the orientation required to pass through the hatch without additional rotation. This orientation was prioritized because it aligned with the rack's configuration during mass testing and minimized handling complexity. However, it necessitated a wider corridor to accommodate turning. The second orientation represented the global minimum corridor width achievable but required rotating the rack after hatch entry.

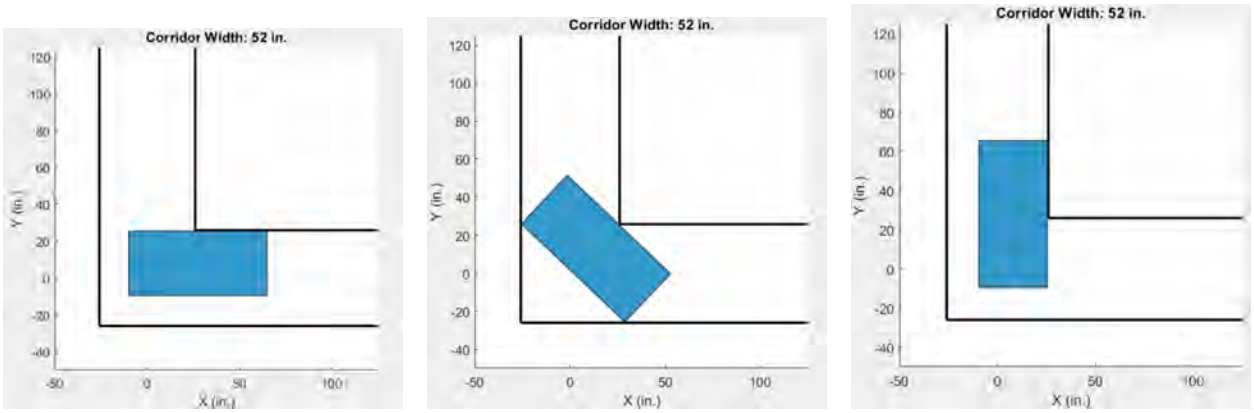

Figure 80: Orientation 1 Simulation — Dimensions: 1.91 m x 0.90 m

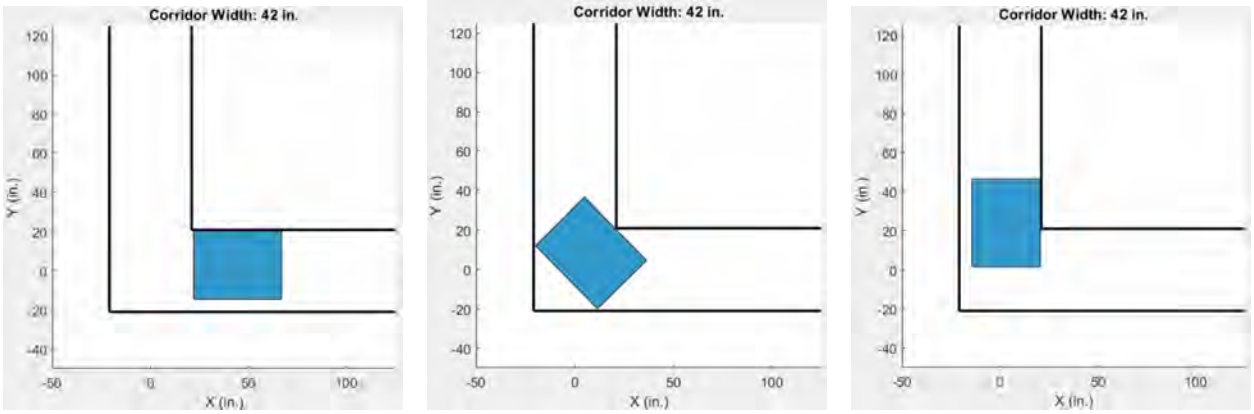

Figure 81: Orientation 2 Simulation — Dimensions: 1.16 m x 0.90 m

The first orientation was selected for physical testing, as it matched the configuration used in underwater and dry land trials. The second orientation was not tested due to concerns about practicality and safety. Specifically, in that configuration, the rack's center of gravity was approximately three feet above ground level, creating a potential tipping hazard when using lifting straps. The team deemed that the elevated center of mass posed risks to both crew and surrounding equipment, making repeatable transport in this orientation infeasible.

In the tested orientation, the rack dimensions were 1.91 m x 0.90 m, resulting in a simulated minimum corridor width of 1.32 m (52 in) for successful corner navigation. In the alternate orientation, the rack dimensions were 1.16 m x 0.90 m, leading to a reduced minimum corridor width of 1.07 m (42 in).

3.6.4 Setup - Benjamin Leazer

The corner testing was conducted in an open space on the top floor of the NBRF at SSL. Four pre-built 80/20 framework structures were used along with corrugated plastic sheets, which were secured to the frameworks using zip ties. These assemblies functioned as the simulated "walls" of the corridor environment.

Rather than using a full corridor, the team focused on replicating the corner section, as this represented the most likely failure point during transport. Each framework structure was rotated onto its side, and two structures were used to form each vertex of the corner: two to simulate the "inside corner" and two for the "outside corner".

Once the wall structures were placed in their approximate positions, a measuring tape was used to calibrate the setup. For each trial, four measurements were taken to confirm the course alignment and ensure consistent corridor width. Two measurements were taken near the corner vertex itself, and two additional measurements were made along the adjoining corridor paths to verify proper alignment and spacing of the simulated walls.

3.6.5 Safety Procedures - Sofia Correia

Standard safety procedures were implemented during the corridor testing, along with specific modifications to the course to minimize risk to the participants. All subjects retained the right to terminate a trial or withdraw from testing at any time, for any reason. Trials were classified as failures if a subject expressed discomfort or lack of confidence in their ability to safely and effectively complete the course.

To reduce the risk of injury during testing, the simulated corridor was constructed using 80/20 aluminum frameworks positioned on their sides. To replicate the spatial constraints of a lunar habitat corridor while ensuring test subject safety, corrugated plastic panels were affixed to the interior sides of the frameworks. This material was selected for its ability to flex under pressure while maintaining structural integrity, reducing the likelihood of injury in the event of accidental contact. Considering the risk that subjects' hands and fingers could at one point be trapped between the rack and the wall, it was important to choose a material that would represent the habitat walls, while still flexing if pressure were applied without injuring the subject. Corrugated plastic provided a safer option as a flat, semi-flexible surface that simulated a rigid boundary without posing the same hazard as metal or hard paneling.

3.6.6 Testing Procedure - Sofia Correia

The rack was initially positioned at one end of the course, oriented horizontally and ready to be lifted. Two subjects aligned themselves with the rack, standing on opposite sides such that the height of rack was between them. Upon the start of the trial, subjects lifted the rack and carried it through the simulated corridor.

If the subjects were able to successfully navigate the full length of the course and complete the 90-degree turn, the trial was deemed a success. The rack was then returned to the starting position, and the width of the corridor was reduced in preparation for the subsequent trial. If the subjects did not feel confident in their ability to safely complete the turn, or if the rack could not be safely maneuvered through the corner, the trial as considered a failure. In this case, the corridor width from the previous successful trial was recorded as the minimum viable corridor width. The initial corridor width was 1.52 meters (60 inches), and the narrowing increments were determined based on subject feedback and observed performance.

Figure 82: Subjects successfully carrying the rack through a corridor of 1.45 meters

3.6.7 Assumptions - Sofia Correia

For this test, several simplifying assumptions were made regarding the environment, equipment, and participants. Due to limitations in available personnel, it was assumed that the test subjects present were sufficiently representative of the physical stature, strength, and mobility of the average trained astronaut. The mock was structures used to simulate the habitat corridors and corners were assumed to accurately reflect the spatial constraints of a lunar habitat. The rack used in testing was weighted using fewer, symmetrically distributed weights; however, it was assumed to sufficiently represent the handling characteristic and maneuvering capabilities of the final weighted rack. Lifting straps were intentionally excluded from testing to simulate the most conservative scenario, where two astronauts are lifting the rack without lifting assistance. It was assumed that if the rack could be safely carried and maneuvered under these conditions, the use of lifting aids would only improve performance. These assumptions enabled the ream to isolate and analyze geometric and ergonomic constraints involved in transporting the rack through the habitat.

3.6.8 Testing Results - Sofia Correia

Test results showed that the most realistic corridor width for successful rack transport was 1.45 meters (57 inches). At this width, two subjects were able to carry the rack around the 90-degree corner with minimal wall contact and low risk of hand entrapment or structural damage to the habitat (Fig. 82). The test began at a corridor width of 1.52 meters (60 inches), which posed no difficulty for the subjects. The corridor was then incrementally narrowed to the resulting 1.45 meters. Although the rack itself physically fit withing a 1.37-meter (54 inch) corridor, subjects were unable to navigate the corner while carrying the rack (Fig. 83), resulting in a trial failure. Subjects felt unsafe maneuvering the rack through corridors narrower than 1.45 meters, citing a high risk of hand entrapment between the rack and the wall, as well as in increased likelihood of damaging the walls.

Figure 83: Subjects failing to carry the rack through a corridor of 1.37 meters

Conclusion

The 1.45-meter corridor provided sufficient clearance for a crew member to pass alongside the rack while it is positioned in a hallway, an important consideration in operational safety within the lunar habitat. Based on subject feedback, physical feasibility, and safety assessments, 1.45 meters was identified as the minimum viable corridor width for safe and efficient rack transportation.

3.7 Future Testing

3.7.1 Rack Installation and Gravitational Environments - Sofia Correia

Given additional time and resources, further testing would focus on evaluating the installation of the rack in a representative lunar habitat. This test would aim to identify any spatial, ergonomic, or operational restrictions on rack installation across potential locations within the habitat.

The test would explore and compare multiple installation methods, evaluating their effectiveness based on subject effort as well as rack stability and integration with existing habitat infrastructure. A goal of the tests would be to identify potential structural attachment points and validate procedures for power and data connections in realistic conditions. Testing could be extended to compare installation performance in rigid versus inflatable habitats, to assess how differences in structure and internal layout would impact installation feasibility.

Installation tests would initially be performed outside the NBRF to refine procedures and collect preliminary data to inform the underwater tests. These procedure would then be validated under simulated lunar gravity conditions within the tank to assess astronaut maneuverability during the mission.

Looking beyond lunar applications, a progression of these test would include adapting and repeating both installation and maneuverability testing under simulated Martian conditions. This would include conducting additional underwater mass handling test to evaluate astronaut performance in the higher gravity environment of Mars, as well as in microgravity, further validating the

rack's versatility across various gravitational environments.

These additional tests would improve confidence in the operational readiness of the rack and ensure its adaptability to a range of habitat configurations and mission environments.

3.7.2 Extended Hardware Testing - Rachel Boschen

While the payload rack has already been tested to validate critical design details, more tests are needed to be ready for flight. The extended hardware testing phase encompasses a critical set of evaluations aimed at verifying the payload rack's physical performance and durability in conditions representative of spaceflight and extraterrestrial surface operations. These tests go beyond initial prototyping and focus on validating the system for deployment in real mission scenarios, where environmental stressors, mechanical loads, and habitat compatibility pose significant engineering challenges. Hardware testing primarily assesses tangible physical elements, such as structural materials, mounting mechanisms, and environmental resilience, to ensure the rack can withstand the rigors of launch, surface deployment, and long-term use on the Moon or Mars. Although the following sections outline key testing efforts, such as structural integrity, thermal resilience, and habitat integration, they are not comprehensive. Instead, they represent the most pressing additional validations needed before the payload rack could be considered flight-ready. Further testing will be required to meet the full suite of safety, mission assurance, and performance standards defined by spaceflight certifying agencies.

3.7.3 Structural Integrity and Durability - Rachel Boschen

To ensure the payload rack is suitable for long-term missions in partial gravity environments, a comprehensive suite of structural integrity and durability tests must be conducted. These evaluations are intended to confirm that the rack can withstand the mechanical stresses associated with transportation, deployment, and daily use on lunar and Martian surfaces. Central to this testing is vibration analysis, which will be performed using a shaker table to simulate the intense loads experienced during launch and landing procedures. These tests will help identify any structural weaknesses or resonant frequencies that could compromise the payload's safety. In addition to dynamic testing, static load tests will apply various forces representative of 1/6g and 1/3g conditions to verify the rack's strength and stability under different gravitational loads. These scenarios will ensure the rack maintains structural integrity whether used on the Moon or Mars. Another critical component of testing involves thermal cycling to reflect the extreme environmental conditions of extraterrestrial surfaces. The rack will be subjected to temperature swings from -180°C to 127°C (for lunar conditions) and -125°C to 20°C (for Martian environments) to determine the materials' resilience, bonding integrity, and potential for thermal fatigue. Successful completion of these tests will validate the payload rack's capacity to perform reliably throughout mission durations that involve variable loads, harsh temperature extremes, and repeated handling by astronauts and robotic systems.

3.7.4 Compatibility with Habitat Interfaces - Rachel Boschen

Verifying that the payload rack integrates seamlessly with various habitat interfaces is essential for mission success, particularly as future surface habitats will likely include a mix of rigid and inflatable structures. This testing phase will focus on ensuring the rack's compatibility with existing and planned interior configurations. Interface testing will involve using full-scale mock-ups of habitat sections to evaluate the rack's ability to align accurately and attach securely to walls, floors, or modular systems. Proper alignment is critical not only for safety but also for optimizing available space within confined habitats. Additionally, testing will assess whether the rack can be deployed, repositioned, or reconfigured easily to adapt to changing mission requirements or crew preferences. Mobility and modularity are especially valuable in environments where efficient use of space and adaptability to scientific or logistical payloads are necessary. These evaluations will involve repeated attachment and detachment cycles to simulate maintenance and daily use scenarios. Through these tests, potential issues such as mechanical mis-alignments, wear and tear at mounting points, or difficulty in manipulating the rack with gloved hands can be identified and resolved. The outcomes will help refine the design for better operational integration and ensure the payload rack supports flexible mission architectures on both the Moon and Mars.

3.7.5 Long-Term Containment and Payload Support - Rachel Boschen

The payload rack's ability to preserve the integrity of stored payloads during long-duration missions is a critical consideration for supporting scientific experiments and essential logistics. To address this, a series of environmental simulations will be conducted in controlled chambers designed to replicate habitat interior conditions, including oxygen-rich atmospheres and consistently low humidity. These chambers will help assess the rack's materials and construction methods for compatibility with sustained exposure to such atmospheres, preventing degradation, corrosion, or material fatigue over time. Additional tests will include vibration and isolation evaluations to ensure payload stability during normal surface operations, such as rover movements or astronaut interactions. These disturbances, while minor compared to launch vibrations, can accumulate over time and potentially affect sensitive scientific instruments or stored supplies. The goal is to verify that the rack provides sufficient damping and isolation to safeguard payloads from micro-shocks or constant low-level movement. Such testing will also reveal any weaknesses in the containment strategy—such as fasteners, restraints, or internal supports—that could lead to payload shifting, damage, or exposure. Altogether, this test phase will confirm the rack's capacity to maintain environmental control and physical security over extended periods, ensuring mission-critical materials remain stable and functional throughout the mission life-cycle.

3.7.6 Extended Software Testing - Rachel Boschen

The extended software testing effort complements the physical evaluations by focusing on the digital systems that enable automation, crew interaction, and adaptive functionality of the payload rack. Software testing ensures that the system's embedded electronics, user interfaces, and fault management protocols perform reliably under mission conditions, including autonomous operation, time-delayed control, and system fault recovery. Unlike hardware testing, which examines tangible performance under stress, software testing evaluates logic, control processes, and digital

reliability—elements that are often invisible but critical to mission success. The tests described here—including interface usability, simulated mission scenarios, and failure recovery—represent essential next steps in preparing the payload rack for integration into a crewed space environment. These highlights are not an exhaustive checklist but are representative of the advanced software validations needed to bridge the gap between prototyping and flight certification. Additional testing will be required to ensure full compliance with mission-specific software assurance standards.

3.7.7 Control Systems and Interfaces - Rachel Boschen

To support autonomous operation and reduce crew workload, the payload rack incorporates a range of automated control systems and digital interfaces that must be rigorously validated. This testing will ensure that all embedded systems—such as those managing environmental conditions like temperature and pressure—operate reliably under expected mission parameters. Functional testing will verify each system's responsiveness, accuracy, and resilience to fluctuations in power or communication delays. These systems must be tightly integrated with the larger habitat infrastructure, particularly for power, telemetry, and monitoring. In parallel, usability testing of the rack's software interfaces will be performed with human-in-the-loop simulations. These tests will measure how intuitive the user interface is for crew members, especially when wearing gloves or working in reduced lighting or time-sensitive scenarios. Emphasis will be placed on ensuring that all status displays, command functions, and feedback loops are clear and efficient, minimizing the cognitive load on astronauts. Human factors considerations—central to the project's mission—will guide the iteration of interface layouts and operational flow. The objective is to create a seamless and ergonomic user experience that supports both autonomous function and manual control when necessary. These tests will ultimately demonstrate the robustness and crew-compatibility of the rack's digital systems under realistic operational conditions.

3.7.8 Operational Simulations - Rachel Boschen

Testing the operational capabilities of the payload rack in realistic mission scenarios is vital for verifying its adaptability and performance. This will involve a series of simulations that replicate typical and edge-case situations on lunar and Martian missions. These simulations will explore various payload configurations, assessing how well the rack adjusts to different weights, volumes, and operational constraints. Scenarios might include storing scientific instruments, biological samples, or logistical supplies, each with unique handling and environmental requirements. The simulations will also incorporate mission time delays, such as those expected during remote operations from Earth to Mars, to evaluate the effectiveness of asynchronous control systems. This will help determine how the rack behaves under delayed commands and how well it can queue or autonomously manage tasks. Software performance, such as response to sensor feedback or task execution timing, will be carefully monitored. The objective is to ensure the system can operate effectively even when human input is delayed or unavailable. Operational simulations provide a holistic view of the payload rack's performance and allow iterative refinement of software, hardware, and crew procedures. These tests are essential to confirming the system's readiness for deployment in complex, real-world mission contexts.

3.7.9 Failure Recovery - Rachel Boschen

Given the high-stakes nature of extraterrestrial missions, the payload rack's ability to detect, diagnose, and recover from failures with minimal crew involvement is a critical design requirement. To validate this, extensive failure recovery testing will be undertaken. This will begin with fault injection tests in which simulated software errors are introduced to assess how well the system identifies and responds to anomalies. The diagnostic algorithms will be evaluated for their ability to differentiate between critical and non-critical faults, and for their speed in alerting the crew or initiating autonomous recovery protocols. In parallel, hardware fault simulations—such as sensor outages, motor failures, or communication disruptions—will test the system's ability to continue performing essential functions or fail gracefully without compromising safety. Redundancy mechanisms will be closely scrutinized to ensure they provide seamless transitions and maintain operational continuity. These may include backup power supplies, secondary communication paths, or failover logic in control systems. Testing will also include scenarios in which astronauts intervene manually to override or reset the system, evaluating how accessible and efficient those processes are. This rigorous approach to failure recovery ensures the payload rack is robust enough to operate independently while remaining transparent and serviceable to human operators when necessary.

A Appendix A - Reference Information

A.1 Introduction

A.1.1 Work Breakdown Structure - Dev Shanker

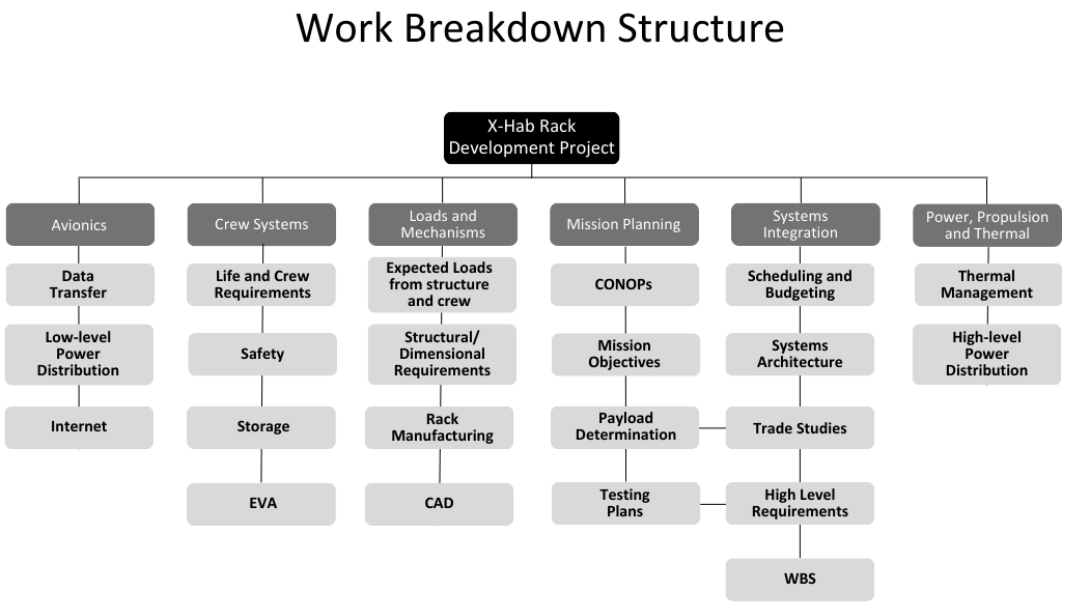

Figure 84: Work Breakdown Structure

The Work Breakdown Structure (WBS) for the X-Hab Rack Development Project is a clear way of organizing tasks and responsibilities for each sub-team, making sure everything is covered systematically. It breaks the project down into six main areas: Avionics, Crew Systems, Loads and Mechanisms, Mission Planning, Systems Integration, and Power, Propulsion, and Thermal. Each of these areas focuses on a critical aspect of the project, making sure nothing important is overlooked.

In this project, the Avionics domain is all about making sure the rack's technology works smoothly. This aspect covers data transfer, low-level power distribution, and internet connectivity, which form the backbone of the rack's electronic systems. This means all components can communicate properly and keep working, whether they're being controlled remotely or used by the crew. Reliable power management is also a must, ensuring that every system on board stays powered without any interruptions. Crew Systems is focused on making the rack safe and user-friendly for astronauts, covering everything from life support and crew safety to storage solutions for EVA (Extravehicular Activity) gear and tools. Loads and Mechanisms (LSM) make sure the rack is

strong and durable, designed to handle the stresses of space without failing, whether it's from crew interactions or external forces.

Mission Planning (MPA) is where the project's big picture comes together. It defines how the rack will be used, its goals, the equipment it needs to carry, and how it will be tested to make sure it works as expected. Systems Integration ensures that all these separate parts work together without a hitch, covering everything from scheduling and budgeting to designing the rack's overall architecture. Finally, Power, Propulsion, and Thermal (PPT) deals with keeping the rack's systems powered, its temperature regulated, and everything running efficiently. By dividing tasks into these focused domains, the WBS makes it easier to manage the project, ensuring that the final product is not just well-built but also reliable, adaptable, and ready for future space missions.

A.1.2 Mission Architecture - Dev Shanker

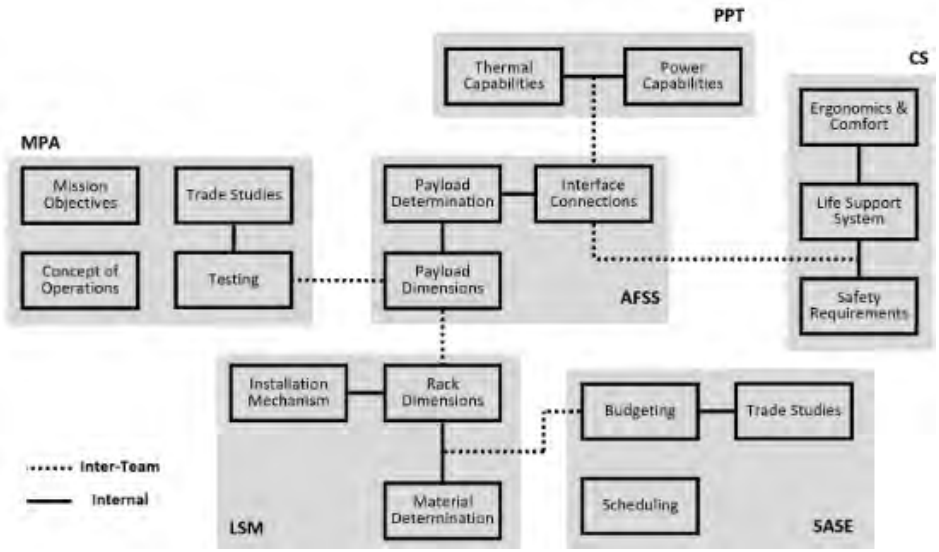

Figure 85: System Architecture

The mission architecture begins with Earth-based design, testing, and integration of a payload rack engineered to operate across microgravity (ISS), 1/6g (Moon), and 1/3g (Mars) environments. These racks must accommodate scientific and logistical payloads while supporting life support interfaces, thermal management, and crew operations. The rack is launched pre-integrated with select payloads, which are subject to mass and volume limits that enable astronauts to transport it under lunar gravity. Launch and surface delivery operations include protective packaging against shock, vibration, and thermal loads.

Once on the lunar surface, the rack is removed from the lander and installed within the habitat. The astronauts then connect the rack to power, data, and environmental systems of the habitat for the use of payload servicing. This ensures mission flexibility and repair-ability over time. The final phase includes commissioning and continuous usage, with provisions for eventual re-purposing or end-of-life disposal.

A.2 Mission Environments

A.2.1 Lunar Environment - Alexa Patnaude

Per the X-Hab documentation as well as our mission statement, the primary intended environment for our rack is the moon

The lunar environment supports short-term surface missions lasting 28 to 60 days, with a typical crew size of 2 to 4 members. Due to the Moon's gravity of 1.62 m/s^2, equipment weight is a moderate concern and must be carefully managed. Resupply missions are only feasible once per year, making it essential to thoroughly plan and allocate all racks, equipment, upgrades, and resources prior to launch. Lunar missions are designed for partial self-sufficiency, capable of operating independently between resupply cycles. These missions serve as critical testbeds for technologies and logistical strategies that may later be used on Mars.

A.2.2 Martian Environment - Alexa Patnaude

Per our mission and vision statements, our rack has adaptability in mind, being able to accommodate both lunar and martian environments.

The Martian environment presents the greatest logistical and operational challenges, requiring a habitat that can autonomously support a crew of four for up to 1200 days. With gravity at 3.71 m/s^2, rack weight is a significant concern. Resupply missions are not feasible during the mission, whether in transit or on the surface, so all supplies must be launched from Earth. This demands precise pre-planning and allocation of racks, spares, and repairs with zero tolerance for shortfalls. Mars missions represent the pinnacle of long-term, deep space exploration and demand complete autonomy in both system design and crew operation.

A.2.3 Rack Number - Nicholas Varro

When looking into the various potential environments of our rack, part of our analysis included investigating the number of racks that could be implemented to properly service each habitat. Knowing the dimensions of the rack, and subsequently its volume, we can roughly estimate the number of rack that could theoretically be implemented into the lunar or Martian habitats. However, unfortunately in our research, due to the low amount of viable information regarding various potential habitats, identifying a specific number of racks proved to be a challenge. Furthermore, since any available information is largely preliminary and not yet concrete, we ultimately decided to forgo further research into the topic of rack number.

A.3 Costing information

A.3.1 Initial Launch Cost Estimations and Analysis - Dev Shanker & Nicholas Varro

An important requirement of our payload rack's design is adaptability with mission environments, specifically in serving both lunar and Martian environments. Due to this, we conducted

analysis on general launch costs to serve as a contextual benchmark. This analysis serves to compare rack production cost to overall launch costs of a particular mission, as well as to explore the potential cost for deploying the rack to the various mission environments.

When looking into launch costs, an important baseline is to explore previous missions to both the lunar and martian environments. Despite information regarding cost of current launch vehicles being largely unavailable, with the exception of SpaceX, we can still utilize data from previous missions to find a generalized trend of decreasing costs for launch as technology continues to evolve. From table 15, we took a look at the budgets of various missions NASA has completed to both the lunar and Martian surface.

Mission Type	**Year**	**Mission Name**	**Cost $M**	**Cost Adjusted $M2025**
Moon	1969	Apollo 11	355	3121
Moon	1969	Apollo 12	375	3297
Moon	1970	Apollo 13	375	3118
Moon	1971	Apollo 14	400	3186
Moon	1971	Apollo 15	445	3545
Moon	1972	Apollo 16	445	3435
Moon	1972	Apollo 17	450	3473
Mars	2011	Curiosity	232.8	334
Mars	2020	Perseverance	243	303

Table 15: NASA Mission Budgets

From the table above, we notice a general trend of decreasing mission costs over time, despite the high, increasing complexity of missions. The Apollo missions, which ranged from $3.121 billion to $3.473 billion (adjusted for 2025), were defined by the high costs of human space exploration, which include extensive life support, crew safety, and the development of the Saturn V. In comparison to the Apollo Missions, the Mars rover missions, Curiosity and Perseverance, exhibit significantly lower costs, at $334 million and $303 million respectively. The reduction of costs here are mainly due to the technological advancements due to robotics, automated mission planning, and cost-efficient launch vehicles. Through using this historical data as a benchmark, our team can better understand the financial impact of deploying the payload rack to lunar and Martian environments, which allow us to refine our design to maintain cost-effectiveness without its mission capability being sacrificed.

A.3.2 Prototype Costing - Nicholas Varro

Table 16 details the projected parts list that was developed by LSM. This list details all of the materials, along with their respective costs, that were expected to be used in construction of the rack. All materials from this list were sourced via 80/20 due to their extensive catalog of various fasteners and modular aluminum systems, along with their reliability from past university projects.

There are 380 parts in total on this list, with costs totaling to $. All costs for table 16 are directly from the 80/20 webpage. This list, while containing materials used to build the rack,

also includes parts to help in the conversion of a single rack to a double rack (or vice-versa) as well as general spare parts. Due to this, not all 380 parts were expected to be physically present on the rack, however all parts were equally important to ensure proper and efficient rack production.

Note: *All listed costs for tables 16, 17, and 18 are taken from late March 2025. Any changes in price due to tariffs or changing economic policies are not reflected in these tables.*

Part ID	Description	Qty	Unit Cost	Total Cost
1515	Beam (1.5'x1.5'x75')	4		
1515	Beam (1.5'x1.5'x73.5')	4		
1515	Beam (1.5'x1.5'x43.5')	4		
1515	Beam (1.5'x1.5'x21')	4		
1515	Beam (1.5'x1.5'x33.5')	6		
4336	Triangle Gusset	28		
4340	Flat Plate 5 Hole	12		
3279	Double Hole T Nut	68		
3285	Triple Hole T Nut	12		
3330	3330 Screw	172		
FL-COU24-100lb	Slider	2		
3005	Bucket Head Socket Cap Screw	32		
3275	Slide-in T Nut	32		
–	**Total**	**380**		

Table 16: Projected Parts List

Part ID	Description	Qty	Unit Cost	Total Cost
4336	Triangle Gusset	28		
4340	Flat Plate 5 Hole	12		
3203	T Nut 5/16-18 Thread	78		
3279	Double Hole T Nut	70		
3285	Triple Holt T Nut	15		
3330	3330 Screw	250		
FL-COU24-100lb	Slider	2		
3005	Bucket Head Socket Cap Screw	32		
3275	Slide-in T Nut	32		
–	**Total**	**519**		

Table 17: Final Parts List

Table 17 presents the final p arts l ist, d etailing w hat w as u ltimately o rdered a nd purchased for production of the rack. The list includes a total of 519 parts, an increase from the originally projected 380. Despite the higher quantity however, total cost was reduced rather significantly to $ from the original $. This cost reduction was largely due to the fact we were able to utilize

repurposed beams from previous projects at SSL, eliminating the need to purchase new material. Along with this, our supplier also changed. We went from 80/20 direct to Rankin Automation, a company that represents various automation companies such as 80/20. With this new supplier, we were able to still order 80/20 materials, but at a discounted unit price which further reduced our spending. Both the reused beam material and supplier change were at the recommendation and guidance of our faculty advisor, and teaching assistants. Rankin Automation is a trusted supplier by the folks at SSL, and since we worked closely with them - orders being placed by Charles Hanner at SSL - we proceeded with them as a supplier.

Furthermore, the increase in total number of parts is largely due to the addition of excess fasteners, particularly with 3330 screws. There was an increase to 250 screws primarily due to the desire to ensure redundancy and avoid any issues in production. This was a strong recommendation from our advisors, and was ultimately incorporated in our order. In regards to tax, we benefited from being a state university, and so our order was tax exempt. Shipping costs were incurred, however there was no specific information on exact amounts as that information was not stated on the order post. However, knowing that beams were not included in the order, and knowing that it would only cost around $ to ship these parts via UPS ground if directly ordered from 80/20, we do not expect the shipping costs to be more than $.

Part ID	**Description**	**Qty**	**Unit Cost**	**Total Cost**
1515	Beam (1.5'x1.5'x75')	4		
1515	Beam (1.5'x1.5'x73.5')	2		
1515	Beam (1.5'x1.5'x43.5')	4		
1515	Beam (1.5'x1.5'x33.5')	4		
1515	Beam (1.5'x1.5'x21')	2		
4336	Triangle Gusset	28		
4340	Flat Plate 5 Hole	8		
3279	Double Hole T Nut	68		
3285	Triple Holt T Nut	8		
3330	3330 Screw	152		
FL-COU24-100lb	Slider	2		
3005	Bucket Head Socket Cap Screw	10		
3275	Slide-in T Nut	10		
–	**Total**	**302**		

Table 18: Prototype Cost

Overall our prototype rack cost $ in total. This total stems from what components actually went into the physical rack not including excess material. The breakdown of what materials were used are expanded in table 18. It should be noted that all of the costs within this table are reflective of Rankin Automation's discounted prices, so costs from 80/20 directly would show an increased cost. Along with this, it is worth nothing that without the beams, the materials only cost $ dollars, approximately half of the price with beams. Since beams used for the prototype were reused from SSL, they were not part of the official order, and thus in calculating the amount actually spent, it would equate to $. Since however we are interested in the overall cost of the prototype rack,

which includes the beams, they are included in the final total. 1515 beams are $ per inch from Rankin Automation.

A.3.3 Launch Costs Revisited - Dev Shanker & Nicholas Varro

As SpaceX's Falcon 9 and Falcon Heavy became the front runners for our calculations and mission planning (see above appendices and sections for further details), we shifted focus from analyzing historical data to looking at current data provided by SpaceX. On their website, SpaceX lists the numerical values for launch costs of both the Falcon 9 and Falcon Heavy (SpaceX, 2022-24). These values are listed via Table 19.

Launch Vehicle	**Cost $M202X**	**Cost Adjusted $M2025**
Falcon 9	69.75 (2024)	72.32
Falcon Heavy	97 (2022)	107.9

Table 19: SpaceX Launch Costs

When looking at the costs that SpaceX lists, we notice that there is only roughly a 35 $M2025 difference between the two vehicles. More so, after calculating and comparing the cost of both the prototype rack and rack made of Al-7075T6, we find that cost of the rack accounts for less than 0.01% of the total launch cost. While we do not have any mission details regarding actual implementation of our racks, making estimating actual launch costs difficult, from the SpaceX data, we can deduce that implementation of the rack will not be the limiting factor in a majority, if not all missions.

The shift to using Space X's launch cost data highlights the impact of commercial spaceflight on cost management. Unlike traditional government-led missions, which are driven by high-cost research and development, SpaceX has highly reduced launch expenses through reusable rockets, manufacturing, and frequent launches. The affordability of these expenses makes space access viable for a wide range of missions, from low Earth orbit to Mars. For our payload rack, this means it can be deployed on various missions without great financial strain. Through leveraging these modern cost structures, our team can ensure the rack remains a versatile and cost-effective solution for future space exploration.

B Appendix B - Evolution of Design

B.1 Design Iteration 1 - Muhammad Chaudhry

When beginning this capstone project, we were faced with a lot of unknowns. With our SDR approaching rapidly at the time, we created this initial design shown in Figure 86. We knew from the mission documents our rack needed to be "modular". So, we created individual cubes with rails inside to slide in an experiment. Then as seen in Figure 86, there are holes which is where we would use rods to connect multiple cubes together. The development of this design was short lived as post NASA SDR we were given significantly more information on the project.

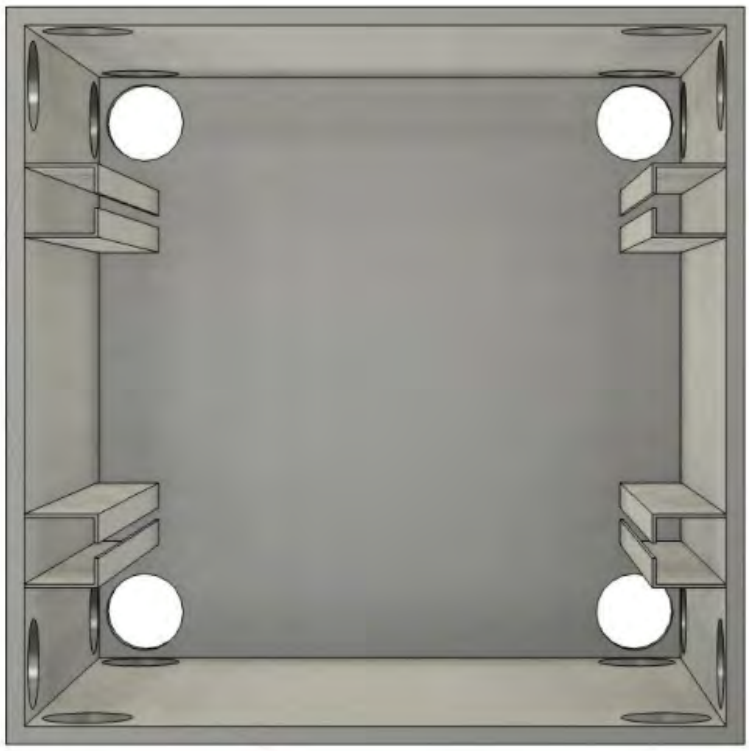

Figure 86: Design Iteration 1

B.2 Design Iteration 2 - Muhammad Chaudhry

Following the NASA SDR, we began designing our rack to fit inside the habitat in Figure 87 (Burke, 2022). Based on this habitat we away from the cube to a more traditional frame for the rack, as seen in Figure 88. The back of the rack is enclosed by sheet metal, which is bolted into the frame. Additionally, the back of the rack is chambered so that it could fit within the 32" hatch as seen in Figure 89, which at the time we believed was a limiting constraint for the rack. This design used MATLAB to determine optimal rack design to maximize internal rack area (573 in^2). The optimization of Figure 89 was done by Ben Leazer in Appendix B.

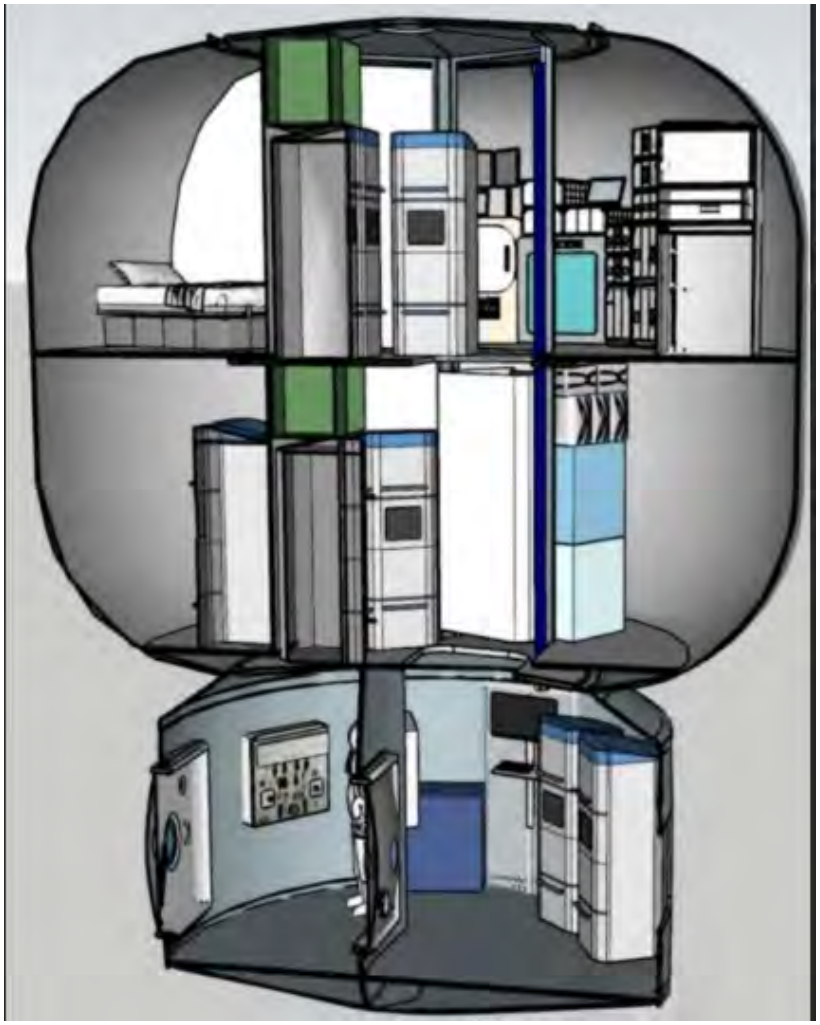

Figure 87: Initial Reference Lunar Habitat

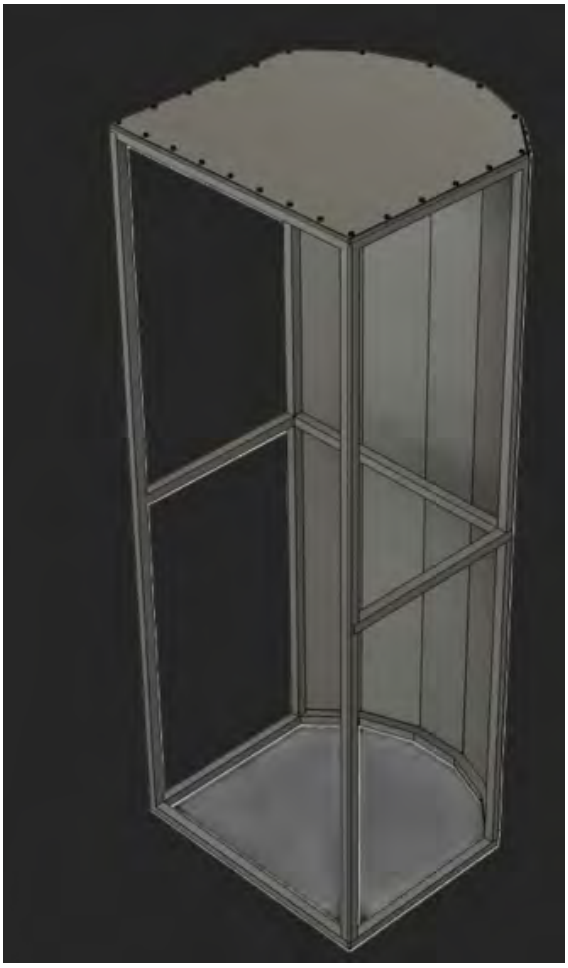

Figure 88: Design Iteration 2

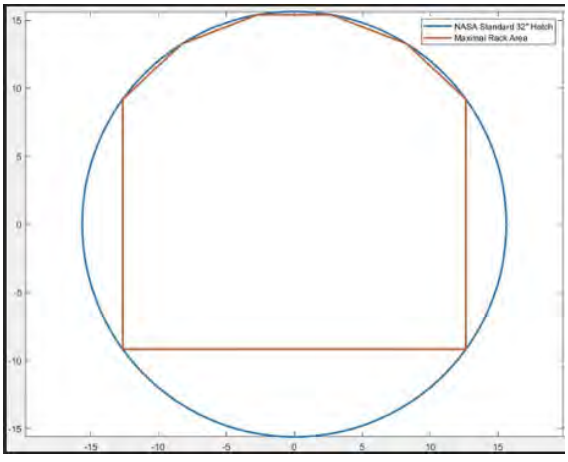

Figure 89: Optimization of Cross-Section

B.2.1 Area-Constrained Design Optimization - Benjamin Leazer

At this stage of the design process, the team was still working to determine the mission requirements that would constrain the rack design. Although NASA had released potential platform concepts for lunar habitat design, no specific dimensions were provided to guide the development. In the *"Moon to Mars eXploration Systems and Habitation (M2M X-Hab) Academic Innovation Challenge – FY25 Solicitation"*, three representative habitat configurations were outlined: a lunar surface habitat, a Moon-to-Mars transfer habitat, and a Mars surface habitat (NASA Exploration Capabilities, 2024). However, none of these included detailed internal dimensions for usable space within the habitats.

In the lunar surface habitat document, the authors explicitly reference the use of Collins Pallets for ECLSS functions, stating that these pallets could pass through a "NASA Standard Hatch" (Burke & Howard, 2022). Upon further investigation, this hatch was identified as a 32-inch circular hatch with a usable pass-through diameter of 31.5 inches (NASA, 2022). Based on this information, the team concluded that the hatch size would constrain the cross-sectional area of the rack.

Beyond the hatch constraint, two additional requirements shaped the rack's design: habitat compatibility and payload compatibility. According to the NASA solicitation document, the rack was not intended for a single habitat, but rather as a standardized payload solution adaptable to a variety of future surface habitation platforms (NASA Exploration Capabilities, 2024). Since most reference habitat concepts feature curved external walls, a design that conformed to a specific curvature, such as the ISPR, would limit adaptability. Therefore, the team opted for a straight-backed design to allow greater flexibility across potential platforms.

To ensure compatibility with most payloads, the design also aimed for cross-compatibility with ISPR payloads. Although specific ISPR payload dimensions are not publicly available, the EXPRESS rack, an add-on to the ISPR, houses payloads that conform to the size of standard middeck lockers, which have a width of 44.5 cm (17.5 in) (NASA, 1984).

Given these constraints, the design requirements were defined as follows: the cross-sectional area of the rack must fit through the 32-inch diameter hatch; the rack must have a minimum internal width of 44.5 cm (17.5 in) to maintain compatibility with ISS IVA testbed payloads; and the rear of the rack must be flat to support use in a range of habitat configurations. As mid-deck lockers are rectangular in shape (NASA, 1984), the team initially considered a square cross-section that would fit through the hatch. To better maximize volume while staying within the circular constraint, the team implemented chamfers on the rear corners, allowing better utilization of the hatch's available area.

To optimize the rack's internal cross-sectional area, the team used Matlab to model the design within a circular envelope of 31.25 inches, providing margin for adjustments and ensuring maneuverability through the hatch. Two separate Matlab scripts were developed: one for a single-chamfer design and one for a double-chamfer configuration. Each script returned the location of edges and vertices that maximized the internal area of the cross section.

The single-chamfer design, as seen in Figure 90a, yielded a cross-sectional area of $0.364\,\mathrm{m}^2$, with an internal width of 63.5 cm and depth of 47.5 cm. The double-chamfer design, as seen in Figure 90b, provided a slightly larger cross-sectional area of $0.370\,\mathrm{m}^2$, with a width of 64.3 cm and depth of 46.7 cm. Although the area increase was only $0.006\,\mathrm{m}^2$, with a proposed rack height of 1.83 m, this translated to an additional 11.0 L ($0.011\,\mathrm{m}^3$) of usable volume. Consequently, the team selected

the double-chamfer design as the preferred configuration.

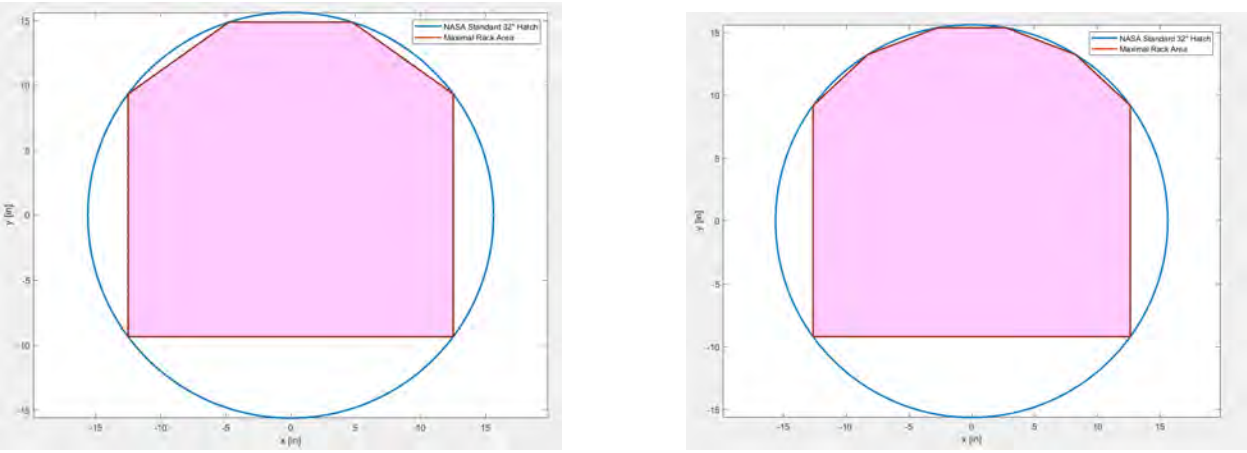

(a) Single-Chamfer Design

(b) Double-Chamfer Design

Figure 90: Matlab Optimization of Cross-Section

B.3 Design Iteration 3 - Muhammad Chaudhry

After this design we were informed by NASA at our PDR that the main hatch constraint was actually 40” x 60”. This allowed us to shift our design to something that was closer in size to the ISPR. At this phase we did not have a concrete way of installing payloads, but we had a middle beam so that you could have two columns for “single size” payloads. Discussion of payload sizes covered in Section 2.5.1, Standardized Payload Sizing. A height of 71”, or 1.8 m, has been used based on the Collins Aerospace ECLSS pallets that are inserted throughout the mock lunar habitat in Figure 87. With the Collins pallets being one of the few structures we could base dimensions on during this phase of design, we opted to keep our height close to the Collins pallet, which is 72”, deducting 1” due to the pallets curved top (Burke, 2022). With this information, our team decided that dimensions of 30” x 40” x 71”, the 30” x 40” is similar in dimension to the ISPR, which could be good in terms of having some level of fluidity between old and new systems. Figure 91 shows our design for Iteration 3.

Figure 91: CAD Model of Design Iteration 3

B.4 Design Iteration 4 - Muhammad Chaudhry & Grace Johnson

Moving forward, two main designs for incorporating a modular rail system for payloads to be loaded and unloaded were considered. The first of these designs, seen in Figure 92, featured a series of ”notches” going up the height of each member. A horizontal bar could slide into these slots, with a rail attached to the inside, which a payload could slide on. More details on rail selection can be found in Section 3.1.2. The main concern for this design was structural integrity of members, given that we were introducing large stress concentrations and taking out a lot of mass with these ”notches.” Additionally, this design leaves room for a lot of free vibration, which we would like to reduce.

Figure 92: CAD Model of Notched Design for Payload Rail Integration

The second design, seen in Figures 93 and 94, featured a series of bolt holes going up the height of each member. A horizontal bar could slide up and down the front and back sides of the rack and be bolted into place. These bars would have a rail attached to the inside, which a payload could slide on. More details on rail selection can be found in Section 3.1.2. This design would allow for payloads to be much more secure, especially on launch and landing where they experience increased vibration. A main concern for this design was accessibility – astronauts would have to easily be able to bolt these bars and screw nuts on the back. Payloads also needed to be slid in through the side, which would require the astronauts to remove side panels to change payloads out.

Figure 93: CAD Model of Bolted Design for Payload Rail Integration

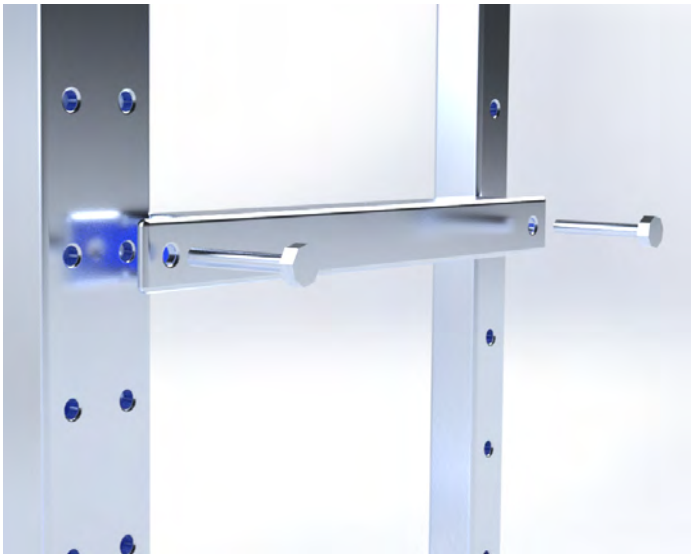

Figure 94: Close-up Exploded View of Connection Points for Horizontal Members in Bolted Design

B.5 Design Iteration 5 - Muhammad Chaudhry & Grace Johnson

Since we still had more room to work with given our 40" x 60" hatch size, we as a team decided to increase our rack cross-sectional dimensions to 35" x 45". The back 8" of depth would be dedicated to wiring, cooling, maintenance, and servicing in this design, as seen in Figure 95, giving us 14.38 ft^3 for maintenance volume. This design iteration also increases the allowable payload width when compared to the previous iterations, giving us 47.74% more payload volume. Given the increased rack dimensions, we decided to go forward with a modified bolted design for payload

housing. The horizontal bars are now attached on the sides of members, not front and back, so that payloads can be slid in the front. These bars have 2" of length cut out on each side so that each bolt can be capped on the inside, as seen in Figure 96. However, feedback from Preliminary Design Review indicated that there cannot be any loose nuts or bolts roaming around the space habitat. A suggestion was made to use spring-loaded pins instead, which we later incorporated into the current design described in Section 2.1.1.

Figure 95: CAD Model of Bolted Design for Payload Rail Integration

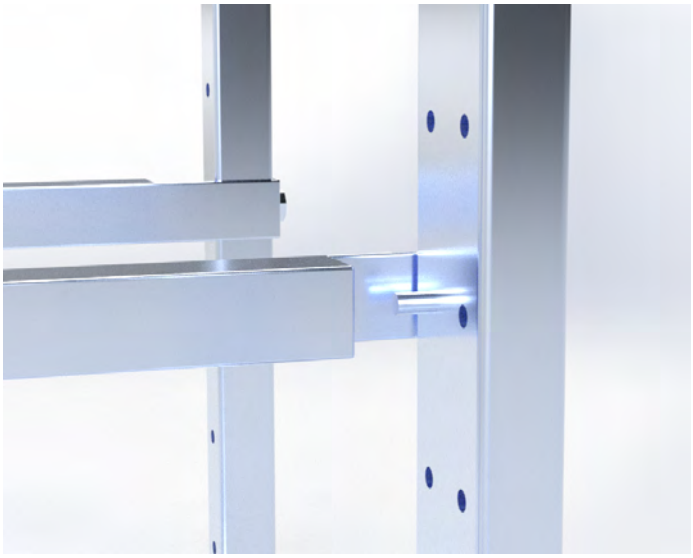

Figure 96: Close-up View of Cut-Out and Bolt for Horizontal Members in Design Iteration 5

B.6 Vertical Member Cross-Sectional Dimension Optimization – Grace Johnson

The first iteration of vertical member optimization was done on Design Iteration 5 and focused exclusively on the maximum yield and ultimate strength limitations of Al7075-T6. These material properties of Al7075-T6 were taken from *Mechanics II: Mechanics of Materials* by James Dally, Robert Bonenberger, and William Fourney. At the time of this preliminary analysis, the rack design was as seen in Figure E of Appendix B. A square cross-section for all corner members was assumed with constant wall thickness for symmetry and ease of manufacturing. For center members, a rectangular cross-section with one outer length assumed twice that of the other was used. For the first approach of optimization, a yield safety factor of 1.0 and ultimate safety factor of 1.4 were used according to NASA prototype specifications (NASA Johnson Space Center, 2014). Critical stress due to Euler buckling was calculated using equation (34) for various combinations of outer length and wall thickness dimensions. Matlab code for this process can be found in Appendix C. Chosen geometry exhibited a predicted critical stress closest to the limiting material constraint of 593 MPa ultimate strength with a safety factor of 1.4. Using this approach, the cross sections of vertical members in the rack frame had an outer length of 28.6 mm and wall thickness of 1.60 mm. This would lead to a yield margin of safety of 0.355 and ultimate margin of safety of 0.0668. The resulting design and dimensions incorporated into the rack frame can be seen in Figure J. After receiving feedback during the in-class Preliminary Design Review, this approach was modified. Instead of optimizing solely to material properties, the team was advised to optimize to launch loading. See Section 3.2.1 for finalized optimization approach and results. Note that before total rack mass at launch was finalized, other iterations were conducted using the same approach detailed in Section 3.2.1, but with different results depending on the mass used.

B.7 Earth Frame Testing Model - Muhammad Chaudhry

Part Type	Quantity	Dimensions (in)
1515	4	1.5 x 1.5 x 70.9
1515	4	1.5 x 1.5 x 43.5
1515	3	1.5 x 1.5 x 67.9
1515	4	1.5 x 1.5 x 33.5
1545	2	1.5 x 4.5 x 67.9
1545	2	1.5 x 4.5 x 33.5
4332	32	-
4340	12	-
3330	112	5/16-18 x .687
3278	64	-
3279	12	-
3285	12	-

Red - Beam
Green - Fastener
Orange - Screw
Blue - T Nut

Figure 97: Earth Frame - Parts List

B.8 Unused Load Cases - Muhammad Chaudhry

Before our in-class CDR, we conducted load cases, which involved the max axial loads. In the model in Figure 98, we applied 6 g's to the racks frame excluding payloads. Fixed the bottom face of the rack. Upon launch the rack may be fixed in a variety of orientations, such as the back and bottom fixed. In this case we only fixed the bottom to look at a "worse case" scenario.

The maximum displacement is 3.482 mm, shown highlighted in red. The maximum stress experienced by the rack is 27.41 MPa. Both can be seen in Figure 99 & 100, respectively.

In the second load case seen in Figure 101, we have a fixed bottom. We have a model "shelf" attached to the rails. With a uniform load of 784.8 N = 80 kg * 9.81 m/s^2, 80 kg (LSM-8). To simplify the model, instead of having a spring-loaded pin, we have a bonded connection between the rail/horizontal member and our vertical member.

The maximum displacement is 0.4642 mm, shown by highlighted red. Area near rails sees deflection in range of 4.642e-2 to 9.284e-2 mm. The maximum stress experienced by the rack is 8.921 MPa. Both can be seen in Figure 102 & 103 respectively.

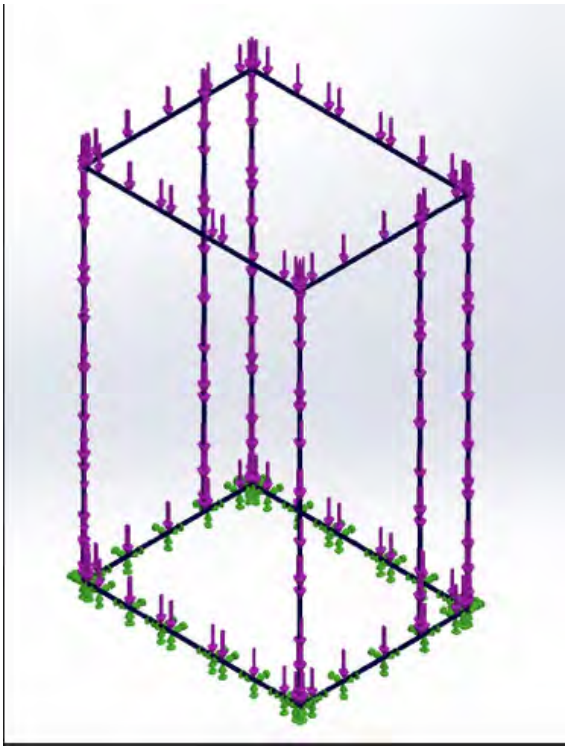

Figure 98: Only Rack - Load Case 1

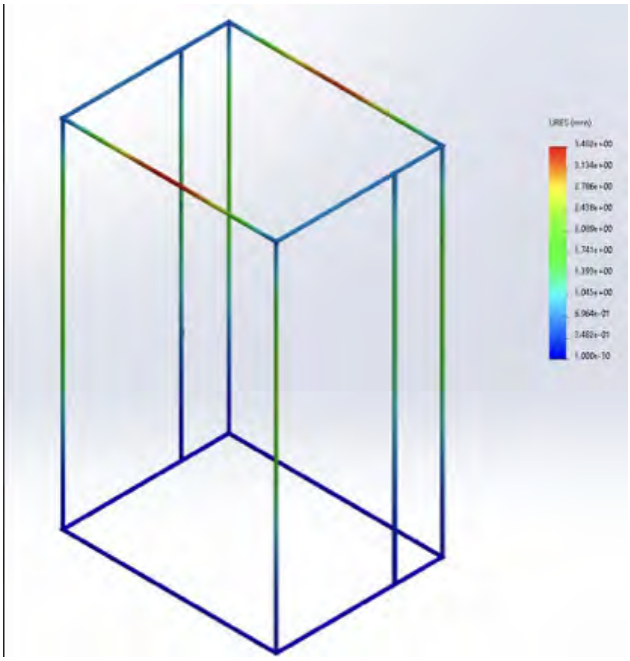

Figure 99: Deformation Plot

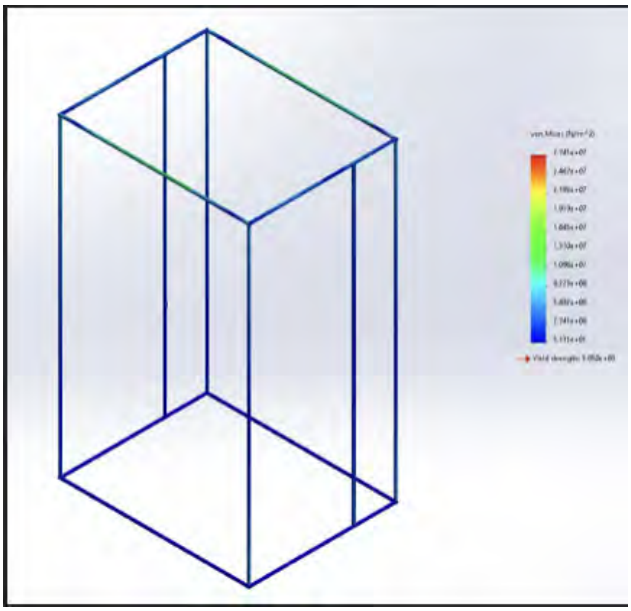

Figure 100: Stress Plot

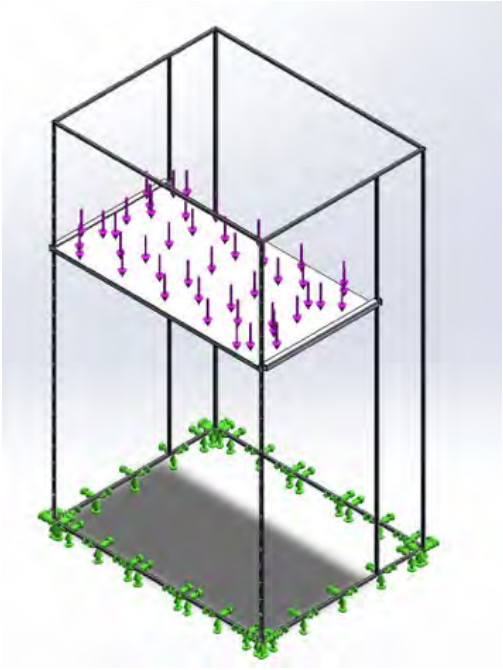

Figure 101: Single Shelf - Load Case 2

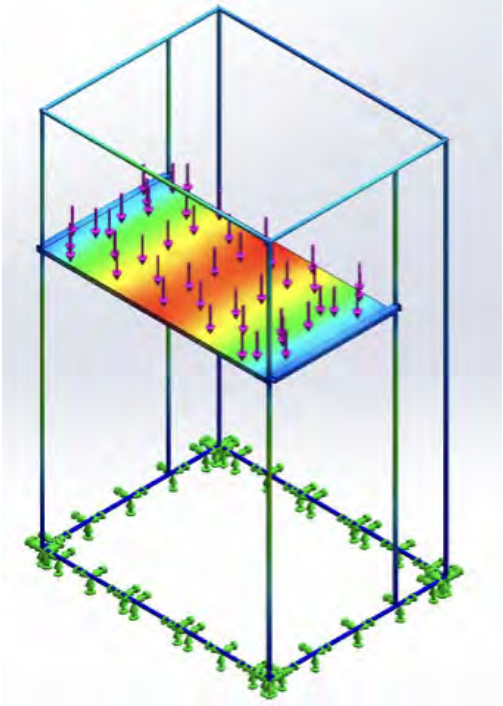

Figure 102: Deformation Plot

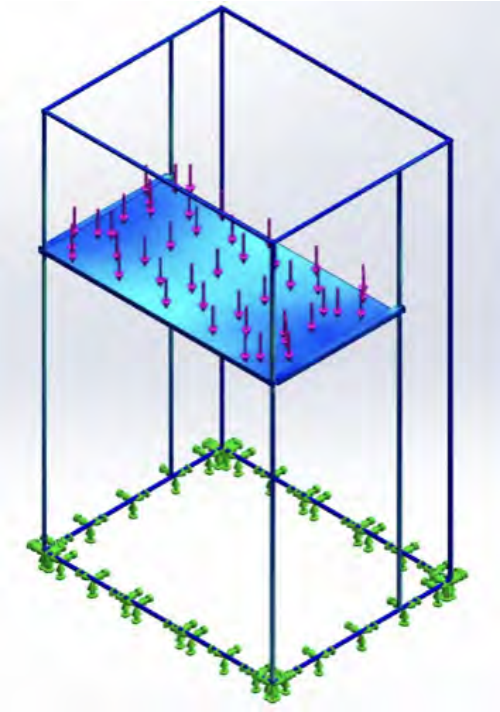

Figure 103: Stress Plot

C Appendix C - Code

C.1 Vertical Member Cross-Sectional Dimension Optimization – Grace Johnson

C.1.1 Final Approach

Figure 104: Page 1 of Matlab Code for Finalized Optimization of Vertical Rack Frame Members Based on Euler Buckling

Figure 105: Page 2 of Matlab Code for Finalized Optimization of Vertical Rack Frame Members Based on Euler Buckling

Figure 106: Page 3 of Matlab Code for Finalized Optimization of Vertical Rack Frame Members Based on Euler Buckling

Figure 107: Page 4 of Matlab Code for Finalized Optimization of Vertical Rack Frame Members Based on Euler Buckling

C.1.2 First Approach

Figure 108: Page 1 of Matlab Code for Initial Optimization of Vertical Rack Frame Members Based on Euler Buckling

Figure 109: Page 2 of Matlab Code for Initial Optimization of Vertical Rack Frame Members Based on Euler Buckling

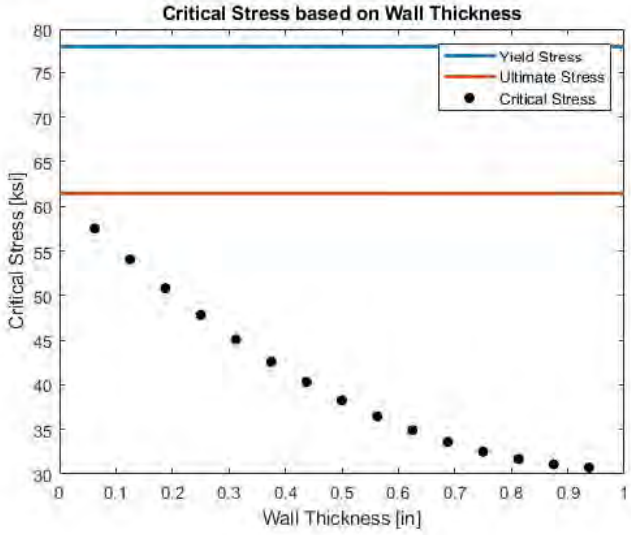

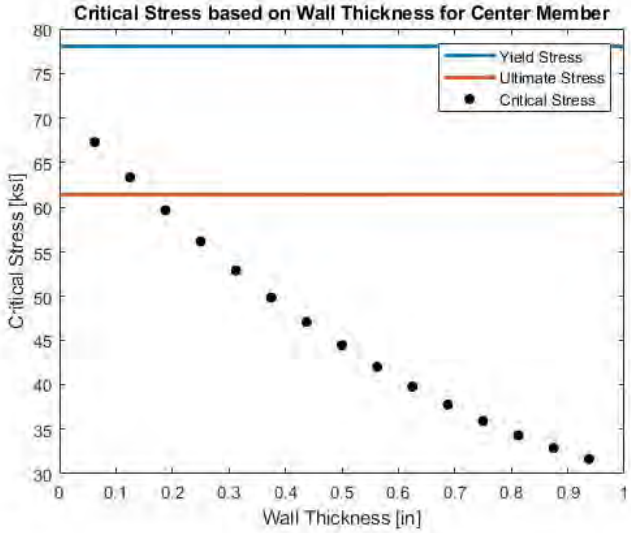

Published with MATLAB® R2023b

Figure 110: Page 3 of Matlab Code for Initial Optimization of Vertical Rack Frame Members Based on Euler Buckling

C.2 Horizontal Member Cross-Sectional Dimension Optimization – Grace Johnson

Figure 111: Page 1 of Matlab Code for Optimization of Horizontal Rack Frame Members Based on Beam Bending

Figure 112: Page 2 of Matlab Code for Optimization of Horizontal Rack Frame Members Based on Beam Bending

C.3 Cold-Plate Geometry Iterations - Luke Bieneman

Figure 113: Page 1 of Iterating Cold-Plate Geometries

Figure 114: Page 2 of Iterating Cold-Plate Geometries

Figure 115: Page 3 of Iterating Cold-Plate Geometries

Figure 116: Page 4 of Iterating Cold-Plate Geometries

Figure 117: Page 5 of Iterating Cold-Plate Geometries

C.4 Corridor and Corner Simulation - Benjamin Leazer

Figure 118: Page 1 of Corridor-Sizing Simulation

Figure 119: Page 2 of Corridor-Sizing Simulation

Figure 120: Page 3 of Corridor-Sizing Simulation

C.5 Design Iteration 2 Optimization - Benjamin Leazer

C.5.1 Single Chamfer

Figure 121: Page 1 of Single-Chamfer Optimization

Figure 122: Page 2 of Single-Chamfer Optimization

Figure 123: Page 3 of Single-Chamfer Optimization

Figure 124: Page 4 of Single-Chamfer Optimization

C.5.2 Double Chamfer

Figure 125: Page 1 of Double-Chamfer Optimization

Figure 126: Page 2 of Double-Chamfer Optimization

Figure 127: Page 3 of Double-Chamfer Optimization

Figure 128: Page 4 of Double-Chamfer Optimization

Figure 129: Page 5 of Double-Chamfer Optimization

Figure 130: Page 6 of Double-Chamfer Optimization

D Appendix D - Power and Thermal Analysis

D.1 Cold-Plate Analysis Equations and Assumptions - Luke Bieneman

D.1.1 Cold-Plate Geometry Analysis

1. Channel Geometry
Hydraulic Diameter (m):

$$D_h = \frac{2wh}{w+h} \tag{36}$$

Cross-sectional Area (m²):

$$A = w \cdot h \tag{37}$$

Wetted Perimeter (m):

$$P_{\text{wet}} = 2(w+h) \tag{38}$$

Heat Exchange Surface Area (m²):

$$A_{\text{surf}} = P_{\text{wet}} \cdot L_{\text{total}} = 2(w+h) \cdot N \cdot L_{\text{plate}} \tag{39}$$

2. Fluid Flow and Reynolds Number
Flow Velocity (m/s):

$$v = \frac{\dot{m}}{\rho A} \tag{40}$$

Reynolds Number:

$$Re = \frac{\rho v D_h}{\mu} \tag{41}$$

3. Friction and Pressure Drop
Friction Factor:

$$f = \begin{cases} \frac{64}{Re}, & Re < 2300 \quad \text{(laminar)} \\ 0.316 \cdot Re^{-0.25}, & Re \geq 2300 \quad \text{(turbulent)} \end{cases} \tag{42}$$

Frictional Pressure Drop (Pa):

$$\Delta P_{\text{friction}} = f \cdot \frac{L_{\text{total}}}{D_h} \cdot \frac{\rho v^2}{2} \tag{43}$$

Local (Minor) Losses (Pa):

$$\Delta P_{\text{local}} = K \cdot \frac{\rho v^2}{2} \quad \text{with} \quad K = 2 + N \tag{44}$$

Total Pressure Drop:

$$\Delta P_{\text{total}} = \Delta P_{\text{friction}} + \Delta P_{\text{local}} \tag{45}$$

4. Convective Heat Transfer

Nusselt Number:

$$Nu = \begin{cases} 3.66, & Re < 2300 \quad \text{(laminar)} \\ 0.023 \cdot Re^{0.8} \cdot Pr^{0.3}, & Re \geq 2300 \quad \text{(turbulent)} \end{cases} \tag{46}$$

Convective Heat Transfer Coefficient:

$$h = \frac{Nu \cdot k}{D_h} \tag{47}$$

Log-Mean Temperature Difference (Approx.):

$$\Delta T_{\log} \approx T_{\text{plate}} - \left(\frac{T_{\text{in}} + T_{\text{out}}}{2} \right) \tag{48}$$

Maximum Convective Heat Transfer (W):

$$Q_{\text{conv}} = h \cdot A_{\text{surf}} \cdot \Delta T_{\log} \tag{49}$$

5. Assumptions

- Water is used as the coolant.
- Fluid properties are treated as constant:

$$\rho = 1000\,\text{kg/m}^3, \quad \mu = 8.9 \times 10^{-4}\,\text{Pa} \cdot \text{s}, \quad c_p = 4182\,\text{J/kg} \cdot \text{K}, \quad k = 0.6\,\text{W/m} \cdot \text{K}$$

- Heat load from electronics: $Q = 560$ W.
- Mass flow rate: $\dot{m} = 193$ kg/hr ≈ 0.0536 kg/s.
- Max outlet temperature: $T_{\text{out}} \leq 19°\text{C}$.
- Wall temperature: $T_{\text{plate}} = 22°\text{C}$.
- Inlet temperature: $T_{\text{in}} = 4°\text{C}$.
- Minor loss coefficients: $K = 2 + N$ (1 inlet + 1 outlet + N U-turns).
- Flow direction is along plate length ($L_{\text{plate}} = 660.4$ mm).
- Turns are spaced across plate depth ($W_{\text{plate}} = 508.6$ mm).
- Channel pitch (turn spacing) $= w + 2$ mm.
- Configurations that exceed plate geometry are skipped in simulation.
- Geometries varied by channel height (1 - 5 mm), width (2 - 20 mm), number of passes (4 - 40)

D.1.2 Matlab Iterated Results

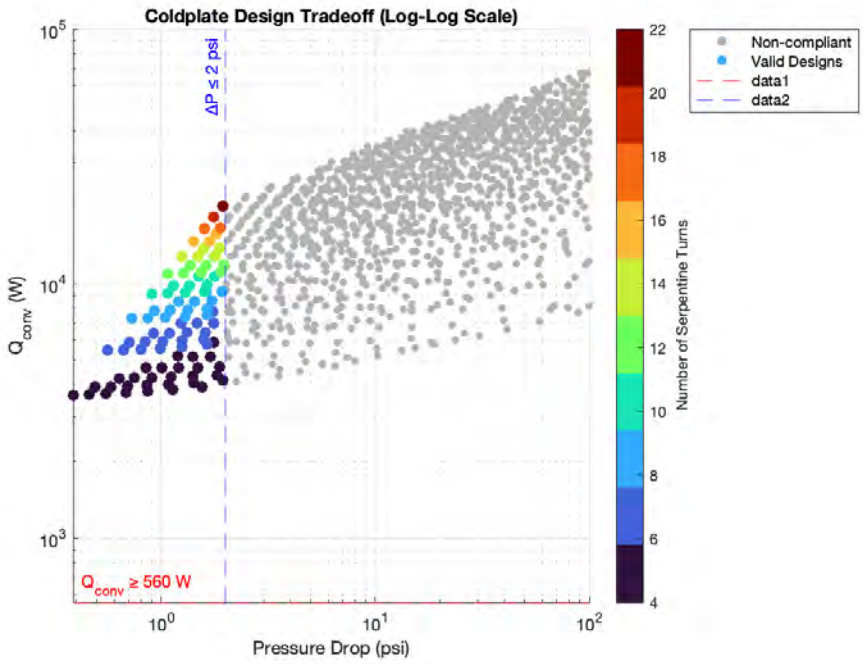

Figure 131: Cold-Plate Geometry Iterations

Category	Height (m)	Width (m)	Turns	Re	Q_{conv} (W)	ΔP (Pa)
Min ΔP	0.005	0.020	4	4819	3656	2662
Max Q ($\Delta P \leq 2$ psi)	0.005	0.020	22	4819	20106	13347

Table 20: Highlighted Cold-Plate Designs

Conclusions A cold-plate with dimensions 660.4 mm (W) x 508.6 mm (D) x 10 mm (t) and single serpentine channel would have its best pressure drop performance or thermal performance at the above channel dimensions and number of turns. Note: Q_{conv} is the convective capability of the design and is thus an overestimate. The efficiency of the cold-plate would require more detailed modeling. What can be concluded more definitively though, is that a shorter path will minimize pressure drop, whereas a longer path will maximize heat transfer. Furthermore, a larger channel area will provide better performance provided the Reynolds Number is turbulent.

D.1.3 Cold Plate Material Trade Study

Material	Properties		Heat Transfer		Mass and Efficiency	
	ρ (kg/m³)	k (W/m · K)	R_{cond} (K/W)	$\dot{Q}$ Q(W per K)	m m (kg)	$\dot{Q}/m$ Q/m (W/K · Kg)
Aluminum 6061	2700	167	0.000299	3340	1.35	2474
Copper	8960	385	0.000130	7700	4.48	1719
Titanium	4500	21.9	0.00228	438	2.25	195
Stainless Steel 304	8000	16.2	0.00309	324	4	81
Graphite	2250	200	0.00025	4000	1.125	3556

Table 21: Material Properties for Cold Plate Design

Assumptions:

- One-dimensional, steady-state heat conduction through the plate
- Flat contact surface with uniform heat flux
- Plate material has uniform thermal conductivity
- No internal heat generation
- Negligible interface/contact resistance
- Plate area: $A = 0.1\,\text{m}^2$
- Plate thickness: $L = 0.005\,\text{m}$

Equations:

Conduction Thermal Resistance

$$R_{\text{cond}} = \frac{L}{kA} \tag{50}$$

Heat Transfer per Unit Temperature Difference

$$Q = \frac{\Delta T}{R_{\text{cond}}} = \frac{kA}{L} \tag{51}$$

Plate Mass

$$m_{\text{plate}} = \rho A L \tag{52}$$

Conclusions

Aluminum-6061 provides the most heat transfer per kg of cold-plate mass outside of graphite, but without the structural limitations that come alongside it. Copper provides the most absolute heat transfer although it is the most dense material analyzed. Lastly, graphene composites or coatings promise great thermal conductivity, but the material science is relatively new and comes with similar structural issues to graphite.

D.1.4 Coolant Trade Study

Coolant	Properties				Flow Rate and Efficiency	
	ρ (kg/m³)	C_p (J/kg · K)	k (W/m · K)	Viscosity (mPa · s)	$\dot{m}$ (kg/s)	Heat Dissipation (W/K)
Water (Cold)	1000	4200	0.622	1.57	0.0333	139.86
Water (Moderate)	998	4182	0.598	0.98	0.0332	138.98
PAO	800	2100	0.14	10	0.0266	55.94
Galden HT-110	1780	1050	0.065	2.8	0.0592	62.24
Fluorinert FC-72	1680	1100	0.057	0.64	0.0559	61.54
Ammonia	604	4700	0.51	0.23	0.0201	94.53
Water-Glycol (50/50)	1060	3500	0.425	1.8	0.0352	123.543

Table 22: Coolant Properties for Cold Plate Design

Assumptions:

- Coolants flow through identical cold plates
- Flow is steady and single-phase (liquid only)
- Heat transfer is dominated by fluid specific heat, not detailed convection
- Constant fluid properties evaluated at 17°C, except for water also at 4°C
- Volumetric flow rate: $\dot{V} = 2\,\mathrm{L/min} = 3.33 \times 10^{-5}\,\mathrm{m^3/s}$

Equations:

Mass Flow Rate

$$\dot{m} = \rho \dot{V} \tag{53}$$

Heat Dissipation per Unit Temperature Difference

$$\dot{Q} = \dot{m} C_p = \rho \dot{V} C_p \tag{54}$$

Conclusions

For conductive heat transfer within a cold-plate, water provides the most robust heat dissipation of the coolants analyzed. A water-glycol mixture provides a promising alternative for temperatures below waters freezing point. Both options are also safe for humans within a habitat.

D.1.5 16 Channel Cold-Plate Computational Fluid Dynamics Analysis

First Take

Ansys Fluent Simulation Report

Analyst	lukeb
Date	5/12/2025 12:22 PM

Table of Contents

System Information

Application	Fluent
Settings	3d, pressure-based, SST k-omega
Version	25.1.0-10210
Source Revision	3b709034ad
Build Time	Nov 26 2024 13:33:31 EST
CPU	AMD Ryzen 7 7800X3D 8-Core Processor
OS	Windows

Geometry and Mesh

Mesh Size

Cells	Faces	Nodes
464838	2476922	1803054

Mesh Quality

Name	Type	Min Orthogonal Quality	Max Aspect Ratio
default-solid-1	Poly Cell	0.21797521	32.190018
default-solid	Poly Cell	0.21100841	10.576583

Orthogonal Quality

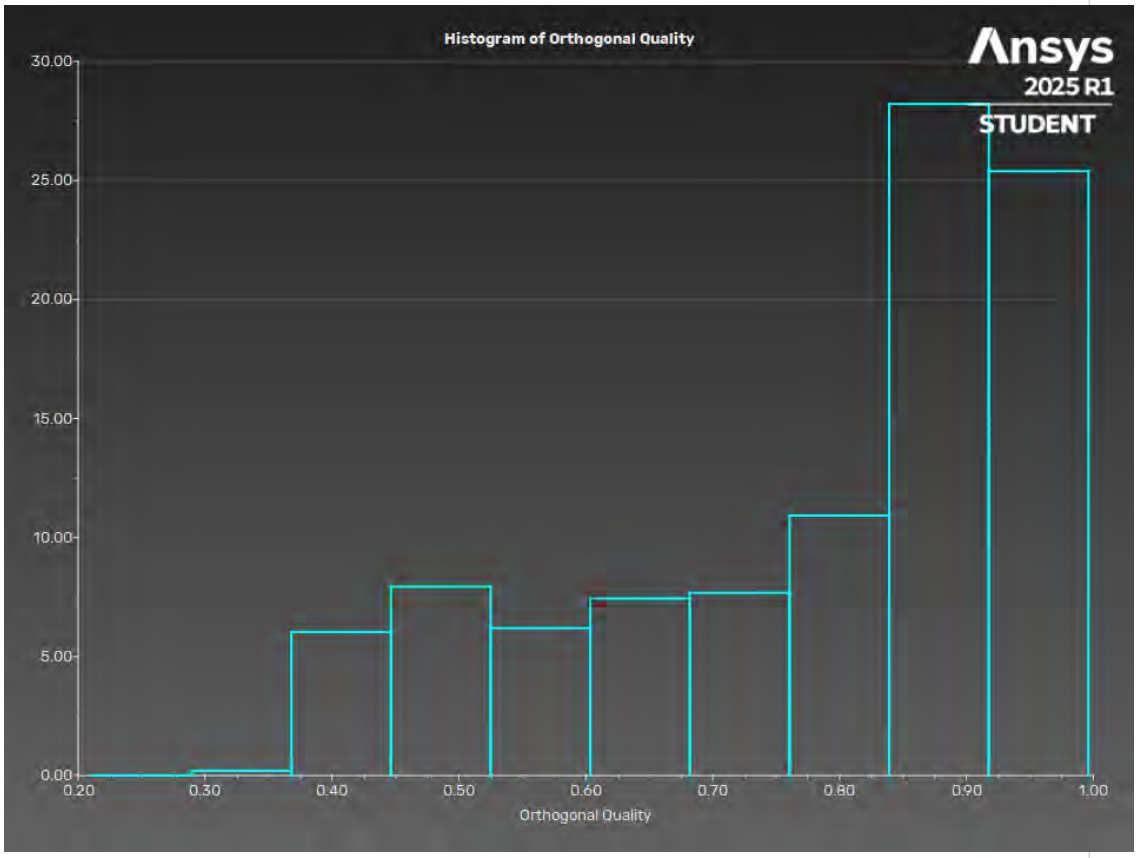

Simulation Setup

Physics

Models

Model	Settings
Space	3D
Time	Steady
Viscous	SST k-omega turbulence model
Heat Transfer	Enabled

Material Properties

− Fluid	
− water-liquid	
Density	998.2 kg/m^3
Cp (Specific Heat)	4182 J/(kg K)
Thermal Conductivity	0.6 W/(m K)
Viscosity	0.001003 kg/(m s)
− air	
Density	1.225 kg/m^3
Cp (Specific Heat)	1006.43 J/(kg K)
Thermal Conductivity	0.0242 W/(m K)
Viscosity	1.7894e-05 kg/(m s)
− Solid	
− aluminum	
Density	2719 kg/m^3
Cp (Specific Heat)	871 J/(kg K)
Thermal Conductivity	202.4 W/(m K)

Cell Zone Conditions

− Fluid	
− default-solid-1	
Material Name	water liquid

Specify source terms?	no
Specify fixed values?	no
Frame Motion?	no
Laminar zone?	no
Porous zone?	no
3D Fan Zone?	no
− Solid	
− default-solid	
Material Name	aluminum
Specify source terms?	no
Specify fixed values?	no
Frame Motion?	no
Solid Motion?	no

Boundary Conditions

− Inlet	
− group1-group2-inlet-default-solid	
Reference Frame	Absolute
Mass Flow Specification Method	Mass Flow Rate
Mass Flow Rate [kg/s]	0.05361
Total Temperature [K]	300
Supersonic/Initial Gauge Pressure [Pa]	0
Direction Specification Method	Normal to Boundary
Turbulence Specification Method	Intensity and Viscosity Ratio
Turbulent Intensity [%]	5
Turbulent Viscosity Ratio	10
− Outlet	
− outlet	
Backflow Reference Frame	Absolute
Gauge Pressure [Pa]	0
Pressure Profile Multiplier	1
Backflow Total Temperature [K]	300
Backflow Direction Specification Method	Normal to Boundary
Turbulence Specification Method	Intensity and Viscosity Ratio
Backflow Turbulent Intensity [%]	5
Backflow Turbulent Viscosity Ratio	10
Backflow Pressure Specification	Total Pressure
Build artificial walls to prevent reverse flow?	no

Radial Equilibrium Pressure Distribution	no
Average Pressure Specification?	no
Specify targeted mass flow rate	no
━ Wall	
━ default-solid-default-solid	
Wall Thickness [m]	0
Heat Generation Rate [W/m^3]	0
Material Name	aluminum
Thermal BC Type	Coupled
Enable shell conduction?	no
Wall Motion	Stationary Wall
Shear Boundary Condition	No Slip
Wall Surface Roughness	Standard
Wall Roughness Height [m]	0
Wall Roughness Constant	0.5
Convective Augmentation Factor	1
━ default-solid:1	
Wall Thickness [m]	0
Heat Generation Rate [W/m^3]	0
Material Name	aluminum
Thermal BC Type	Heat Flux
Heat Flux [W/m^2]	1667
Enable shell conduction?	no
Convective Augmentation Factor	1
━ default-solid-default-solid-shadow	
Wall Thickness [m]	0
Heat Generation Rate [W/m^3]	0
Material Name	aluminum
Thermal BC Type	Coupled
Enable shell conduction?	no
Convective Augmentation Factor	1

Reference Values

Area	1 m^2
Density	1.225 kg/m^3
Enthalpy	0 J/kg
Length	1 m

Pressure	0 Pa
Temperature	288.16 K
Velocity	1 m/s
Viscosity	1.7894e-05 kg/(m s)
Ratio of Specific Heats	1.4
Yplus for Heat Tran. Coef.	300
Reference Zone	default-solid-1

Solver Settings

− Equations	
Flow	True
Turbulence	True
Energy	True
− Numerics	
Absolute Velocity Formulation	True
− Pseudo Time Explicit Relaxation Factors	
Density	1
Body Forces	1
Turbulent Kinetic Energy	0.75
Specific Dissipation Rate	0.75
Turbulent Viscosity	1
Energy	0.75
Explicit Momentum	0.5
Explicit Pressure	0.5
− Pressure-Velocity Coupling	
Type	Coupled
Pseudo Time Method (Global Time Step)	True
− Discretization Scheme	
Pressure	Second Order
Momentum	Second Order Upwind
Turbulent Kinetic Energy	Second Order Upwind
Specific Dissipation Rate	Second Order Upwind
Energy	Second Order Upwind
− Solution Limits	
Minimum Absolute Pressure [Pa]	1
Maximum Absolute Pressure [Pa]	5e+10
Minimum Static Temperature [K]	1

Maximum Static Temperature [K]	5000
Minimum Turb. Kinetic Energy [m^2/s^2]	1e-14
Minimum Spec. Dissipation Rate [s^-1]	1e-20
Maximum Turb. Viscosity Ratio	100000

Run Information

Number of Machines	1
Number of Cores	4
Case Read	12.019 seconds
Iteration	56.462 seconds
AMG	35.372 seconds
Virtual Current Memory	2.74891 GB
Virtual Peak Memory	2.85808 GB
Memory Per M Cell	4.56055

Solution Status

Iterations: 80

	Value	Absolute Criteria	Convergence Status
continuity	3.07809e-06	0.001	Converged
x-velocity	2.017612e-05	0.001	Converged
y-velocity	1.260431e-05	0.001	Converged
z-velocity	0.000101829	0.001	Converged
energy	8.298646e-07	1e-06	Converged
k	0.003247662	0.001	Not Converged
omega	0.001976995	0.001	Not Converged

Report Definitions

pressure	30246.88	Pa
outlet-temp	301.8335	K
total-heat-transfer	1158.628	W

Plots

Residuals

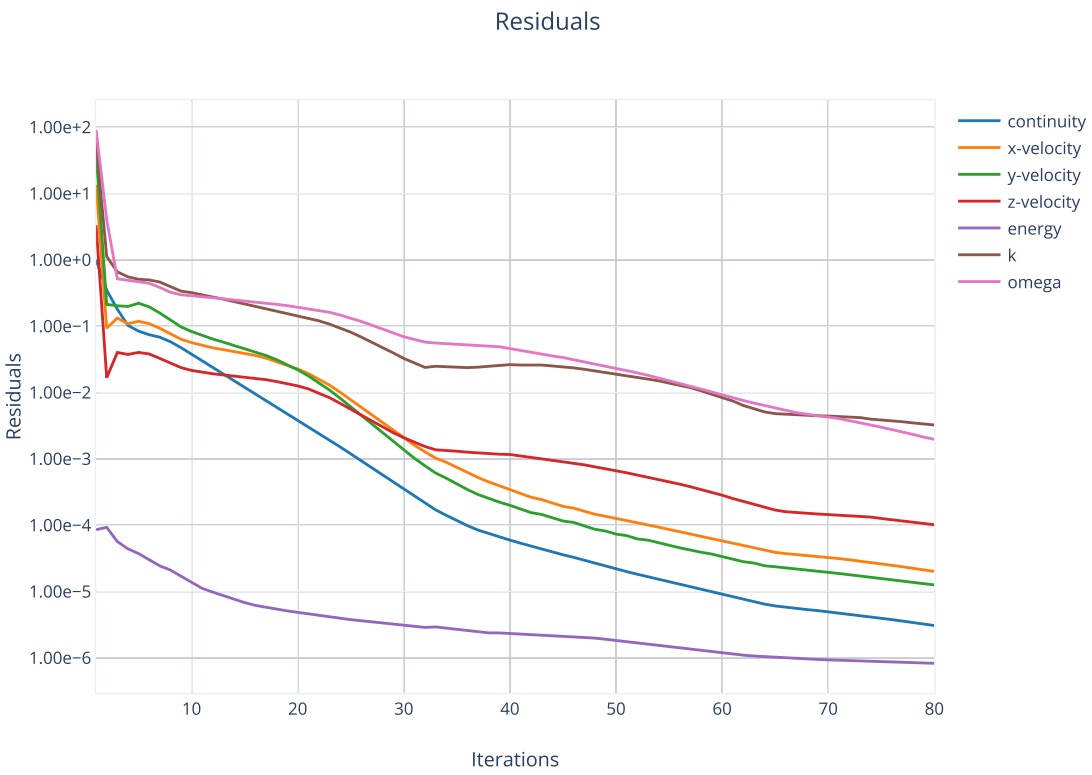

pressure

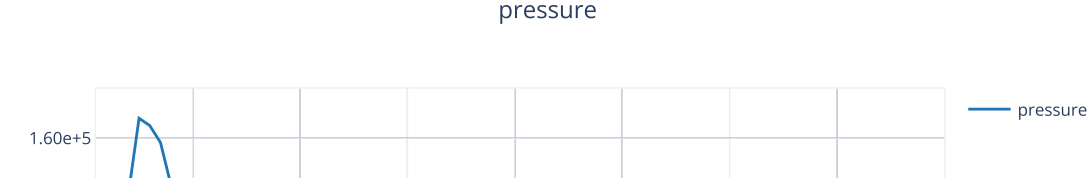

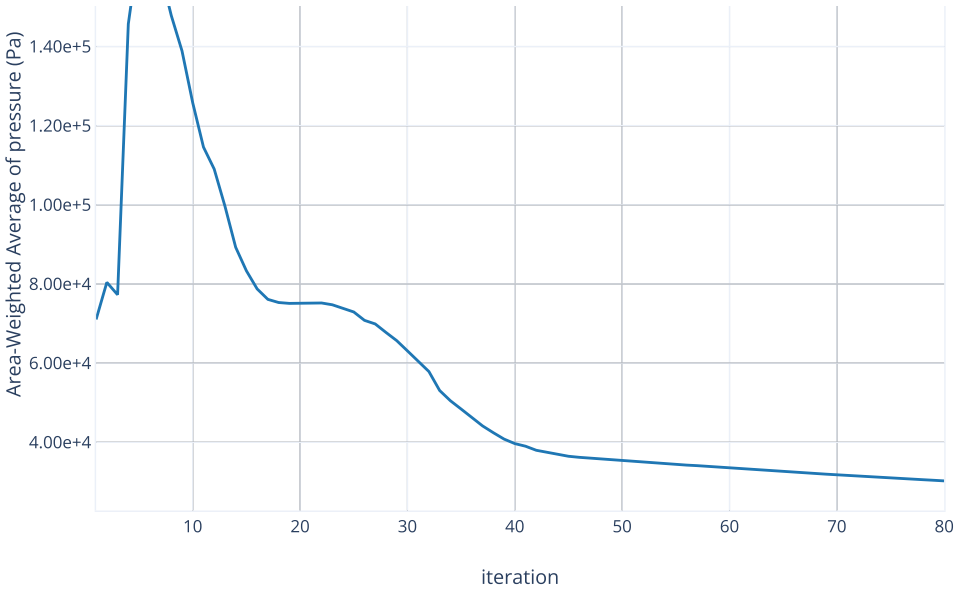

outlet-temp

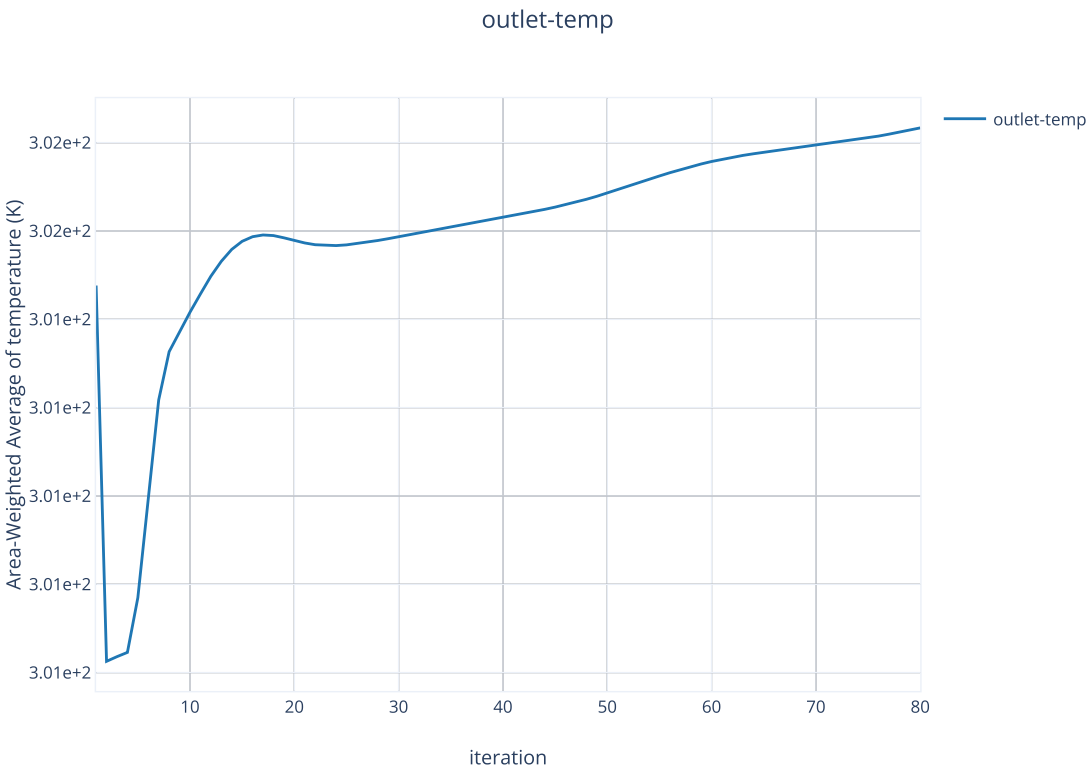

total-heat-transfer

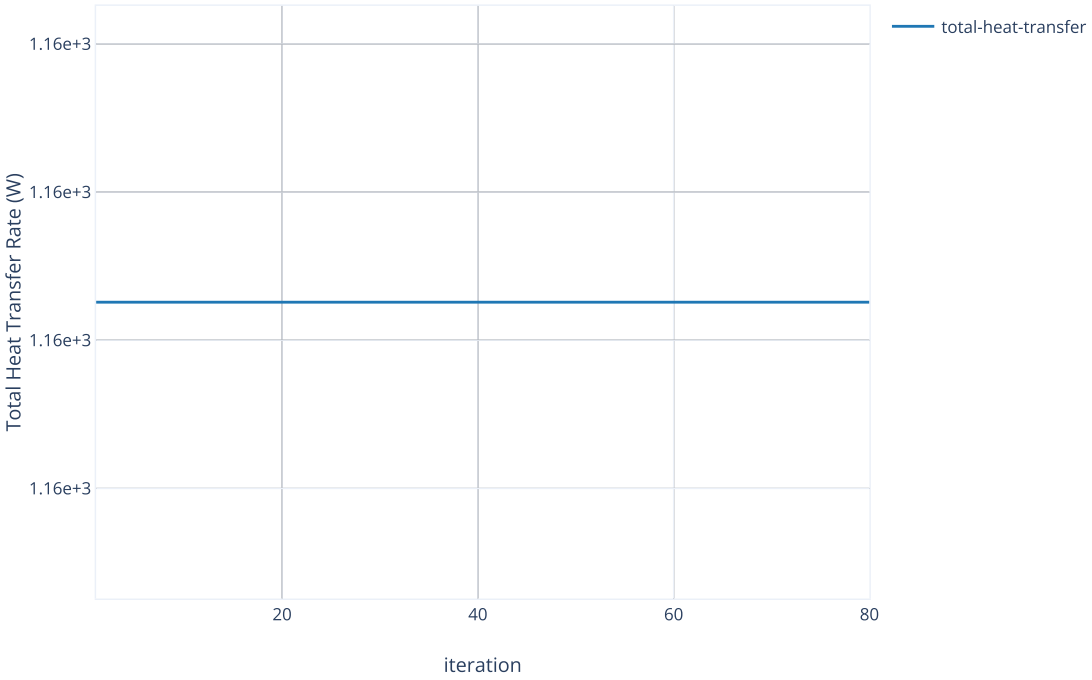
total-heat-transfer
Total Heat Transfer Rate (W)
1.16e+3
1.16e+3
1.16e+3
1.16e+3
20
40
60
80
iteration

Contours

contour-1

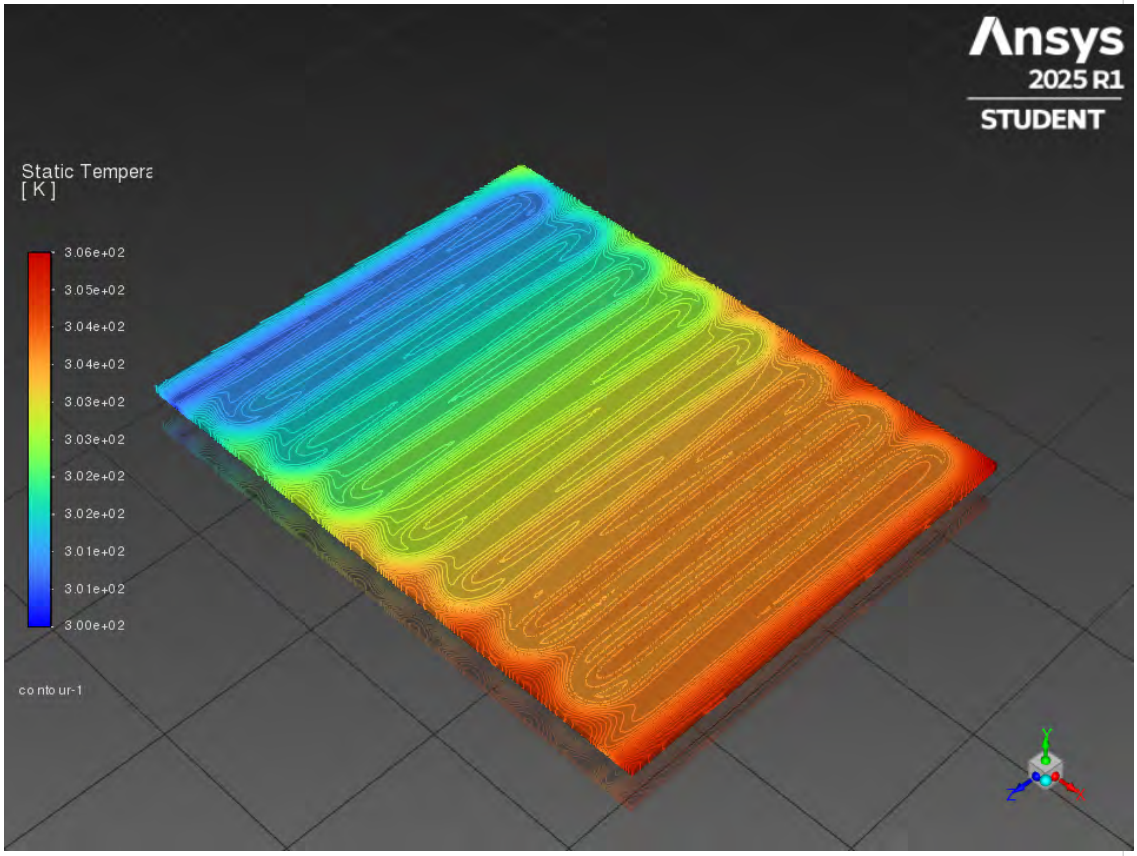

Conclusions

A Computational Fluid Dynamics (CFD) Analysis was performed on a 16 channel Aluminum cold-plate with dimensions 660.4 mm (W) x 508.6 mm (D) x 10 mm (t) and 5 mm (H) x 20 mm (W) channels. The inlet temperature was 300K (27C) with a mass flow rate of 193 kg/hr. The resulting outlet temperature was 302K (29C) and pressure drop of 30247 Pa (4.39 psi), with a total heat transfer of 1159 W. A few conclusions can be drawn from this:

- Both the pressure drop and heat transfer were significantly worse than the analytical analysis predicted.
- Temperature drop was very small (< 2 C)
- Temperature distribution across the cold-plate surface is heavily biased towards the inlet in a serpentine design.

These conclusions provide possible paths for further optimization:

- Shortening channels to decrease pressure drop
- Increasing turbulence within channels for better convective heat transfer to coolant
- Changing the internal channel layout

One possible variation that addresses all of these conclusions is the addition of multiple shorter individual channels with turbulent features with the channels (ribs, fins, etc.) Although, this has the cost of needed more inlet/outlets and more external tubing.

Second Take

Ansys Fluent Simulation Report

Analyst	lukeb
Date	5/12/2025 12:23 PM

Table of Contents

System Information

Application	Fluent
Settings	3d, pressure-based, SST k-omega
Version	25.1.0-10210
Source Revision	3b709034ad
Build Time	Nov 26 2024 13:33:31 EST
CPU	AMD Ryzen 7 7800X3D 8-Core Processor
OS	Windows

Geometry and Mesh

Mesh Size

Cells	Faces	Nodes
464838	2476922	1803054

Mesh Quality

Name	Type	Min Orthogonal Quality	Max Aspect Ratio
default-solid-1	Poly Cell	0.21797521	32.190018
default-solid	Poly Cell	0.21100841	10.576583

Orthogonal Quality

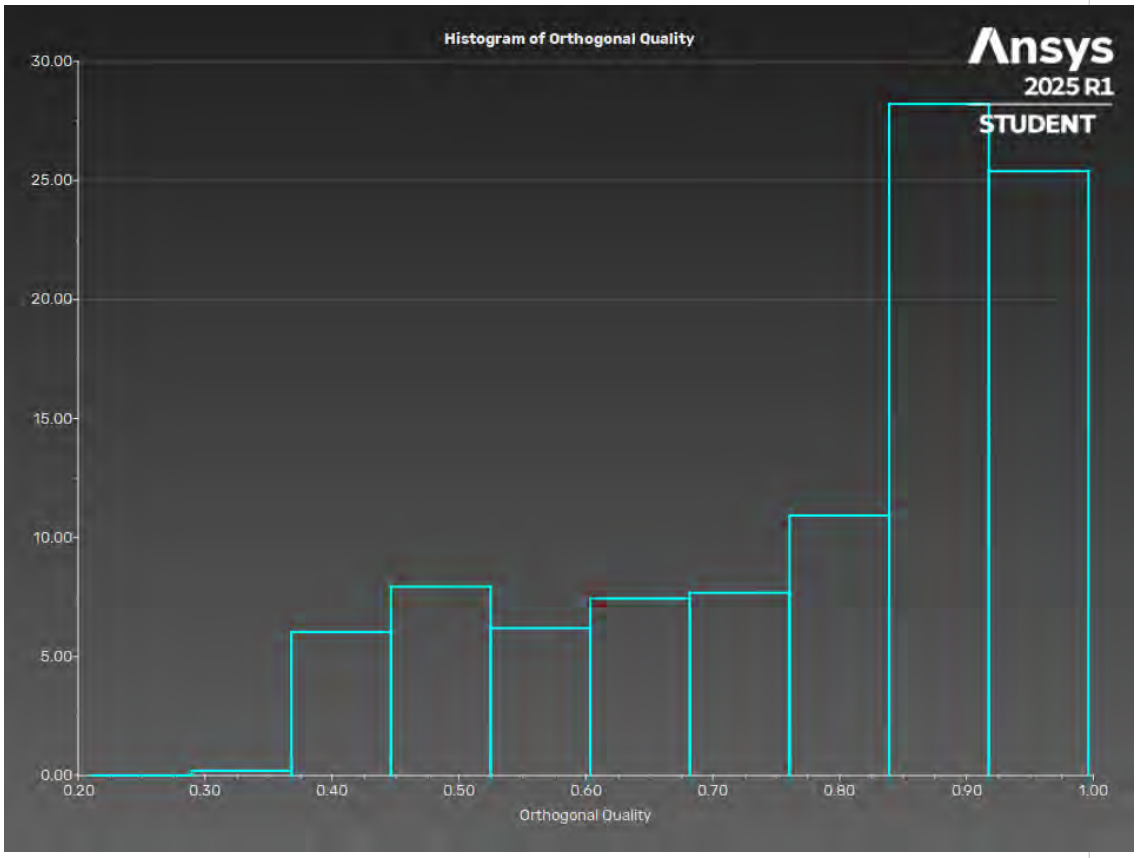

Simulation Setup

Physics

Models

Model	Settings
Space	3D
Time	Steady
Viscous	SST k-omega turbulence model
Heat Transfer	Enabled

Material Properties

− Fluid	
− water-liquid	
Density	998.2 kg/m^3
Cp (Specific Heat)	4182 J/(kg K)
Thermal Conductivity	0.6 W/(m K)
Viscosity	0.001003 kg/(m s)
− air	
Density	1.225 kg/m^3
Cp (Specific Heat)	1006.43 J/(kg K)
Thermal Conductivity	0.0242 W/(m K)
Viscosity	1.7894e-05 kg/(m s)
− Solid	
− aluminum	
Density	2719 kg/m^3
Cp (Specific Heat)	871 J/(kg K)
Thermal Conductivity	202.4 W/(m K)

Cell Zone Conditions

− Fluid	
− default-solid-1	
Material Name	water liquid

Specify source terms?	no
Specify fixed values?	no
Frame Motion?	no
Laminar zone?	no
Porous zone?	no
3D Fan Zone?	no
− Solid	
− default-solid	
Material Name	aluminum
Specify source terms?	no
Specify fixed values?	no
Frame Motion?	no
Solid Motion?	no

Boundary Conditions

− Inlet	
− group1-group2-inlet-default-solid	
Reference Frame	Absolute
Mass Flow Specification Method	Mass Flow Rate
Mass Flow Rate [kg/s]	0.05361
Total Temperature [K]	277
Supersonic/Initial Gauge Pressure [Pa]	0
Direction Specification Method	Normal to Boundary
Turbulence Specification Method	Intensity and Viscosity Ratio
Turbulent Intensity [%]	5
Turbulent Viscosity Ratio	10
− Outlet	
− outlet	
Backflow Reference Frame	Absolute
Gauge Pressure [Pa]	0
Pressure Profile Multiplier	1
Backflow Total Temperature [K]	277
Backflow Direction Specification Method	Normal to Boundary
Turbulence Specification Method	Intensity and Viscosity Ratio
Backflow Turbulent Intensity [%]	5
Backflow Turbulent Viscosity Ratio	10
Backflow Pressure Specification	Total Pressure
Build artificial walls to prevent reverse flow?	no

Radial Equilibrium Pressure Distribution	no
Average Pressure Specification?	no
Specify targeted mass flow rate	no
━ Wall	
━ default-solid-default-solid	
Wall Thickness [m]	0
Heat Generation Rate [W/m^3]	0
Material Name	aluminum
Thermal BC Type	Coupled
Enable shell conduction?	no
Wall Motion	Stationary Wall
Shear Boundary Condition	No Slip
Wall Surface Roughness	Standard
Wall Roughness Height [m]	0
Wall Roughness Constant	0.5
Convective Augmentation Factor	1
━ default-solid:1	
Wall Thickness [m]	0
Heat Generation Rate [W/m^3]	0
Material Name	aluminum
Thermal BC Type	Heat Flux
Heat Flux [W/m^2]	5000
Enable shell conduction?	no
Convective Augmentation Factor	1
━ default-solid-default-solid-shadow	
Wall Thickness [m]	0
Heat Generation Rate [W/m^3]	0
Material Name	aluminum
Thermal BC Type	Coupled
Enable shell conduction?	no
Convective Augmentation Factor	1

Reference Values

Area	1 m^2
Density	1.225 kg/m^3
Enthalpy	0 J/kg
Length	1 m

Pressure	0 Pa
Temperature	288.16 K
Velocity	1 m/s
Viscosity	1.7894e-05 kg/(m s)
Ratio of Specific Heats	1.4
Yplus for Heat Tran. Coef.	300
Reference Zone	default-solid-1

Solver Settings

− Equations	
Flow	True
Turbulence	True
Energy	True
− Numerics	
Absolute Velocity Formulation	True
− Pseudo Time Explicit Relaxation Factors	
Density	1
Body Forces	1
Turbulent Kinetic Energy	0.75
Specific Dissipation Rate	0.75
Turbulent Viscosity	1
Energy	0.75
Explicit Momentum	0.5
Explicit Pressure	0.5
− Pressure-Velocity Coupling	
Type	Coupled
Pseudo Time Method (Global Time Step)	True
− Discretization Scheme	
Pressure	Second Order
Momentum	Second Order Upwind
Turbulent Kinetic Energy	Second Order Upwind
Specific Dissipation Rate	Second Order Upwind
Energy	Second Order Upwind
− Solution Limits	
Minimum Absolute Pressure [Pa]	1
Maximum Absolute Pressure [Pa]	5e+10
Minimum Static Temperature [K]	1

Maximum Static Temperature [K]	5000
Minimum Turb. Kinetic Energy [m^2/s^2]	1e-14
Minimum Spec. Dissipation Rate [s^-1]	1e-20
Maximum Turb. Viscosity Ratio	100000

Run Information

Number of Machines	1
Number of Cores	4
Case Read	12.692 seconds
Iteration	339.22 seconds
AMG	191.152 seconds
Virtual Current Memory	2.76481 GB
Virtual Peak Memory	2.97682 GB
Memory Per M Cell	4.58893

Solution Status

Iterations: 100

	Value	Absolute Criteria	Convergence Status
continuity	0.003871417	0.001	Not Converged
x-velocity	3.614214e-07	0.001	Converged
y-velocity	1.737271e-06	0.001	Converged
z-velocity	4.657185e-07	0.001	Converged
energy	9.960743e-08	1e-06	Converged
k	5.66838e-06	0.001	Converged
omega	3.899e-06	0.001	Converged

Report Definitions

pressure	26728.53	Pa
outlet-temp	284.7536	K
total-heat-transfer	3475.194	W

Plots

Residuals

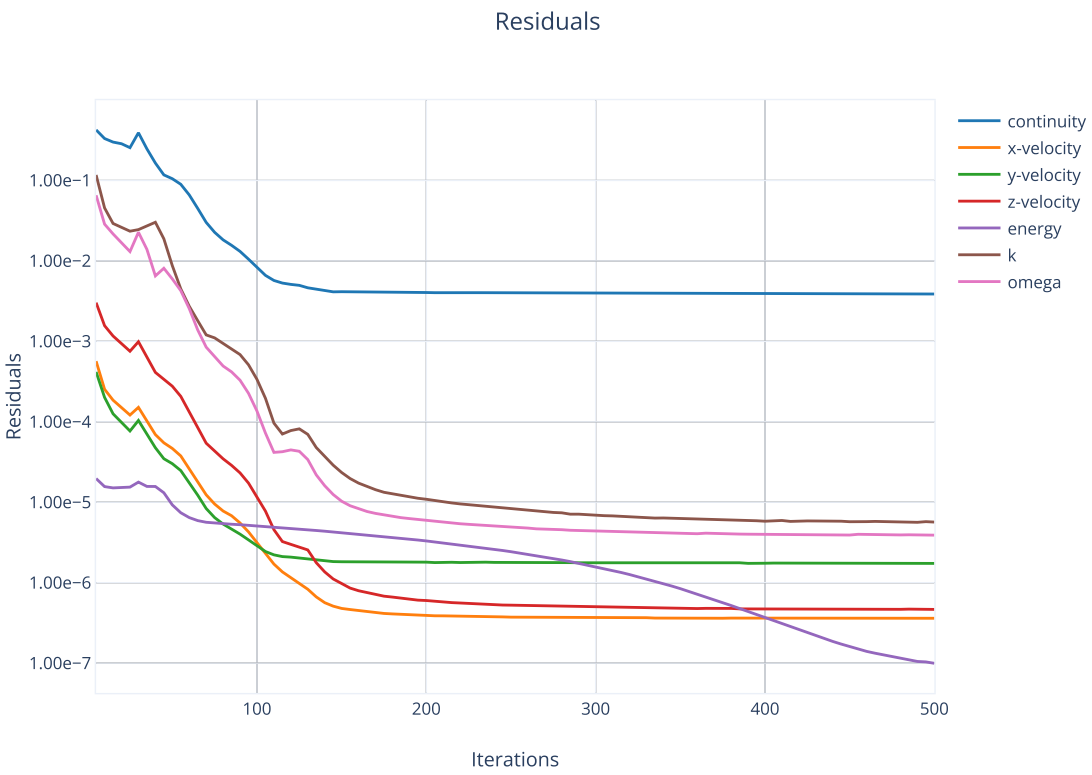

pressure

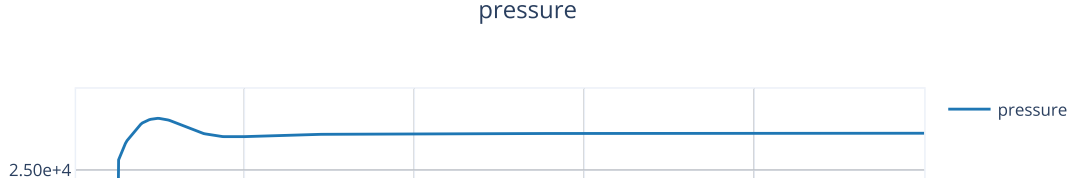

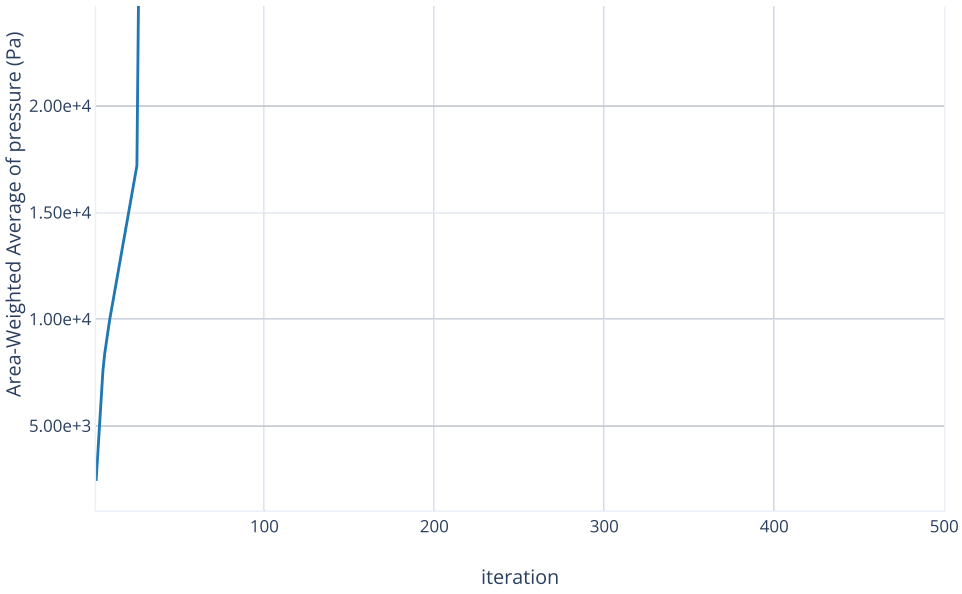

outlet-temp

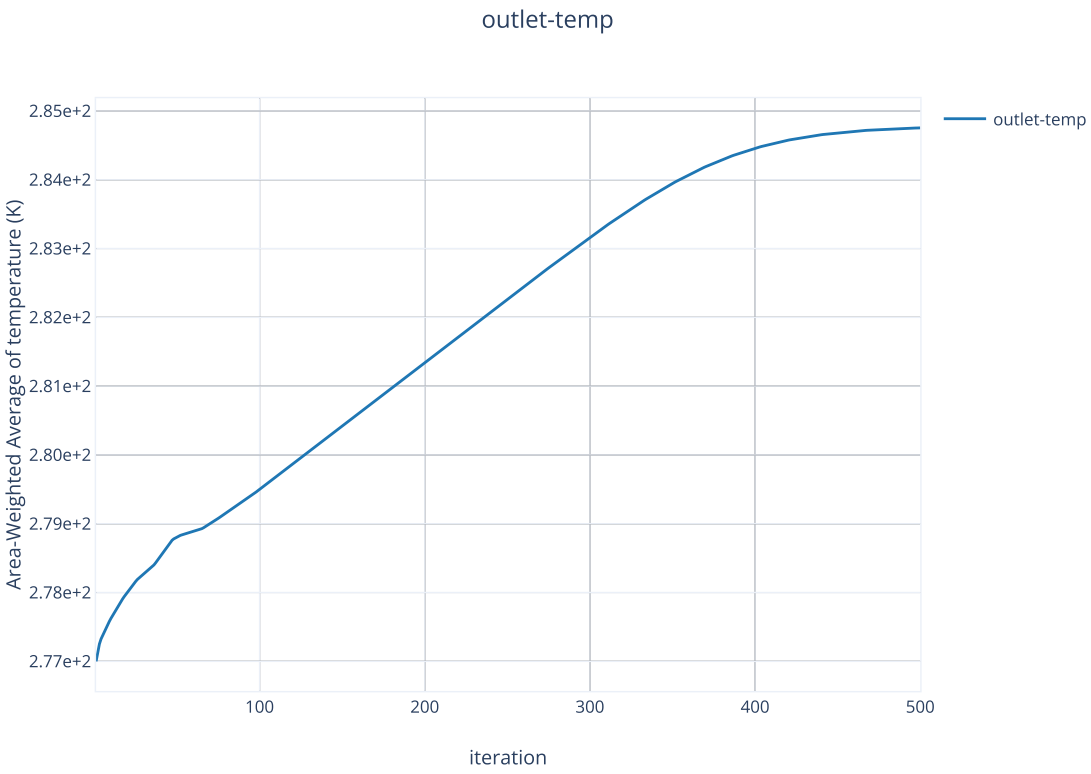

total-heat-transfer

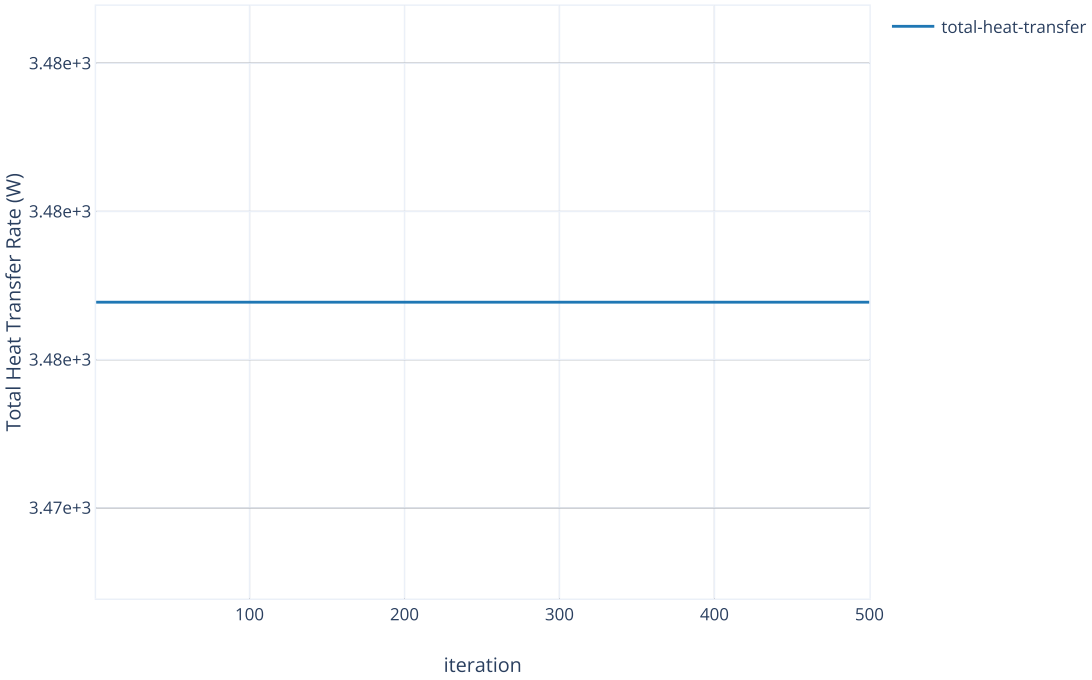
total-heat-transfer
3.48e+3
3.48e+3
3.48e+3
3.47e+3
Total Heat Transfer Rate (W)
100
200
300
400
500
iteration

Contours

contour-1

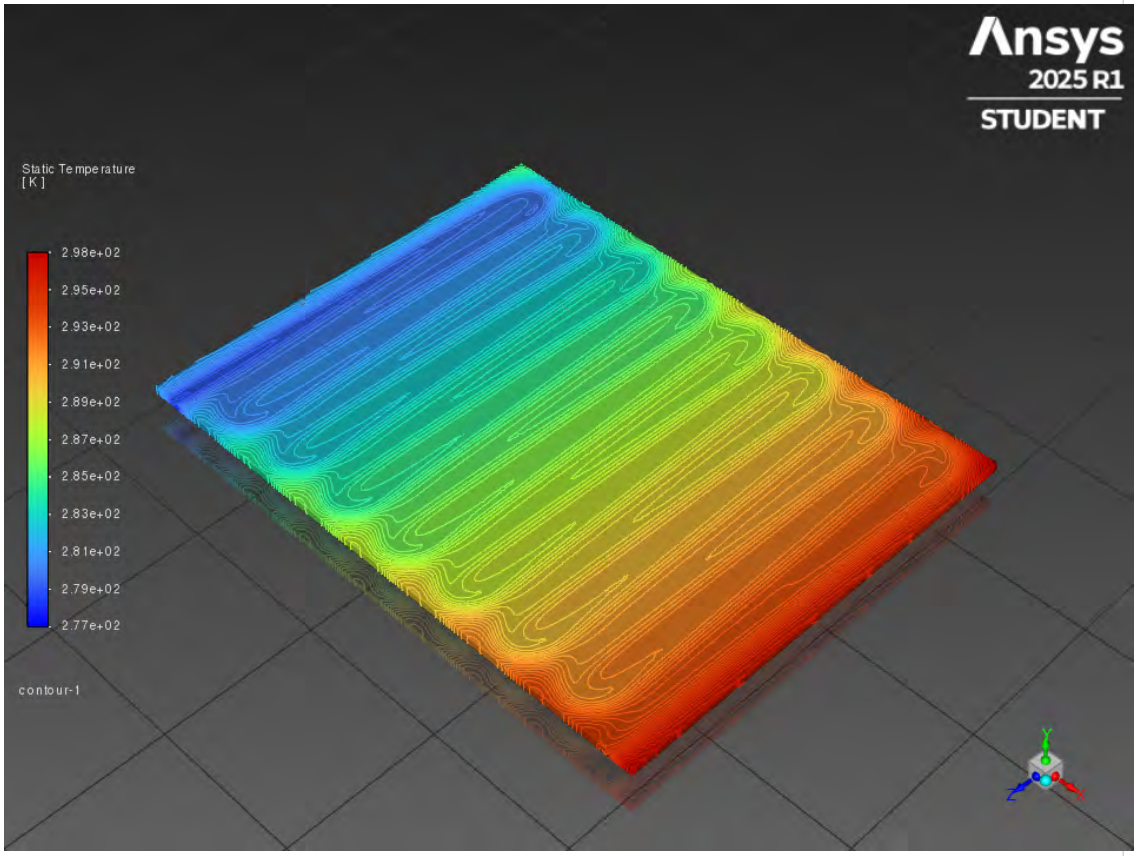

Conclusions

The second take CFD analysis was performed with parameters more representative of the mission, a larger heat flux to determine a steady-state outlet temperature, and more revised model. The two key changes were an inlet temperature or 277 K (4 C) and a surface mass flux of 5000 W/m^2. The resulting pressure drop across the plate was 26729 Pa (3.88 psi), outlet temperature of 284.7 K (12 C), and total heat transfer of 3475 W. This second take CFD analysis demonstrates the thermal capabilities of an aluminum-water cold-plate with the geometry given are more than sufficient for 560 W payloads. This simulation demonstrates similar drawbacks to the previous: the serpentine channel layout in a cold-plate this large creates a large temperature and pressure gradient across the payload

D.2 Air-Cooling Equations and Assumptions - Raymond Encarnacion

D.2.1 Convective Heat Transfer Equations

Thermal Load (W):

$$\dot{Q} = \dot{m} c_p \Delta T \tag{55}$$

Volumetric Flow Rate (m^3/s):

$$\dot{V} = \frac{\dot{m}}{\rho_{\text{air}}} \tag{56}$$

Total Noise Level (dB):

$$L_{total} = 10 log_{10}(10^{L_1/10} + 10^{L_2/10} + \ ... \ 10^{L_n/10}) \tag{57}$$

D.2.2 Assumptions

- Moderate temperature water is used as the coolant for the air-cooling system.
- Heat load from air-cooling system: $\dot{Q}$ = 560 W
- Mass flow rate from MTL: $\dot{m}$ = 198 kg/hr
- Cabin Temperature: T_{in}= 18 °C
- Max Payload Temperature: T_{in}= 38 °C
- Specific heat of air: $c_{p,air}$ = 1004 J/kg-°C
- Air Density on Earth: $\rho = 1.225 kg/m^3$

E Appendix E - Payload Definition - Sofia Correia

To demonstrate that the payload rack meets the scientific and operational standards established by existing infrastructure currently in use aboard the International Space Station (ISS), an analysis was conducted to evaluate whether a variety of real and conceptual payloads could be accommodated by the rack's geometry and interfaces. This assessment included existing ISS-based and possible future scientific payloads based on emerging mission needs.

E.1 Existing Scientific Payloads

Several scientific payloads currently used aboard the ISS were used as references, such as:

- **MERLIN (Microgravity Experiment Research Locker Incubator)** – Provides a thermally controlled environment for biological and physical science experiments, with an operating temperature range between 253 K and 321.5 K (–20 °C to 48.5 °C). It supports a payload mass of approximately 13.6 kg and has dimensions of 419 mm (W) × 259 mm (D) × 170 mm (H). The system uses both air and water cooling. (University of Alabama, 2025)
- **ELF (Electrostatic Levitation Furnace)** – Used for experiments regarding materials science, this payload levitates samples using electrostatic force and melts them via laser heating. Its dimensions are 887 mm (W) × 785 mm (D) × 590 mm (H), and it operates with a maximum power draw of 550 W. (Japan Aerospace Agency, 2020)
- **MSG (Microgravity Science Glovebox)** – A sealed, ventilated environment for biological and chemical research in microgravity. It measures 904 mm (W) × 635 mm (D) × 498 mm (H), requires gaseous nitrogen, and operates at +28 V DC with a usable current of 7 amperes. (Thompson, 2014)
- **ExPRESS Locker** – Scientific payloads are either inserted into, or replace the ExPRESS Locker within the rack. Each locker measures 460 mm (W) × 544 mm (D) × 272 mm (H). (Thompson, 2014)

Each of these payloads fall within the structural and volumetric limits of the rack design. The rack's adjustable rail system allows payloads of different volumes to be securely mounted at various heights, and its integrated power, data, and life support interfaces ensure compatibility with electrical and environmental requirements.

E.2 Future Payload Concepts

The rack is also designed with future lunar exploration and scientific needs in mind. Unlike the ISS, lunar habitats must account for partial gravity, increased exposure to cosmic radiation, and dust mitigation challenges. The rack's modularity, removable panels, and enclosed volume make it adaptable do these differing constraints.

Potential future payloads include:

- **Lunar Agriculture Systems** – Designed to support food production and plant research, these systems require flexible vertical clearance and environmental controls. The rack accommodates them with adjustable rail heights and built-in interfaces for power, lighting, humidity regulation, and air composition management.
- **Lunar Tissue Growth Chambers** – Intended to study the effect of partial gravity on biological systems, these payloads require precise thermal, lighting, and atmospheric control. The rack supports multiple experiment chambers with modular sizing and servicing access, as well as integrated systems for temperature control, lighting, and atmosphere regulation.
- **Cosmic Radiation Detection and Space Weather Monitoring** – The payload may include instruments to measure galactic cosmic rays (GCRs), solar particles, and radiation impacts on biological samples. The rack can provide power, data, and environmental support for both instrumentation and living tissue payloads.

This assessment confirms the rack's compatibility with a wide variety of current and anticipated payloads. Its structural adaptability, integrated interfaces, and emphasis on serviceability make it suitable for the existing and evolving demands of lunar surface missions.

F Appendix F - ECLSS Overview - Colin Keller

F.1 Overview

At the heart of every crewed spacecraft, orbital station, and future planetary outpost lies the Environmental Control and Life Support System (ECLSS)—a highly integrated suite of subsystems responsible for maintaining a habitable environment. These systems not only manage atmospheric composition and pressure, but also enable water recovery, temperature and humidity regulation, waste processing, and fire detection and suppression (NASA, 2010). Yet just as important as the functions themselves is the hardware platform that houses and interfaces with these systems. This is where standardized rack architectures such as the Collins Rack, ISPR, and EXPRESS Rack (EXpedite the PRocessing of Experiments to the Space Station) come into play.

ECLSS is not a monolithic device, but rather a network of modules distributed across several racks—each performing distinct roles. For instance, on the International Space Station (ISS), these subsystems are arranged across integrated racks that align with international payload standards and modularity requirements. The International Standard Payload Rack (ISPR) is the foundational design standard for full-sized equipment racks on the ISS. Measuring approximately 2 meters tall, 1 meter wide, and 0.86 meters deep, with a usable volume of roughly 1.57 cubic meters, the ISPR accommodates life science payloads, hardware experiments, and life support components (NASA, 2001). It includes internal utilities such as data buses, cooling loops, power interfaces (120V DC), and air or water cooling depending on the hardware housed within. ISPRs are a cornerstone of NASA's modular infrastructure strategy, ensuring that large payload elements—such as the Water Recovery System (WRS) or Carbon Dioxide Removal Assembly (CDRA)—can be swapped out, maintained, and interfaced with other systems via standardized mechanical and electrical ports (NASA, 2010).

Among the rack variants used on the ISS, the Collins Rack—a term not always formalized in public-facing NASA documentation but referring to racks developed or modified by Collins Aerospace—plays a specialized role in life support and avionics. Collins Aerospace, a major NASA contractor and systems integrator, has contributed to both environmental and structural systems aboard the ISS. Their rack contributions may involve flight-certified avionics enclosures, atmospheric regulators, oxygen control panels, and humidity control hardware integrated into modular frames (Collins Aerospace, 2022). The so-called "Collins racks" are typically synonymous with high-reliability systems supporting either the ECLSS infrastructure or avionics environments requiring precise thermal management and EMI shielding. They are often tailored for flight segment integration where system-specific constraints—like gas flow or thermal gradient control—demand custom or semi-custom rack architecture, while still maintaining a degree of standardization for ISS compatibility.

Another major rack class used in both ECLSS and science payloads is the EXPRESS Rack. Originally designed to provide fast turnaround for scientific experiments aboard the ISS, EXPRESS Racks are also used to house life support components and interfaces due to their modularity and service integration. These racks can support up to ten standardized payload drawers (called "lockers"), each capable of hosting a small payload experiment, fluid processing unit, or sensor suite. With built-in connections for power, command and data handling, temperature control, and video

monitoring, EXPRESS Racks are a versatile platform for integrating secondary ECLSS functions, such as trace contaminant monitors or microbial sampling units (NASA, 2008). This design promotes parallel development and deployment of hardware, enabling systems to evolve independently while maintaining plug-and-play operability.

The interaction between rack architecture and ECLSS performance is often quite fascinating. For instance, the Water Recovery System (WRS)—which recycles urine, humidity condensate, and other wastewater into potable water—is composed of multiple modular elements, including a Urine Processor Assembly (UPA), Water Processor Assembly (WPA), and associated Multi-filtration Beds. These are each installed in ISPR-formatted racks and require seamless integration with thermal loops and power systems (Carter et al., 2008). Similarly, the Carbon Dioxide Removal Assembly (CDRA) resides within ISPR housing and contains alternating beds of zeolite-based adsorbents that cyclically trap and vent CO_2. These racks must be designed to facilitate both autonomous function and rapid crew maintenance, as adsorbent beds and other components degrade over time and require replacement.

Further integration challenges arise when dealing with multiphase fluids, biological waste, and particulate matter—all of which are common in ECLSS subsystems. Systems such as the Temperature and Humidity Control (THC) module are integrated into pressurized segments using rack-level ducting and condensate removal systems, while also demanding direct thermal rejection through ISS cooling loops (NASA, 2001). Racks involved in THC operations must incorporate hydrophobic filters, anti-microbial surfaces, and drainage systems, adding layers of engineering complexity to their design. These requirements make it essential that racks like the ISPR or EXPRESS variants are built with redundant power buses, EMI protection, and structural reinforcement to mitigate vibration and acceleration loads during launch and installation.

A final note must be made regarding the logistics infrastructure tied to these racks—particularly in how consumables, replacement filters, and system components are delivered. Cargo Transfer Bags (CTBs) and pallet systems such as the Mid-deck Locker Equivalent (MLE) are designed to interface directly with rack mounts, allowing crew members to install or replace elements quickly. Racks often include slide rails, restraint bars, and tethering hooks to accommodate CTBs in both temporary and permanent storage configurations. This harmonization between life support infrastructure and logistics hardware is a non-negotiable component of modern spacecraft and habitat design.

F.2 Atmosphere Control and Supply (ACS)

The Atmosphere Control and Supply (ACS) subsystem plays a foundational role in the Environmental Control and Life Support System (ECLSS) aboard crewed spacecraft such as the International Space Station (ISS). It is tasked with generating, storing, and regulating the composition and pressure of the cabin atmosphere, ensuring a safe and breathable environment for the astronauts onboard. Within the ISS, the ACS is physically implemented through modular hardware housed in standardized rack enclosures—most notably within the International Standard Payload Rack (ISPR) format and specialized racks developed by Collins Aerospace. These racks provide the structural and utility interfaces necessary to integrate life support functionality into the broader station architecture, enabling ACS components to operate continuously and autonomously for months or even years at a time (NASA, 2010; Collins Aerospace, 2022).

A central component of the ACS subsystem is the Oxygen Generation Assembly (OGA), which

uses electrolysis to split purified water into its constituent elements: hydrogen and oxygen. The oxygen is introduced directly into the cabin environment to replenish what is consumed by crew respiration, while the hydrogen is typically vented overboard or routed to the Sabatier system, which can convert it into methane and water (NASA, 2015). This process not only supports oxygen recycling but also enhances overall water recovery efficiency. Because electrolysis does not produce nitrogen, the ACS subsystem is also responsible for maintaining the proper balance of atmospheric gases by using pressurized nitrogen tanks. These tanks, mounted externally on the station's truss or airlock modules, can inject nitrogen into the cabin as needed to maintain Earth-like atmospheric conditions—generally around 14.7 psi total pressure with an oxygen partial pressure near 21 kPa (NASA, 2008). This balance is critical not just for crew health, but also for minimizing flammability risk and supporting system compatibility across various modules.

F.3 Temperature and Humidity Control (THC)

The Temperature and Humidity Control (THC) subsystem is a critical element of the Environmental Control and Life Support System (ECLSS) architecture aboard the International Space Station (ISS) and future crewed vehicles. Its primary function is to maintain a stable thermal environment and control moisture levels within habitable areas, both of which are essential for crew health, equipment functionality, and the safe operation of scientific payloads. Unlike terrestrial HVAC systems that rely heavily on convection, THC systems in microgravity must be engineered around the unique fluid and thermal dynamics of orbit. This includes leveraging forced airflow, liquid-cooled loops, and phase-change mechanisms to remove excess heat and humidity generated by the crew, onboard systems, and external environmental conditions. Central to the effectiveness and modularity of this subsystem is its integration within rack-based platforms such as the International Standard Payload Rack (ISPR) and advanced systems developed by Collins Aerospace, both of which are designed to support thermal control components in a compact, serviceable, and interoperable format.

F.4 Atmosphere Revitalization (AR)

The Atmosphere Revitalization (AR) subsystem is one of the core elements of the Environmental Control and Life Support System (ECLSS), tasked with continuously filtering and purifying the cabin air to ensure a safe, breathable environment for astronauts. While the Atmosphere Control and Supply (ACS) subsystem maintains gas composition and pressure, AR ensures that the internal atmosphere remains clean, chemically balanced, and biologically safe by removing carbon dioxide, trace contaminants, and excess humidity. This process, although invisible to the crew, is essential for preventing hypercapnia, toxic gas buildup, and equipment degradation. Within the context of long-duration missions aboard the International Space Station (ISS), these functions are modularized into specialized hardware units installed within standardized rack systems—most notably the International Standard Payload Rack (ISPR) and enhanced systems provided by Collins Aerospace. The design and implementation of these racks ensure that AR functions remain accessible, maintainable, and interoperable across the station's integrated life support infrastructure (NASA, 2015).

F.5 Fire Detection and Suppression (FDS)

The fire detection and suppression system is located on or near all powered racks where a fire may be of concern. These systems will differ from rack to rack as payload definitions are finalized. When triggered, this system will flash red LED's and the connected system/laptop will indicate which sensors went off. Crew members, in the event it happens, also have the ability to manually trigger said event notification. At this point, after a fire is located, crews will have strict protocols to follow on how to suppress and/or isolate it. For example, for each locations where a fire may be of concern, if need be, there is a port loaded with a fire suppressant in the event it cannot be put out by other means (NASA, SSP51721).

F.6 Waste Management (WM)

The waste management system on a rack deals with the collection, processing, and storage of human waste. The system is divided into two main parts, the commode and urinal. In the urinal, urine is collected and pretreated with oxone and sulfuric acid before being sent to the urine processor. In the commode, air is pulled in such that human fecal matter is drawn into a waste bag inside of a waste canister. This bag is then compressed inside of the waste canister to allow for the next bag to be positioned inside. The canister is rated to hold approximately 28 defecations before signaling the crew to be cleaned (NASA, 2022).

F.7 Water Recovery Management (WRM)

The water recovery management system operates to supply the crew with water for consumption and payloads while also collecting waste water for processing. The two most important subsystems this system houses are the water processing assembly and urine processor assembly. The water processing assembly takes in waste water and humidity condensate and outputs potable water used for experiments, water electrolysis for O_2, and drinking. This system drastically reduces the need for water resupply missions and promotes self-sustainability (NASA, 2024).

F.8 ECLSS Glossary

Table 23: Glossary of ECLSS Systems
(N/A - Not public information)

G Appendix G - References

Akin, D. L. (2023, July). *Developing an integrated logistics infrastructure for lunar surface habitats* (ICES-2023-454). 52nd International Conference on Environmental Systems, Calgary, Alberta, Canada. Texas Tech University Institutional Repository. https://ttu-ir.tdl.org/server/api/core/bitstreams/b3886a6c-8d96-4f74-a075-f69a41d80e1e/content

Akin, D. L. (2025). *Overview of underwater ballasting for partial gravity testing* [Class handout]. ENAE484: Space Systems Design, University of Maryland.

Anderson, M. S., & Ewert, M. K. (2015). *Status of the Atmosphere Revitalization Subsystem on ISS*. https://ntrs.nasa.gov/api/citations/20150022318/downloads/20150022318.pdf

Briggs, A., & Napier, N. (2022). *NASA Universal Waste Management System and Toilet Integration Hardware: Operations on ISS*. https://ntrs.nasa.gov/api/citations/20220005710/downloads/NASA%20Universal%20Waste%20Management%20System%20and%20Toilet%20Integration%20Hardware%202022%20final%20draft.pdf

Burke, C. J., & Howard, R. L. (2022). *Internal layout assessment of a lunar surface habitat*. https://doi.org/10.2514/6.2022-4266

Callahan, M. R., & Sargusingh, M. J. (2024). *Status of the ISS Water Recovery System*. https://ntrs.nasa.gov/api/citations/20240005472/downloads/ICES%202024-317%20Status%20of%20ISS%20Water_Final.pdf

Carter, D. L., Tobias, B. C., & Callahan, M. R. (2008). *Development of the Water Recovery System for the International Space Station*.

Collins Aerospace. (2022). *Life Support and Environmental Systems*. https://www.collinsaerospace.com/

Data Device Corporation. (n.d.). *MIL-STD-1553 Data Bus Couplers*. https://www.ddc-web.com/en/mil-std-1553-data-bus-couplers

Davis, T., Adams, J., Fisher, E., Prickett, G., & Smith, T. (1999). *EXPRESS rack technology for space station*. https://ntrs.nasa.gov/api/citations/19990008536/downloads/19990008536.pdf

European Space Agency (ESA). (2014). *European users guide to low gravity platforms* (Issue 2). https://www.esa.int/Science_Exploration/Human_and_Robotic_Exploration/Research/European_user_guide_to_low_gravity_platforms

Glass, M. (2010, July). *Performance comparison: Solid State Power Controllers vs Electromechanical Switching*. https://powerdevicecorp.com/resources/FileManager/power/whitepapers/SSPCvsbreakersWP.pdf

International Space Station Program. (2015, October). *Pressurized Payloads Interface Requirements Document* (Rev. R). https://ntrs.nasa.gov/api/citations/20190001390/downloads/20190001390.pdf

ISS National Laboratory. (n.d.). *Expedite the processing of experiments to the Space Station - ISS National Lab*.https://issnationallab.org/facilities/expedite-the-processing-of-experiments-to-the-space-station/

Japan Aerospace Exploration Agency. (2020) *ELF: Experiment – International Space Station*. JAXA Kibo Utilization Office. https://iss.jaxa.jp/en/kiboexp/pm/elf/humans-in-space.jaxa.jp

Layne, L. L., & Urie, D. M. (2003). Life Support Systems for Spacecraft and Lunar/Martian Habitats. Journal of Spacecraft and Rockets, 40(4), 525–532.

Miedza, B., & Behrens, B. (1997). *Cold-Plate Development for Space Station Application*. https://adsabs.harvard.edu/full/1997ESASP.400..299M

NASA. (2021). *SSP 51721: Environmental Control and Life Support System (ECLSS) Design Document for ISS*. https://ntrs.nasa.gov/api/citations/20210009936/downloads/SSP%2051721-Baseline.pdf

NASA. (2010). *Environmental Control and Life Support System (ECLSS) Fact Sheet*. https://www.nasa.gov

NASA. (2008). EXPRESS Rack Overview. https://www.nasa.gov

NASA. (2023, November). *NASA-STD-3001 Volume 2 Revision D: Human system integration standards*. NASA. https://www.nasa.gov/wp-content/uploads/2023/11/nasa-std-3001-vol-2-rev-d-with-signature.pdf

NASA. (2022, July). *International docking system standard (IDSS) interface control document (ICD)* (Rev. F). https://www.internationaldockingstandard.com/download/IDSS_IDD_Revision_F.pdf

NASA. (1984, March). *Orbiter middeck/payload standard interfaces control document* (NASA Technical Memorandum No. 19850018529). National Space Transportation Systems Program Office. https://ntrs.nasa.gov/api/citations/19850018529/downloads/19850018529.pdf

NASA. (2022, March 2). *Quick start guide to payload design.* https://www.nasa.gov/wp-content/uploads/2020/10/pdguide_payloadengineering_20220302.pdf

NASA. (2015). *Water Recovery System: Status and Performance Summary.* NASA TP-2015-218928.

NASA Exploration Capabilities. (2024, March 6). *Moon to mars exploration systems and habitation (M2M X-Hab) academic innovation challenge – FY25 Solicitation* [Solicitation]. National Space Grant Foundation. https://spacegrant.org/wp-content/uploads/2024/03/M2M-X-Hab-Challenge-Solicitation-2025.pdf

NASA Johnson Space Center. (2015, October). *Pressurized Payloads Interface Requirements Document International Space Station Program.* https://ntrs.nasa.gov/api/citations/20190001390/downloads/20190001390.pdf

NASA Johnson Space Center. (2014). *JSC-65828B-Chg1: Spacecraft Design and Verification of Space Systems.* NASA. https://standards.nasa.gov/sites/default/files/standards/JSC/B/1/JSC-65828B-Chg1.pdf

NASA. (n.d.). Space Station Research Investigation. NASA. https://www.nasa.gov/mission/station/research-explorer/investigation/#id=1571

National Aeronautics and Space Administration. (2014, June). *Loads and Structural Dynamics Requirements for Spaceflight Hardware.*

National Space Transportation System Program Office. (1984, March). *Orbiter middeck/payload standard interfaces control document.* https://ntrs.nasa.gov/api/citations/19850018529/downloads/19850018529.pdf

Online Metals. (n.d.). *Order 0.19" aluminum sheet 7075-T6 online, thickness: 3/16".* https://www.onlinemetals.com/en/buy/aluminum/0-19-aluminum-sheet-7075-t6/pid/12664

Online Metals. (n.d.). *0.19" Aluminum Sheet 7075-T6.* https://www.onlinemetals.com/en/buy/aluminum/0-19-aluminum-sheet-7075-t6/pid/12664

O'Neill, J., Bowers, J., Corallo, R., Torres, M. A., & Stapleton, T. J. (2019). *Environmental control and life support module architecture for deployment across deep space platforms.* 49th International Conference on Environmental Systems.

S. W. Thompson, L. P. Jordan, and G. N. Flores. (2014) *An Overview of ExPRESS, WORF, and MSG Platforms.* NASA Marshall Space Flight Center. https://ntrs.nasa.gov/api/citations/20140011706/downloads/20140011706.pdf?attachment=true

Smith, A. M. (2013). The space elevator: Dynamics and control. *Acta Astronautica, 90*(2), 345–353. https://www.sciencedirect.com/science/article/pii/S0094576513002373

SpaceX. (2022, March 22). Capabilities & Services (2024). Retrieved from https://web.archive.org/web/20220322170331/https://www.spacex.com/media/Capabilities&Services.pdf

SpaceX. (2024). Capabilities & Services. Retrieved from http://spacex.com/humanspaceflight

SpaceX. (2021). Falcon user's guide. https://www.spacex.com/media/falcon-users-guide-2021-09.pdf

TFAWS NASA. (n.d.). *An Advanced Design of an Isothermal Coldplate*. https://tfaws.nasa.gov/TFAWS07/Proceedings/TFAWS07-1024.pdf.

Thermal Space. (2018, April 23). *Custom cold plate or thermal interface plate for precise temperature control*. https://thermal-space.com/cold-plate-design-and-fabrication/.

Thompson, S., Jordan, L. P., & Flores, G. N. (2014). *An overview of EXPRESS Rack, Microgravity Science Glovebox, and sub-rack facilities for materials science research*. Materials LAB Workshop. https://ntrs.nasa.gov/api/citations/20140010107/downloads/20140010107.pdf

Thompson, S. W., & Lake, R. E. (2014, October). *Conducting research on the International Space Station using the EXPRESS Rack Facilities*. NASA. https://ntrs.nasa.gov/api/citations/20140016876/downloads/20140016876.pdf

Various Authors. (n.d.). *Material properties reference table*. [PROPS.pdf].

University of Alabama. (2024) *MERLIN*. University of Alabama at Birmingham, Engineering and Innovative Technology Development. https://www.uab.edu/engineering/eitd/projects/cold-stowage/merlinuab.edu

Wieland, P. O. (1998). Living together in space: The design and operation of the life support systems on the International Space Station (NASA Reference Publication 1998-206956). National Aeronautics and Space Administration, Marshall Space Flight Center.